This is to certify that the
dissertation entitled

SCANNING PROBE RECOGNITION MICROSCOPY:
RECOGNITION STRATEGIES

presented by

QIAN CHEN

has been accepted towards fulfillment
of the requirements for the

Ph. D. degree in Department of Electrical & Computer Engineering

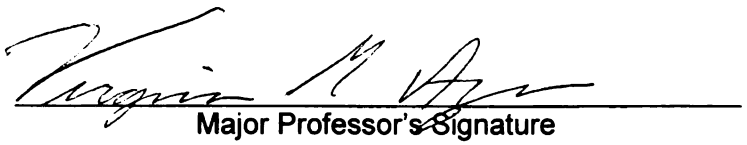

Major Professor's Signature

12 DECEMBER 2007

Date

SCANNING PROBE RECOGNITION MICROSCOPY: RECOGNITION STRATEGIES

By

Qian Chen

A DISSERTATION

Submitted to
Michigan State University
in partial fulfillment of the requirements
for the degree of

DOCTOR OF PHILOSOPHY

Department of Electrical & Computer Engineering

2007

ABSTRACT

SCANNING PROBE RECOGNITION MICROSCOPY:
RECOGNITION STRATEGIES

By

Qian Chen

Scanning Probe Recognition Microscopy (SPRM) is a specially modified Scanning Probe Microscopy (SPM) system designed and developed by our research group in partnership with Veeco Instruments. In Scanning Probe Recognition Microscopy, the SPM system itself is given the ability to automatically track regions of interest during scanning through incorporation of recognition–based tip control. The recognition capability is realized by using algorithms and techniques in image processing, pattern recognition and computer vision fields. Adaptive learning and prediction are also implemented to make the object detection and tracking procedures quicker and more reliable. The major contribution of SPRM includes: (1) decreasing overall operation time; (2) providing the ability to quantitatively measuring properties while maintaining the uniformity of experimental environment; (3) sequentially measuring topographic, mechanical and chemistry properties of the same sample surface through repetitive high resolution scanning in the appropriate mode; (4) properties measuring in situations which are inaccessible by standard SPM. SPRM measurements of the surface roughness, elasticity and surface chemistry of 2D nanoscale electrospun carbon nanofibers are given in detail as an example of SPREM analysis in a situation that is not fully accessible by SPM. The 3D nanoscale electrospun nanofibers are the components of a tissue scaffold for regenerative medicine. These scaffolds are used for neural cells re-growth in a damaged spinal cord. The candidate's thesis research is therefore to design and

implement the recognition strategies that allow SPRM properties extraction along tissue scaffold nanofibers, to perform the first quantitative measure of multiple properties that have been shown to be important in neural cell re-growth and, by doing so, to contribute significant understanding to the cure of presently incurable paralysis.

ACKNOWLEDGMENT

I would like to sincerely thank my major advisor, Dr. Virginia Ayres, for her support all the way through the program. She not only gives me technical guidance, but also teaches me about how to be face difficulties and tackle difficulties. I really appreciate her encouragement and consideration. I would like to thank Dr. Lalita Udpa for her guidance and support. She inspires me in many aspects and keeps me moving forward. I would also like to express my gratitude to Dr. Marcos Dantus and Dr. Hayder Radha for their precious advices and kindness as my committee members.

I would like to thank Yuan Fan for his consideration and friendship during the cooperation. Thanks are also extended to Benjamin Jacobs for his help in nanocircuits experiments.

I thank Dr. Sally Meiners, Ijaz Ahmed, Roberto Delgado-Rivera and Suzan Harris for their generous help when I was visiting their lab to study for spinal cord repair.

I would like to express my appreciation to my husband, Xiangdong Peng, and my parent, Jiwen Chen and Fengying Ma, for their love and support through all these years. Without them, I can not get this far. Finally, to my lovely son, Kevin, he makes me motivated and feels truly blessed.

TABLE OF CONTENTS

LIST OF TABLES viii

LIST OF FIGURES ix

INTRODUCTION 1

Part I SPRM INSTRUMENTATION DEVELOPMENT 5
CHAPTER 1
IMAGING TECHNIQUES USED IN NANOBIOLOGY 7
1.1 Optical Microscopies 7
1.2 Electron Microscopies 10
1.3 Brief Introduction of Scanning Probe Microscopy in Biology and Medicine ... 12

CHAPTER 2
SCANNING PROBE MICROSCOPY IMAGING TECHNIQUES 14
2.1 Fundamentals of SPM 14
2.1.1 Block diagram 16
2.1.2 Operation modes 18
2.2 Advantages and Limitations of SPM 20
2.2.1 Advantages 20
2.2.2 Limitations 20
2.3 Improvement of SPM Start of Art 21

CHAPTER 3
SCANNING PROBE RECOGNITION MICROSCOPY 23
3.1 SPRM System Functionalities 24
3.1.1 Recognition ability 24
3.1.2 Auto-tracking capability and region of interest 24
3.1.3 Real-time result display capability 24
3.1.4 Property analysis capability 25
3.2 SPRM Prototype System Structure 25
3.3 SPRM System Design & Software Development 26
3.4 SPRM Recognition Algorithm 28
3.4.1 Preprocessing: Wavelet-based image segmentation 28
3.4.2 Feature detection 31
3.5 SPRM Operation Modes 35
3.6 Novelty & Importance of SPRM versus State of the Art AFM 36
3.6.1 Novelty and importance of SPRM versus standard SPM 36
3.6.2 Novelty and importance of SPRM versus optical techniques 38
3.6.3 Novelty and importance of SPRM versus HRTEM 39

Part II SPRM APPLICATIONS IN NANOBIOLOGY 41
CHAPTER 4
MOTIVATION & BACKGROUND OF SPRM IN TISSUE ENGINEERING 42
4.1 Introduction of Tissue Engineering: Spinal Cord Repair 42
4.2 Environmental Nanoscale Cues for Cell Growth 44
4.3 Ultimate Goal 50

CHAPTER 5
SPRM AUTO-TRACKING IMPLEMENTATION ON TISSUE SCAFFOLD NANOFIBERS 52
5.1 Importance of Auto-Tracking of Individual Nanofibers 52
5.2 SPRM Auto-Tracking Capability 55
5.3 Examples of SPRM 60

CHAPTER 6
NANOFIBER PROPERTIES ANALYSIS BY USING SPRM 62
6.1 Tissue Scaffold Samples and Experimental Parameters 62
6.2 Nanofiber Property Analysis by Using SPRM 64
6.2.1 Surface roughness 64
6.2.2 Elasticity 71
6.3 Comparison of Nanofiber Diameter by Transmission Electron Microscopy 77
6.4 Comparison of Nanofiber Properties by Transmission Electron Microscopy 80
6.5 Conclusion & Discussion 81

CHAPTER 7
CELL RESPONSE ANALYSIS 83
7.1 Tissue Scaffold Samples & Experimental Techniques 86
7.1.1 Tissue scaffold samples 86
7.1.2 SPRM Properties investigation of nanofibers 87
7.2 First Model System: Fibroblasts on 2D versus Nanoscale 3D Nanofibers 95
7.2.1 Cell culture 96
7.2.2 Experimental investigation of fibroblasts response 97
7.2.3 Comparison of fibroblasts response and conclusion 100
7.3 Second Model System: Astrocytes on 2D versus Nanoscale 3D Nanofibers 101
7.3.1 Cell culture 102
7.3.2 Experimental investigation of astrocytes response 102
7.3.3 Conclusion 104

CHAPTER 8
8 ELECTROSPINNING PARAMETERS 105
8.1 Introduction 106
8.2 Experimental Setting 108
8.3 Experimental Results 109
8.4 Discussion and Conclusion 113

Part III CONCLUSION & FUTURE WORK 115
CHAPTER 9
9 CONCLUSION & DISCUSSION 115
9.1 Conclusion 115
9.2 Discussion 116

CHAPTER 10
10 FUTURE WORK 117
10.1 Improvement of SPRM Recognition Capability 117
10.2 Extended Work in Spinal Cord Repair 117
10.3 Extension of SPRM to Additional Research Problems: Nanocircuits 118

REFERENCE 123

LIST OF TABLES

Table 2-1 Multimode SPM Scanner Specifications [32] 18

Table 2-2 Operation Modes of AFM 19

Table 6-1 Surface Roughness Statistical Analysis 70

Table 6-2 Elasticity/Area Map Statistical Analysis 77

Table 6-3 Nanofiber Diameter Measurements Using TEM and AFM Images 79

LIST OF FIGURES

Figure 2-1 Block diagram of Atomic Force Microscopy 16

Figure 3-1 Block diagram of Scanning Probe Recognition Microscopy 26

Figure 3-2 Software design diagram 27

Figure 3-3 Schematic of overall approach. Reproduced from Figure 2, Reference: Q. Chen, Y. Fan, L. Udpa, and V.M. Ayres, Vol. 2, Issue 2, pp. 181-189, Int. J. Nanomedicine (2007) 28

Figure 3-4 Edge detection based on wavelets (a) original image, (b) edge image when scale = 2, (c) edge image when scale = 10 30

Figure3-5 Segmentation (a) the edge image after dilation, (b) the edge image after threshold, (c) the segmented object 31

Figure 3-6 The definition of the Edge Feature is based on (a) AFM images; (b) Continuous wavelet transformed (CWT) images. (c) Pixel intensities on horizontal and vertical lines clearly show the Edge Feature for each cell type. Reproduced from Figure 4, Reference: Q. Chen, Y. Fan, L. Udpa, and V.M. Ayres, Vol. 2, Issue 2, pp. 181-189, Int. J. Nanomedicine (2007) 35

Figure 4-1 Cellular constituents of the blood-brain barrier. Images from reference [55] 44

Figure 4-2 SEM micrograph showing the bone marrow cell morphology on substrates with different surface roughness, Images from reference [59] 45

Figure 4-3 Movements of National Institutes of Health 3T3 cells on substrates with a rigidity gradient (*a*) A cell moved from the soft side of the substrate toward the gradient. The cell turned by ~90° and moved into the stiff side of the substrate. Note the increase in spreading area as the cell passed the boundary. (*b*) A cell moved from the stiff side of the substrate toward the gradient. The cell changed its direction as it entered the gradient and moved along the boundary. Bar, 40 μm. Images from reference [60] 46

Figure 4-4 Peptide modification enhances the ability of nanofibers to promote axonal regrowth. Rostral is to the left. G, host-graft interface. Curves were adjusted in Adobe Photoshop for each panel to enhance the visibility of the axons against the autofluorescence of the nanofibers. (A) Neurofilament M-labeled axons were observed within the implant of unmodified nanofibers. (B) Axonal growth was more robust within the implant of nanofibers modified with the D5' peptide. Bar, 150 μm. (C) Axons were observed on the surface of the nanofibers following folds

in the nanofibrillar fabric. The top of the image is ~ 300 μm ventral to the top of the spinal cord. Bar, 300 μm. Single arrows in (B) and (C) denote axons growing more or less parallel to the axis of the spinal cord. Double arrows denote axons that deviated from a parallel path. Reference: S. Meiners, I. Ahmed, A. S. Ponery, N. Amor, S. L. Harris, V. Ayres, Y. Fan, Q. Chen, R. Delgado-Rivera, and A. N. Babu, Polymer International, vol. 56, pp. 1340-1348, 200 48

Figure 4-5 Astrocytes cultured on even bare nanofibers adopted a stellate morphology (a) that is typical of their in vivo counterparts, whereas astrocytes cultured on poly-L-lysine (PLL) coated plastic coverslips had a flat, cobblestone appearance (b) which is never seen in the body. To date, PLL has been required for astrocyte growth in culture. Reference: S. Meiners, I. Ahmed, A. S. Ponery, N. Amor, S. L. Harris, V. Ayres, Y. Fan, Q. Chen, R. Delgado-Rivera, and A. N. Babu, Polymer International, vol. 56, pp. 1340-1348, 2007 50

Figure 5-1 Off-line segmentation results at scan size equals 15 microns a) AFM height image; b) Recovered image by reading exported ASCII file; c) Off-line segmentation results using thresholding method. 53

Figure 5-2 Off-line segmentation results at scan size equals 3 microns (a) AFM height image; (b) Recovered image by reading exported ASCII file; (c) Off-line segmentation results by using thresholding method. 53

Figure 5-3 Different types of regions on tissue scaffold nanofibers: Data point (1) is out of region of interest; data point (2) is right on top of a nanofiber; data point (3) is on the side of a nanofiber. Scan size: 10 microns [62]. 54

Figure 5-4 SPRM auto-tracking capability to scan along individual nanofibers (a) AFM height image; (b)-(g) A series of images shows the time sequence of scanned results by using SPRM. [62] 55

Figure 5-5 Flow chart of auto-tracking scan 56

Figure 5-6 SPRM scan along individual nanofibers in a tissue scaffold. Left image is the standard AFM image, region in black box are target scan region by SPRM. Right image shows the scan result of using SPRM, two individual nanofibers are scanned one after the other, other regions not scanned are padded 0 for display. 57

Figure 5-7 Scan plan to stay on individual nanofiber (a) without boundary prediction; (b) with boundary prediction 58

Figure 5-8 Demonstration of Scan angle in imaging Tissue scaffold nanofibers using SPRM (a) horizontal scan direction; (b)vertical scan direction 59

Figure 5-9 (a) Standard AFM image of tissue scaffolds with scan size equals 6 microns; (b) simulation scan result of SPRM by using horizontal scan direction; (c) real-time scan result of SPRM by using horizontal scan direction. 60

Figure 5-10 (a) Standard AFM image of tissue scaffolds with scan size equals 6 microns; (b) simulation scan result of SPRM by using vetical scan direction; (c) real-time scan result of SPRM by using vertical scan direction..... 61

Figure 6-1 AFM and SEM images of electrospun carbon nanofiber tissue scaffolds. (a)-(c) AFM images of Sample A, B and C. The scan area of each image is 5 square microns and the z-height projection is 1500 nanometers. (d)-(f) SEM images of Sample A, B and C. The scan area of each image is 20 square microns. Reproduced from Figure 1, Reference: Y. Fan, Q. Chen, et al. in press, Vol. 2, Issue 4, *Int. J. Nanomedicine* (2007)..... 64

Figure 6-2 surface roughness calculation of Scanning Probe Microscopy..... 65

Figure 6-3 Circle fit based on Kåsa method. Reproduced from Figure 5, Reference: Y. Fan, Q. Chen, et al. in press, Vol. 2, Issue 4, *Int. J. Nanomedicine* (2007)..... 67

Figure 6-4 (a) Characteristic tip-dilation artifacts (b) The cross section of a real AFM nano fiber image and the best fit circle. Reproduced from Figure 6, Reference: Y. Fan, Q. Chen, et al. in press, Vol. 2, Issue 4, *Int. J. Nanomedicine* (2007)..... 68

Figure 6-5 SPRM analysis of surface roughness (a) AFM image; (b) surface roughness map of an individual nanofiber..... 69

Figure 6-6 Histograms of surface roughness (a) Sample A; (b) Sample B; (c) Sample C. Reproduced from Figure 3, Reference: Y. Fan, Q. Chen, et al. in press, Vol. 2, Issue 4, *Int. J. Nanomedicine* (2007)..... 70

Figure 6-7 Force volume imaging of Atomic Force Microscopy..... 72

Figure 6-8 Tip probing position (a) tip probes top of nanofiber, force is normal to sample surface; (b) tip probes side of nanofiber, force is not normal to sample surface... 73

Figure 6-9 Force distance records the indentation of tip into soft sample..... 73

Figure 6-10 (a) force curve, both approach part and retract part are displayed; (b) force distance curve, only approach part curve is displayed, which is used to calculate elasticity property..... 74

Figure 6-11 Elasticity histograms for (a) Sample A; (b) Sample B; (c) Sample C. Reproduced from Figure 4, Reference: Y. Fan, Q. Chen, et al. in press, Vol. 2, Issue 4, *Int. J. Nanomedicine* (2007)..... 76

Figure 6-12 TEM images of (a) Sample A; (b) Sample B; (c) Sample C, with corresponding selective area electron diffraction (SAED) images shown beneath. Reproduced from Figure 7, Reference: Y. Fan, Q. Chen, et al. in press, Vol. 2, Issue 4, *Int. J. Nanomedicine* (2007) 81

Figure 6-13 Close up images (a) Sample B; (b) Sample C. Reproduced from Figure 8, Reference: Y. Fan, Q. Chen, et al. in press, Vol. 2, Issue 4, *Int. J. Nanomedicine* (2007) 81

Figure 7-1 (a) Characterization ofS2R+ cells: A, Morphology of cell. Many cells display broad circumferential lamellipodia; B. Protrusive activity (time-lapse sequence). Lamellipodium protrudes with regular and smooth outline. Dotted line shows the initial position of the cell edge. Time in min:sec. C. Actin cytoskeleton (phalloidin staining). Circumferential lamellipodium is rich in actin. D. Structural organization of lamellipodia; (b) Characterization of BG2 cells. A. Morphology of cell population. Cells display polarized lamella. B. Protrusive activity (time-lapse sequence). Leading edge moves forward by combination of filopodial (arrowheads) and lamellipodial protrusion. Dotted line shows the initial position of the cell edge. Time in min:sec. C. Actin cytoskeleton (phalloidin staining). D. Structural organization of lamellipodia. Images from reference [80] 85

Figure 7-2 Four target substrates (a) 2D: planar plastic coverslip; (b) NANS: Non-activated nanofibers; (c) SANS: surface-activated nanofibers, functionalized with amine group; (d) SANS + XL + D5/FGF-2: crosslinked and modified with D5 peptide or FGF-2 growth factor. 87

Figure 7-3 Histogram of surface roughness map for (a) NANS: unmodified nanofibers; (b) SANS + XL + FGF-2: crosslinked and FGF-2 modified nanofibers. AFM images of these two substrates are shown as the inside images, scan size: 5 μm. 88

Figure 7-4 Box plots of elasticity for two different nanofiber substrates SAN+XL+FGF-2 and NAN. The top images are AFM images of these nanofibers, scan size: 5 μm. Points shown as crosses on AFM images are the positions where force curves are collected to calculate elasticity. 89

Figure 7-5 In vivo astrocyte-capillary system: astrocytes are pointed by arrows in (a); FGF-2s are dots pointed by arrows in (b). S. Meiners, et al. UMDNJ 90

Figure 7-6 Repulsive regime versus attractive regime in Phase Imaging..... 91

Figure 7-7 Force distance curve showing the division between the two regimes, this curve was taken on a SANS+XL+FGF-2 nanofiber sample. 92

Figure 7-8 Characteristic morphologies of a-HSA antibody (a) phase attractive mode; (b) phase repulsive mode [81] 93

Figure 7-9 surface chemistry characteristics (a) height image of SANS+XL+ FGF-2, Z range for height image is 500 nm; (b) height image of NANS, Z range is 1000 nm; (c) phase image of SANS+XL+FGF-2 at repulsive mode, Z range is 75 °; (d) phase image of NANS at repulsive mode, Z range is 20 °; (e) phase image of SANS+XL+FGF-2 at attractive mode, Z range is 75 °; (f) phase image of NANS at attractive mode, Z range is 20 °. Image scan size is 1 μm. 95

Figure 7-10 Fibroblasts cultured on 2D surface. (a) Phase contrast microscopy of live cells, and (b) Optical microscopy of fixed cells indicate similar morphologies. Reproduced from Figure 1, Reference: Q. Chen, Y. Fan, et al, Mater. Res. Soc. Symp FF. Proc. (2007) 97

Figure 7-11 Fibroblasts cultured on amine coated nanofibers. (a) Phase contrast microscopy of live cells, and (b) Optical microscopy of fixed cells indicate similar morphologies. Reproduced from Figure 2, Reference: Q. Chen, Y. Fan, et al. Mater. Res. Soc. Symp FF. Proc. (2007) 97

Figure 7-12 AFM images of 3T3 NIH fibroblast cultured on 2D surface. (a) Deflection image of a typical fibroblast; (b) Close-up deflection image of top right region; (c) Close-up deflection image of top left region; (d) Close-up deflection image of bottom right region; (e) Height image of vertex region for another cell showing structures (close-up deflection image in inset). Reproduced from Figure 3, Reference: Q. Chen, Y. Fan, et al. Mater. Res. Soc. Symp FF. Proc. (2007) 98

Figure 7-13 3T3 NIH fibroblast cultured on amine coated nanofibers (SANS). (a) Multiple cell-cell interactions on the SANS are observed in the optical microscopy image. The cells in the black box are shown in close-up AFM images in (b) through (g). (b) through (d): increasing close-up AFM height images; (e) through (g): corresponding increasing close-up AFM deflection images. Reproduced from Figure 4, Reference: Q. Chen, Y. Fan, et al. Mater. Res. Soc. Symp FF. Proc. (2007)..... 99

Figure 7-14 Actin stain + Fluorescent Microscopy images of astrocytes on different substrate (a) astrocytes on 2D substrate imaged at 24 hours; (b) astrocytes on NANS at imaged 24 hours; (c) astrocytes on modified NANS imaged at 24 hours; (d) astrocytes on 2D substrate imaged at 48 hours; (e) astrocytes on NANS imaged at 48 hours; (f) astrocytes on modified NANS imaged at 48 hours..... 102

Figure 7-15 AFM images of astrocytes grown on different substrates for 24 hours (a) 2D substrate; (b) NANS; (c) modified NANS. Image scan size : 50 μm..... 103

Figure 8-1Polymer monomers (a) poly (methyl methacrylate), and (b) poly (ε-caprolactone). (c) Experimental configuration of electrospinning experiment.. 108

Figure 8-2 (a) Field emission SEM of PMMA-based carbon nanofibers and (b) atomic force microscopy of PMMA-based carbon nanofibers with 6% weight of single walled carbon nanotubes added. A 200 micron bore radius resulted in micron-scale

diameter nanofibers. Reproduced from Figure 2, Reference: Rutledge, S.L., Shaw, H. C., Benavides, J. B., Yowell, L. L., Chen, Q., Jacobs, B. W., Song, S. P., Ayres, V. M., Diamond and Related Materials, 2006. 15(4-8): p. 1070-1074 [84] 110

Figure 8-3 Field emission SEM of poly (ε-caprolactone) carbon nanofibers spun at bore radii (a) 152.4, (b) 254.0, and (c) 406.4 microns. As the bore size was increased, a slight increase in fiber diameter with a large decrease in bubble size was observed. Reproduced from Figure 3, Reference: Rutledge, S.L., Shaw, H. C., Benavides, J. B., Yowell, L. L., Chen, Q., Jacobs, B. W., Song, S. P., Ayres, V. M., Diamond and Related Materials, 2006. 15(4-8): p. 1070-1074 [84] 111

Figure 8-4 Mean force distance curves for three nanofibers samples electrospun with different bore radii and the aluminum foil. The mean force distance curve areas increased with increasing bore radius (insets), indicating a decrease in nanofiber elasticity with increasing bore radius. Reproduced from Figure 5, Reference: Rutledge, S.L., Shaw, H. C., Benavides, J. B., Yowell, L. L., Chen, Q., Jacobs, B. W., Song, S. P., Ayres, V. M., Diamond and Related Materials, 2006. 15(4-8): p. 1070-1074 [84] 112

Figure 10-1 Diagram of providing an automatic guide for tissue scaffold design 118

Figure 10-2 SEM images of nano circuits 119

Figure 10-3 Scanning scheme implementation for GaN anocircuit: (a) Image captured by standard SPM, the image side is 5 x 5 microns; (b) Scanning scheme simulation showing lines of the scan plan; (c) Real-time image captured by SPRM system using self-defined scanning scheme along the nanowire. Reproduced from Figure 4, Reference: B.W. Jacobs, V.M. Ayres, M.A. Tupta, R.E. Stallcup, A. Hartman, J.B. Halpern, M-Q. He, M.A. Crimp, A.D. Baczewski, N.V. Tram, Q. Chen, Y. Fan, S. Kumar, L. Udpa , 2006 6th IEEE Conference on Nanotechnology Proceedings ... 120

Figure 10-4 SPRM scan strategy to locate nanowire in nanocircuits (a) AFM images of nanocircuits, the arrow points to the nanowire; (b) simulation scan result shows locating the nanowire by following edges of nanocircuits. Image Size: 50μm. 121

INTRODUCTION

Scanning Probe Microscopy (SPM) is a newly emerging and powerful technique for nanoscale science in biology and medicine. Its great advantages are its direct investigative capability and its inherent resolution which easily and reliably reaches nanometer level, the precise scale for significant investigations of macromolecular biological units. SPM techniques can also function in a liquid ambient environment, which means that biological entities can be investigated under nearly life-like conditions [1-3].

But SPM has limitations in several aspects. One of them is the relatively slow rate of scanning during SPM imaging. It usually takes several minutes to generate a typical image. Another is the heavy dependence on an expert human both as an operator and as an image interpreter. Still another set of issues comes from imaging artifacts.

Our research group designed and developed Scanning Probe Recognition Microscopy (SPRM) system in partnership with Veeco Instruments, which integrates recognition ability into the SPM system to allow the SPM system to automatically track specific regions of interest. Also, additional powerful functionalities are also integrated into the SPRM system, including feature recognition, object classification, auto-tracking and property analysis abilities. Different functionalities can be realized by operating in online or offline modes. Therefore, in addition to saving operation time, SPRM has the advantages of providing more meaningful information about samples automatically, efficiently and accurately. The power of SPRM allows the investigation of many situations in which standard SPM is insufficient.

The candidates' original research contributions to the development of SPRM are as

follows. One major contribution has been development of a set of recognition strategies that provide mathematical criteria that guides the auto-tracking. The recognition strategies are grounded on the imaging processing concept of feature definition. A feature is any relevant aspect of a system. It must be probable of precise mathematical definition in terms of a test criterion. The candidate's contribution is to define the first set of features within Scanning Probe Microscope data. These features were then used as part of the feedback loop which guided the auto-tracking implementation. Another major contribution by the candidate was the first adaptation of SPRM for investigation of a significant nanobiomedical problem, analyzing nanoscale 3D cues for spinal cord repair research. The candidate also made significant contributions to the development of the auto-tracking implementation, and to material properties analyses.

The dissertation is divided into three parts. In the first part, the main focus is the instrumentation design and development of the new Scanning Probe Recognition Microscopy capability. The second part focuses on the successful application of SPRM system in analyzing nanoscale 3D cues for spinal cord repair research. The third part summaries the conclusions from the present research and identifies the future work.

In the instrumentation part: the first chapter introduces the commonly used imaging techniques to set both SPM and the new SPRM within the context of techniques used for nanoscale investigations, and particularly for nanobiological investigation. Then the fundamentals of SPM, which is the base instrument of SPRM, are addressed in chapter 2. Chapter 2 discusses the fundamental elements of SPM, its advantages, its limitations and the current start of art. Chapter 3 discusses the new functionalities built in SPRM and the basic design and development of SPRM and how these address issues in SPM.

In the second part, the main focus is using SPRM to investigate a very important research topic: spinal cord repair. In Chapter 4, motivation and background of SPRM in spinal cord repair are addressed. Chapter 5 discusses the auto-tracking ability of SPRM which enables the system to scan only on individual nanofibers within the tissue scaffolds used for regenerative medicine, thereby, collecting the first accurate nanofiber properties analyses. In Chapter 6, the topographic, mechanical and chemical properties of nanofibers which influence neural cell attachment are addressed and analysis of these properties are done by using SPRM. Cell responses to different substrates are explored and compared in Chapter 7. Chapter 8 discussed the correlation of electronspinning parameters with nanofiber properties analysis. The last part of this dissertation summarizes the conclusions reached from the candidate's research, along with discussion of the future research directions.

Part I SPRM

Instrumentation Development

Part I SPRM INSTRUMENTATION DEVELOPMENT

A new SPM-based technique, Scanning Probe Recognition Microscopy (SPRM), is presented in this dissertation. The new SPRM system improves several aspects of SPM, including speed, accuracy and flexibility. Also, the SPRM system enables the investigation of situations in which SPM is insufficient. SPRM will be an outstanding new tool in the multiple research fields that need nanoscale investigation with SPM techniques.

Nanobiology especially needs techniques that can provide direct observation and analysis of phenomenon at the nanoscale. SPRM has the potential to be widely used in experimental nanobiology. The development of SPRM for applications in nanobiology is multidisciplinary in two respects. One is the development of the new SPRM capability within the overall field of scanning probe microscopy. Another is to set both SPM and the new SPRM within the context of experimental techniques used in nanobiological investigations. As the current state of art techniques used in nanobiology are also those used in nanotechnology in general, discussion of these provides a setting for the development of SPM as well as SPRM. Therefore, the experimental techniques used in nanobiology will be discussed first, followed by discussion of SPM and finally by the discussion of the development of SPRM.

Therefore, the first part of dissertation focuses on the development of the SPRM system. It starts from the most commonly used experimental imaging tools in current nanobiology researches. Then SPM techniques are introduced, the advantages and limitations of SPM are emphasized, and the latest research works to improve SPM

performance are addressed. Finally, the design and development of the new SPRM system are discussed in detail to enhance the performance of SPM.

CHAPTER 1

1 IMAGING TECHNIQUES USED IN NANOBIOLOGY

The present SPRM system is successfully used to investigate many research topics in nanobiological field. Therefore, a survey of imaging techniques commonly used to investigate nanobiological phenomenon is addressed and comparisons between them are also discussed.

1.1 Optical Microscopies

(1) Phase contrast microscopy

Phase contrast microscopy is an optical microscopy illumination technique in which small phase shifts in the light passing through a transparent specimen are converted into amplitude or contrast changes in the image [4]. It is preferable used to bright field microscopy to provide contrast of transparent specimens such as living cells or small organisms.

(2) Fluorescence microscopy

Fluorescence microscopy is an optical microscopy technique used to study the properties of specimens using the phenomena of fluorescence and phosphorescence in addition to reflection and absorption. It is one of the most ubiquitous tools in biomedical laboratories. In fluorescence microscopy, the sample under investigation becomes itself the light source. The fluorescence microscopy is based on the phenomenon that certain material emits energy detectable as visible light when irradiated with the light of a specific wavelength. The sample can either be fluorescing in its natural form like chlorophyll and some minerals, or treated with fluorescing chemicals. Fluorescence

microscopy has 3 strengths. First, it has high biological specificity. Second, it is highly sensitive in the imaging of cells and tissues. The exquisite sensitivity and image contrast allows biological structures to be imaged on the submicron length scale. Third, it is a minimally invasive imaging technique, which gives it the ability to study biological structure and function in vivo[5].

But in a thick sample, the signals from multiple sample places are integrated to form the final image. Since there is little correlation between the structures at different depths, the final image becomes fuzzy.

Fluorescence microscopy can be implemented in other more advanced configurations to enable novel imaging modes. Two particularly important configurations, confocal microscopy and two-photon microscopy, are discussed.

(3) Confocal microscopy

Confocal microscopy is an optical imaging technique that can obtain 3D sections in thick specimens by using a spatial pinhole to eliminate out-of-focus light or "flare" in specimens that are thicker than the focal plane. It achieves blur-free images of thick specimens at various depths, at the cost of obtaining fluorescence signal from only a single point in the specimen.

There has been a tremendous explosion in the popularity of confocal microscopy in recent years, due in part to the relative ease with which extremely high-quality images can be obtained from specimens prepared for conventional fluorescence microscopy. It has been used extensively to investigate microstructures in cells and in the imaging of tissues[6].

In laser scanning confocal microscopy, a fluorescent specimen is illuminated by a

point laser source, and each volume element is associated with a discrete fluorescence intensity. Laser scanning confocal microscopy offers several advantages over conventional fluorescence microscopy including controllable depth of field, the elimination of image degrading out-of-focus information. The primary advantage is the ability to serially produce thin optical sections through fluorescent specimens that have a thickness ranging up to 50 μm or more[7]. Advances in confocal microscopy have made possible multidimensional views of living cells and tissues that include image information in the x, y and z dimensions as a function of time and presented in multiple colors (using two or more fluorophores). The disadvantages of confocal microscopy are primarily the limited number of excitation wavelengths available with common lasers, which occurs over very narrow bands and are expensive to produce in the UV region. Another downside is the harmful nature of high intensity laser irradiation to living cells and tissues. Finally the best spatial resolution obtained to date is on the order of 400 nm, which is still too large to explore macromolecular resolution processes which have 1-10 nm resolution requirement.

(4) Two-photon microscopy

Two-photon microscopy is an alternative to confocal microscopy for the 3D imaging of thick specimens. Two-photon microscopy uses non-linear absorption of two photons to induce fluorescence that is confined to a very small region. A laser beam is scanned laterally across the sample to generate 2D fluorescence images from an extremely thin optical section within the sample. This optical section can be varied in depth, building up a stack of images to produce a 3D rendering the sample. An excellent demonstration of the ability of two-photon imaging for deep tissue imaging is in the neurobiology area[8].

The major advantage of two-photon microscopy is its ability to permit high-resolution and high-contrast imaging from deep within intact living tissue. Two-photon microscopy is particularly useful for live imaging of thick samples because it has less photodamage compared with confocal microscopy. Since two-photon microscopy obtains 3D resolution by the limitation of the region of excitation instead of the region of detection as in a confocal system, photodamage of biological specimens is restricted to the focal point. Photodamage at the focal plane will still occur, as with the confocal, but there isn't damage above and below the plane of focus. The disadvantages of two-photon microscopy lie in the following aspects: Pulsed lasers are generally much more expensive; the microscope requires special optics to withstand the intense pulses; the two-photon absorption spectrum of a molecule may vary significantly from its one-photon counterpart; and wavelengths greater than 1400 nm may be significantly absorbed by the water in living tissue. Finally the best obtained two-photon microscopy resolution to date is on the order of 50 nm which is still above the desired 1-10nm resolution.

1.2 Electron Microscopies

The transmission electron microscope (TEM) operates on the same basic principles as the light microscope but uses the quantum wavelike nature of electrons instead of light pass through the object. It is an imaging technique whereby a beam of electrons is transmitted through a specimen, then an image is formed, magnified and directed to appear. In TEM, electrons are focused by two or more electron lenses to form a greatly magnified image onto photographic film or a charge coupled device camera. The image produced by TEM is 2D and the brightness of a particular region of the image is proportional to the number of electrons that are transmitted through the specimen at that

position on the image. The resolution of light microscope is limited by the wavelength of light. Since "light source" of TEM is electrons. The resolution of a TEM is limited by the electron wavelength: $\lambda = \frac{h}{p}$, where h = Plank's constant 6.6×10^{-34} $(J \cdot s)$ and p is the electron's momentum. Because the electrons wavelengths are much shorter than optical wavelengths, it is possible for TEM to get a much higher resolution. The resolution of a TEM easily reaches the Angstrom (10^{-10} m) level.

In nanobiology, the TEM excels as a diagnostic tool with respect to the detection and identification of both abnormal tissue anatomy and the pathogens responsible for the disease [9]. The key problem in the use of TEM for nanobiology investigations is the sample preparation. The specimens must be very thin and able to withstand the high vacuum present inside the instrument. Biological specimens must be frozen, sectioned while frozen into electron transparent slice around 10 nm thick, coated with a thin around 10 nm conductive film of gold and imaged in Cryo-TEM that maintains the biological tissues in its frozen state. Therefore, there is always the question of how well the TM section represents the living state. Also the field of view is relatively small, raising the possibility that the region analyzed may not be characteristic of the whole sample. There is also the potential that the frozen sample may be damaged by the electron beam.

The latest advancement in electron microscopy is 3D reconstruction of cellular components at a resolution that is on the order of magnitude of atomic structures. The method for reconstruction of 3D images of single, transparent objects recorded by TEM is called electron tomography (ET). With improvements in instrumentation, data collection methods and techniques for computation, ET may become a preferred method for imaging isolated organelles and small cells [10]. Its resolution is excellent. Its main

disadvantages are that the sectioned and coated biological specimens do not ideally represent the dynamic living state, and that, as discussed, the sample preparation and instrumentation requirement is intensive.

1.3 Brief Introduction of Scanning Probe Microscopy in Biology and Medicine

The family of Scanning Probe Microscopy techniques has revolutionized studies of nanostructures. The key capability of SPM is that, through a controlled combination of feedback loops, detectors and piezoelectric actuation, it enables direct investigations of atomic to nanometer scale phenomena. A key difference between scanning probe and optical microscopies is that in scanning probe microscopies, a tip is in actual direct interaction with a nanoscale object rather than viewing its image. The SPM record for contributions in nanobiology and medicine includes an impressive number of firsts: the first direct observations of DNA and RNA by atomic force microscopy [11], the first direct investigations of receptor sites by atomic force microscopy [2, 12], the first direct investigations of cellular water pore sites by atomic force microscopy [13, 14] , the first direct investigations of ion channels by atomic force microscopy [15], the first direct investigations of ligand docking by functionalized tip atomic force microscopy [16], atomic force microscope investigations of surface and submembranous structures on living cells [17, 18] including cancer cells [19-21], the first direct investigations of the binding of fluorescently conjugated lectins to cell surface glycoproteins by near-field optical microscopy [22], and many more important first direct studies.

Atomic Force Microscopy (AFM) is one of the most widely used techniques in SPM family. It was developed specifically for nanoscale investigations of biological samples, which are largely nonconductive [23]. It has been successfully used to image many

biological samples ranging from genetic material to cells to bone [24].

Studies can be done under physiological conditions in AFM allow us to image biological processes [25]. Studies can also be performed at the macromolecular level of resolution. For example, AFM images of transcription complexes have been obtained of RNA polymerase in complex with DNA [26]. Such studies detailing the structure-function relationship of transcription process are key in furthering understanding of gene expression.

AFM can also be operated in force scan mode, which allows for the measurement of adhesion forces between receptors and their corresponding binding partners, or ligands [27]. It can also serve as a microindenter that probes cells revealing information about their mechanical properties. The mechanical properties of cells play an important role in such essential physiological processes such as cell migration and cell division [28].

Scanning tunneling microscopy (STM) has the highest resolution of all SPM family. It is highly desirable for use in investigation of molecular biology and medicine [29]. DNA and RNA structures have been successfully investigated by using STM [30].

The above examples document why SPM is emerging as a powerful tool for investigations in nanobiology and medicine. The drawbacks that limit the widespread use of SPM in nanobiology, and therefore the new biomedical knowledge that it could generate, are those previously given: slow scan speed, imaging artifacts and dependence on an expert human operator. A detailed discussion of SPM operation and the root causes of its drawbacks are given in Chapter 2.

CHAPTER 2

2 SCANNING PROBE MICROSCOPY IMAGING TECHNIQUES

2.1 Fundamentals of SPM

Scanning Probe Microscopy (SPM) is emerging as a powerful technique for nanoscale science in biology and medicine because it provides direct real-time information at the nanoscale with in-vitro level sample preparation. It can be used as an imaging device, which allows for the acquisition of atomic-level images of biological structures as well as to measure forces of interactions between two opposing surfaces down to the single-molecule level. Its great advantages are its direct investigative capability and its inherent resolution which easily and reliably reaches the nanometer level, the precise scale for significant investigations of biological units. Therefore, SPM resolution exceeds that of the optical techniques and reaches the correct level, and SPM sample preparation is much less drastic than that required by the electron microscopy techniques. SPM techniques can be operate in air, liquid or vacuum environment, which means that biological entities can be investigated under nearly life-like conditions. In addition to its use as an imaging technique, SPM can also be used as an interactive device as shown in investigations of receptor-ligand binding. The interactive capabilities of SPM are just beginning to be recognized and exploited.

Scanning Probe Microscopy (SPM) is a branch of microscopy that forms images of surfaces using a sharp probe in near-field interaction with the surface to scan the specimen. An image of the surface is obtained by mechanically moving the probe in a raster scan of the specimen, line by line, and recording the probe-surface interaction as a

function of position. The SPM family includes Scanning Tunneling Microscopy (STM), Atomic Force Microscopy (AFM), Near-Field Scanning Optical Microscopy (NSOM) and others. STM was developed in the early 1980's. The significance of its invention was recognized by the award of the Nobel Prize in Physics in 1986 [31], one of only four such awards given for the development of a revolutionary new instrument. This invention was quickly followed by the development of other techniques in SPM family. AFM is one of the most important later techniques. Despite the number of types of SPM and modes in which they can be operated, the underlying operation is the same for them all. A sharp probe undergoes a near-field interaction with a sample surface during a piezoelectric raster-motion scan of the surface, thereby producing a map of the interaction. Each different type of SPM is characterized by the nature of the local probe and its interaction with the sample surface. The inherent resolution is atomic level for STM and nanometer level for AFM.

However, SPM has several limitations. The speed of SPM imaging is one key limitation. In most SPM techniques, a sharp tip is scanned across a sample to image its topography and material properties. It typically takes 1 to 100 minutes to obtain a high-quality image. The use of SPM would increase dramatically if the speed of SPM could match that of other scanning microscopes such as confocal and scanning electron microscopes. Moreover, there are many experiments, such as watching biological processes that simply cannot be done without faster imaging.

SPM is human operator intensive and a long learning curve is required to become truly expert operator. Insufficient instruments and teachers create a cycle of limited use of a powerful capability.

2.1.1 Block diagram

The research work presented in this dissertation is mainly based on AFM, but it can be extended to all the SPM family easily. Therefore, AFM is discussed in detail as a typical rather than a specific example. The block diagram of AFM is shown in Figure 2-1.

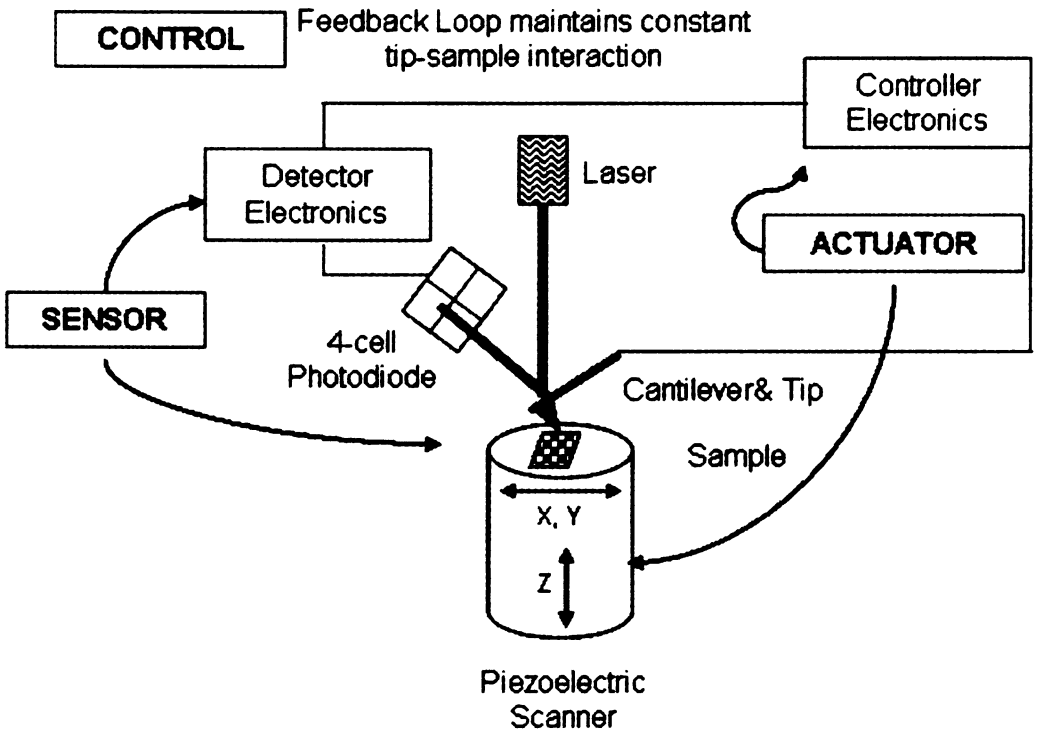

Figure 2-1 Block diagram of Atomic Force Microscopy

(1) Cantilever & tip

The AFM consists of a microscale cantilever with a sharp tip (probe) at its end that is used to scan the specimen surface. The cantilever is typically silicon or silicon nitride with a tip radius of curvature on the order of nanometers. When the tip is brought into proximity of a sample surface, forces between the tip and the sample lead to a deflection of the cantilever according to Hooke's law. Depending on the situation, forces that are measured in AFM include ion-ion repulsive forces, Van der Waals forces, capillary forces, chemical

bonding, electrostatic forces, Casimir forces, solvation forces etc. The cantilever should have a small spring constant, and the tip should have a radius of curvature less than 20~50nm and a cone angle between 10~20 degree. Material used to make AFM tips are usually Silicon and Silicon Nitride for hardness greater than the majority of sample surfaces, and for ease of fabrication using standard semiconductor industry micromachine

(2) Sensor & photodiode

Typically, the deflection of cantilever is measured using a laser spot reflected from the top of the cantilever into a four-cell (quad) photodiode. The four elements of the quad photodiode (position sensitive detector) are combined to provide different information depending on the operating mode. The amplified differential signal between the top two elements and the two bottom elements provides a measure of the deflection of the cantilever. In this way, the photodiodes can detect the movement of the beam, and therefore the movement of the cantilever and tip. The vertical movement of the tip is thereby measured as a voltage change.

(3) Scanner

Traditionally, the sample is mounted on a piezoelectric scanner, which can move the sample in the z direction for maintaining a constant force by receiving signal from feedback control unit, and the x and y directions for scanning the sample. The scanners are made from piezoelectric material, which expands and contracts proportionally to an applied voltage. The scanner is constructed by combining independently operated piezo electrodes for X, Y and Z into a single tube, forming a scanner which can manipulate samples with extreme precision in 3 dimensions.

Table 2-1 Multimode SPM Scanner Specifications [32]

Model	Scan Size	Vertical Range
AS-0.5 ("A")	0.4μmx0.4μm	0.4μm
AS-12 ("E")	10μmx10μm	2.5μm
AS-12V("E" vertical)	10μmx10μm	2.5μm
AS-130("J")	125μmx125μm	5.0μm
AS-130V("J" vertical)	125μmx125μm	5.0μm
AS-200	200μmx200μm	8.0μm

(4)Feedback control

If the tip were scanned at a constant height, there would be a risk that the tip would collide with the surface, causing damage. Hence, in most cases a feedback mechanism is employed to adjust the tip-to-sample distance to maintain a constant relationship between the tip and the sample. The type of relationship kept constant depends on the mode of operation. The feedback control unit takes its input from the sensor and yield an output to the scanner that maintains a fixed tip-sample interaction.

2.1.2 Operation modes

The AFM can be operated in a number of modes [33], depending on the requirements of applications. Different operation modes have different force of interaction between the tip and sample surface as shown in Table 2-2. The most commonly used operation modes are contact mode and tapping mode.

Table 2-2 Operation Modes of AFM

Mode of Operation	Force of Interaction
contact mode	strong (repulsive) - constant force or constant distance
non-contact mode	weak (attractive) - vibrating probe
tapping mode	strong (repulsive) - vibrating probe
lateral force mode	frictional forces exert a torque on the scanning cantilever

Contact AFM measures topography by sliding the probe's tip across the sample surface. It can be operated in both air and fluids. It can have relatively high scan rate (throughput). Rough samples with extreme changes in vertical topography can sometimes be scanned more easily in Contact mode. However, Lateral (shear) forces may distort features in the image. The forces normal to the tip-sample interaction can be high in air due to capillary forces from the adsorbed fluid layer on the sample surface. The combination of lateral forces and high normal forces can result in reduced spatial resolution and may damage soft samples (i.e., biological samples, polymers, silicon) due to scraping between the tip and the sample.

Tapping Mode™ AFM measures topography by tapping the surface with an oscillating tip. This eliminates shear forces, which can damage soft samples and reduce image resolution. Therefore, soft samples can be imaged and image resolution can be improved by using Tapping Mode. Tapping Mode is available in air and fluids too. It has relatively higher lateral resolution on most samples (1 nm to 5 nm), lower forces and less damage to soft samples imaged in air. Lateral forces are virtually eliminated, so there is no scraping. However, it has slightly slower scan rate than contact mode AFM.

2.2 Advantages and Limitations of SPM

2.2.1 Advantages

The SPM has several advantages over the scanning electron microscope (SEM). Unlike the electron microscope which provides a two-dimensional projection or a two-dimensional image of a sample, the SPM provides a true three-dimensional surface profile[34].

Additionally, samples viewed by SPM do not require any special treatments (such as metal/carbon coatings) that would irreversibly change or damage the sample. While an electron microscope needs an expensive vacuum environment for proper operation, most SPM modes can work perfectly well in ambient air or even a liquid environment. This makes it possible to study biological macromolecules and even living organisms.

In principle, SPM can provide higher resolution than SEM. It has been shown to give true atomic resolution in ultra-high vacuum (UHV). UHV AFM is comparable in resolution to Scanning Tunneling Microscopy and Transmission Electron Microscopy.

2.2.2 Limitations

A disadvantage of SPM compared with the scanning electron microscope (SEM) is the image size. The SEM can image an area on the order of millimeters by millimeters with a depth of field on the order of millimeters. The SPM can only image a maximum height on the order of 10 micrometers. While a 12 inch water scan area capability has been developed to serve the semiconductor fabrication community. The wide scan area is paid for by a loss of resolution. SPM as it was developed was intended for high resolution imaging of a nanoscale representative area.

Nonlinearity issue of piezo is also a problem. Nonlinearity means that when a linear voltage ramp is applied to piezo, the peizo moves in a nonlinear motion. It will introduce artifacts SPM images.

Another inconvenience is that at high resolution, the quality of an image is limited by the radius of curvature of the probe tip, and an incorrect choice of tip for the required resolution can lead to image artifacts, as can any tip damage that occurs while scanning.

SPM can not scan images as fast as an SEM, requiring several minutes for a typical scan, while an SEM is capable of scanning at near real-time after the chamber is evacuated. The relatively slow rate of scanning during SPM imaging often leads to thermal drift in the image, making the SPM microscope less suited for measuring accurate distances between artifacts on the image.

SPM images can be affected by hysteresis of the piezoelectric material and cross-talk between the (x,y,z) axes that may require software enhancement and filtering. Such filtering can "flatten" out real topographical features.

2.3 Improvement of SPM Start of Art

SPM speed is limited by the slowest components in its entire control loop. High-speed AFM techniques developed to improve the speed [35] are an active research area. Improvement of scanning speed has been made by using smaller cantilevers[36], faster scanners[37] and better controllers[38, 39] [40].

In an independent but related development by the Veeco co-principal investigator of the present project. Veeco's new Easy-AFM offers ability to automatically adjust scan parameters by choosing scan parameters which make new parameter-based feedback loops more stable. The scan rate can be increase when the feedback loop is stabilized.

Therefore, Easy-AFM reduces the time for initial setup and adjustment of parameters, enabling a faster path to sophisticated, high-quality images[41]. Easy-AFM was developed with integration with SPRM in mind.

CHAPTER 3

3 SCANNING PROBE RECOGNITION MICROSCOPY

Our research group designed and developed the Scanning Probe Recognition Microscopy in partnership with Veeco Instruments. Scanning Probe Recognition Microscopy integrates recognition ability in Scanning Probe Microscopy to allow us to adaptively follow and investigate specific regions of interest. Therefore, The SPM system itself is given the ability to auto-focus on regions of interest through incorporation of recognition-based tip control. The recognition capability is realized using techniques in pattern recognition and image processing fields. Adaptive learning and prediction are also implemented to make detection and recognition procedures quicker and more reliable. The new SPRM system has the advantages of saving operation time, providing powerful feature/property analysis ability etc. The powerful functionalities of the new SPRM system will be explained in detail in the following section.

The candidate's contribution is to define the first set of features within Scanning Probe Microscope data. These features were then used as part of the feedback loop which guided the auto-tracking implementation. Another major contribution by the candidate was the first adaptation of SPRM for investigation of a significant nanobiomedical problem, analyzing nanoscale 3D cues for spinal cord repair research. The candidate also made significant contributions to the development of the auto-tracking implementation, and to material properties analyses.

3.1 SPRM System Functionalities

3.1.1 Recognition ability

The new SPRM system can recognize operator defined features of samples under observation, such as edge, shape and so on. This is paradigm shift from the operator defining scanning parameters to the operator defining significant aspects of their problems in the term of features. The recognition ability gives the new SPRM system the power to automatically recognize different types of objects and classify them into groups based on given prior information. SPRM will increase ease of use and work efficiency at the same time.

3.1.2 Auto-tracking capability and region of interest

Based on the recognition capability of the SPRM, auto-tracking capability is built into the SPRM system by combining adaptive learning and prediction techniques. Therefore, the SPRM system is able to automatically scan while focused on only the region of interest instead of raster scanning the whole scan region which includes the background as well as the region of interest. It is very useful especially when the interested regions are sparse on the whole scan region, such as cells on substrate. With SPRM, dramatic operation time can be saved and only meaningful information about the interested region is extracted at the same time of scanning.

3.1.3 Real-time result display capability

The SPRM system provides a real-time scan result display, the same as a standard SPM. The ability enables users to know the scan result in real-time. Then users are able to adjust parameters in real-time according to the displayed scan result. Auto-adjustment

of scan parameters has also been implemented by the Veeco Co-Principal Investigator, Veeco "Easy-AFM" ™ .

3.1.4 Property analysis capability

Combined with auto-tracking capability, the SPRM system has the ability to automatically analyze important properties of objects on sample surface, such as surface roughness, elasticity, etc. In a standard SPM, this would involve manually applied repetitive work which is very time consuming. Also a human operator applied probe may actually access a region of unreliable data points. The new SPRM system has the obvious advantages in convenience, efficiency and accuracy.

3.2 SPRM Prototype System Structure

The Scanning Probe Recognition Microscopy system is built based on standard Scanning Probe Microscopy, its block diagram is shown in the Figure 3-1. Compared with standard SPM setting, the new SPRM system adds Signal Access Module [42], a second computer and embeds new algorithms into the standard SPM computer.

The new SPRM system can get the real-time analog signals from standard SPM through Signal Access Module (SAM). Signals from different ports of SAM include multiple information: height of sample surface, cantilever deflection, and so on. The SPRM software embedded in the controller also sends control signals to Signal Access Module to assist real-time scan result display. All these signals are sampled by an A/D card installed on the second computer. Scan results are displayed in real-time in the second computer by analyzing these sampled signals.

The key recognition and implementation elements are software embedded inside the Veeco SPM controller. The module labeled "SPRM scan plan generation" automatically

generate scan plan in real-time in order to auto-track the region of interest. The scan plan is generated and updated in real-time, and the system has the adaptive learning ability based on previous information.

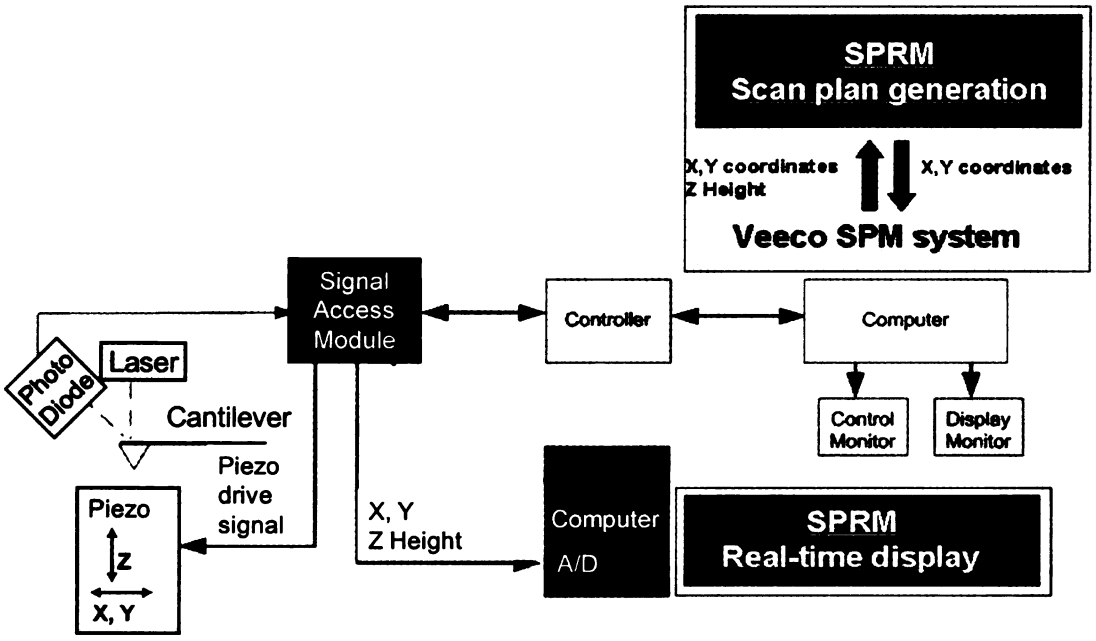

Figure 3-1 Block diagram of Scanning Probe Recognition Microscopy

3.3 SPRM System Design & Software Development

The Scanning Probe Recognition Microscopy software is divided into two parts. One part is embedded in the main SPM controller to generate real-time SPRM scan plan. The other part is responsible for analog signal sampling, data processing and real-time scan result display on the second computer. Object oriented design is used in software design of the first part. There are mainly 6 classes as shown in Figure 3-2.

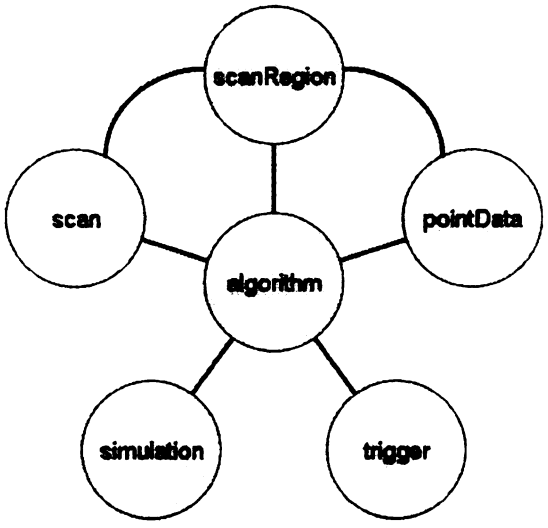

Figure 3-2 Software design diagram

The *algorithm* class includes all algorithms used in SPRM system. It is the key part of the system. It needs to communicate with all other parts.

The *scan* class has the interface with the SPM system to control the parameters associated with scan and to control the real movement of tip.

The *pointData* class defines the information at a single point.

The *scanRegion* class stores information of the scan region.

The *simulation* class enables the software to be run under simulation mode instead of run under real SPM. It is a helpful tool for debugging and testing of the system.

The *trigger* class provides the interface to Signal Access Module of Scanning Probe Microscopy. It makes the analog signal output possible.

The second part of the SPRM software to display real-time scan results is developed by Matlab. The DI sampling card is used in sampling real-time analog signals from Signal Access Module.

3.4 SPRM Recognition Algorithm

Many different algorithms are used in implementation of Scanning Probe Recognition Microscopy. Based on different applications, there are specific algorithms that showed the best recognition results. But there are some common techniques which can be applied to recognize most of observation targets and produce promising results.

The overall recognition/classification procedure consists of three steps as depicted in Figure 3-3.

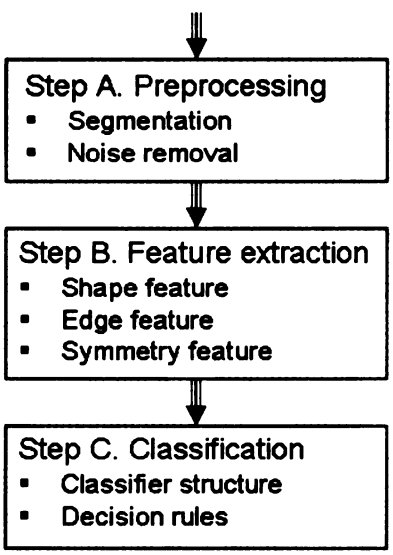

Figure 3-3 Schematic of overall approach. Reproduced from Figure 2, Reference: Q. Chen, Y. Fan, L. Udpa, and V.M. Ayres, Vol. 2, Issue 2, pp. 181-189, Int. J. Nanomedicine (2007)

3.4.1 Preprocessing: Wavelet-based image segmentation

The idea in using wavelet-based multi-resolution analysis is to detect the edges of the target objects. After the edges of target objects are successfully detected, it will be much easier to segment the region of the target objects from the background by calculating the boundary box of the target objects.

Since wavelet analysis is multi-resolution analysis, it is very useful in detecting

edges under different levels of scale. A remarkable property of the wavelet transform is its ability to characterize the local regularity of functions. For an image $f(x,y)$, its edges correspond to singularities, and thus are related to the local maxima of the wavelet transform modulus. Therefore, the wavelet transform is an effective method for edge detection [43].

Two wavelets are respectively the partial derivative along x and y of a 2D smoothing function $\theta(x,y)$.

$$\psi^1(x,y) = \frac{\partial\theta(x,y)}{\partial x} \qquad \textbf{3-1}$$

$$\psi^2(x,y) = \frac{\partial\theta(x,y)}{\partial y} \qquad \textbf{3-2}$$

Let

$$\psi_s^1(x,y) = \frac{1}{s^2}\psi^1(\frac{x}{s},\frac{y}{s}) \qquad \textbf{3-3}$$

$$\psi_s^2(x,y) = \frac{1}{s^2}\psi^2(\frac{x}{s},\frac{y}{s}) \qquad \textbf{3-4}$$

For any image $f(x,y)$, the wavelet transform has two components: $W^1 f(s,x,y) = f * \psi_s^1(x,y)$ and $W^2 f(s,x,y) = f * \psi_s^2(x,y)$, the two components of the wavelet transform are the coordinates of the gradient vector of $f(x,y)$ smoothed by $\theta_s(x,y)$ at scale s.

$$Mf(s,x,y) = \sqrt{\left|W^1 f(s,x,y)\right|^2 + \left|W^2 f(s,x,y)\right|^2} \qquad \textbf{3-5}$$

$Mf(s,x,y)$ is called the modulus of the wavelet transform at the scale s.

$$Af(s,x,y) = \arg\tan(\frac{W^1 f(s,x,y)}{W^2 f(s,x,y)}) \qquad 3\text{-}6$$

$Af(s,x,y)$ is the angle between the gradient vector and the horizontal. At each scale, the edge points are the points (x,y) where the modulus image $Mf(s,x,y)$ is local maximum along the gradient direction given by $Af(s,x,y)$.

This edge detection method is used on an AFM image of cell grown on nanofiber tissue scaffolding. The soothing function to construct wavelets is chosen to be Gaussian function because it has good property of decreasing noise.

(a) (b) (c)

Figure 3-4 Edge detection based on wavelets (a) original image, (b) edge image when scale = 2, (c) edge image when scale = 10

From the edge images, it is clear that when the scale parameter is chosen appropriately, we can detect the edges of the target object, which is the cell in this figure.

The points on the edge image are still broken. We can use dilation operation to connect those edge points. But there are still some noise points on the edge image. Since these noise points have relatively small area compared with the edge points, a filter is designed to count the area of the connected points and then threshold in order to remove those noise points. Finally, the bounding box of the edge points is the boundary of the cell.

Therefore, the cell is successfully segmented as shown in Figure3-5.

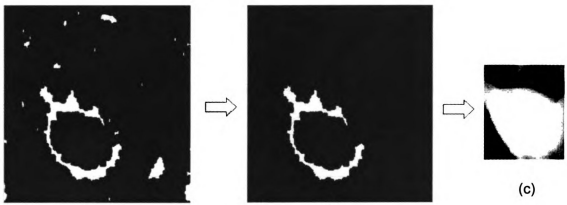

Figure3-5 Segmentation (a) the edge image after dilation, (b) the edge image after threshold, (c) the segmented object

3.4.2 Feature detection

The choice of discriminating properties as features is a key issue to any classifier being successful. Most biological objects have their own shape. We define the shape feature using moments-based methods and give an application of using shape feature to distinguish cells from fibers. Another feature we found important is the edge feature. Many nanobiological objects have inside structure, like nucleus of cells. Therefore, those objects will have both inside edges and outside edges. Therefore, edge enhancement method is used and then edge information is extracted as a feature to represent different inside structures.

3.4.2.1 Shape feature

Moment-based methods may be used to determine a feature representing[44]. A Shape Feature was defined as the ratio of second moments along the major axis ($M_{\min}$) and minor axis ($M_{\max}$):

$$ratio = \frac{M_{\max}}{M_{\min}} \qquad \textbf{3-7}$$

The Shape Feature defined in Equation above has the properties of translation, scale and rotation invariance.

The nuclei of the two kinds of cells have different shapes. The differences in the shape can be quantified by calculating the second moment along the major and minor axes of the image which are orthogonal to each other. The major axis is found using Equation below.

$$\theta = \arctan\left(\frac{2M_{xy}}{M_{xx} - M_{yy} + \sqrt{(M_{xx} - M_{yy})^2 + (2M_{xy})^2}}\right) \qquad \textbf{3-8}$$

Where

$$M_{xx} = \sum_x \sum_y (x - \bar{x})^2 f(x, y) \qquad \textbf{3-9}$$

$$M_{yy} = \sum_x \sum_y (y - \bar{y})^2 f(x, y) \qquad \textbf{3-10}$$

$$M_{xy} = \sum_x \sum_y (x - \bar{x})(y - \bar{y}) f(x, y) \qquad \textbf{3-11}$$

The second moment along the major axis can be calculated using the following equation.

$$M_{\min} = \sum_x \sum_y [(x - \bar{x})\sin\theta - (y - \bar{y})\cos\theta]^2 \qquad \textbf{3-12}$$

The second moment along the minor axis can be calculated using the orthogonality property by the following equation.

$$M_{\max} = \sum_x \sum_y \left[(x - \bar{x})\sin(\theta + 90^\circ) - (y - \bar{y})\cos(\theta + 90^\circ)\right]^2 \qquad \textbf{3-13}$$

3.4.2.2 Boundary enhancement & Edge feature

A continuous wavelet transform is a scale based two-dimensional transformation that allows multiscale/multiresolution analysis of images. The transformed data set $W(\sigma,\tau_1,\tau_2)$ is given by:

$$W(\sigma,\tau_1,\tau_2)=\frac{1}{\sigma}\iint f(x,y)\psi^*(\frac{x-\tau_1}{\sigma},\frac{y-\tau_2}{\sigma})dxdy \qquad \textbf{3-14}$$

Where σ is the scale parameter, τ_1,τ_2 are the translation parameters, * denotes the complex conjugation, and ψ is the generating wavelet function. The scale parameter σ plays a crucial role. Wavelet transforms process data at different scales or resolutions. At each scale it computes the similarity of the image data with the wavelet kernel at the selected scale σ. At large scales, the transform coefficients $W(\sigma,\tau_1,\tau_2)$ are dominant for data from objects in the image which correspond with the larger scale wavelet kernel. Similarly, for small scales, small features are highlighted in the $W(\sigma,\tau_1,\tau_2)$ transform domain. By choosing the appropriate scale, we can get the relevant details from the images that are necessary to perform a particular recognition task across multiple scales.

The multiscale analysis procedure begins by defining a family of functions of varying scales, expressed as

$$\hat{\psi}(\sigma,x,y)=\frac{1}{\left\|\varphi(\frac{x^2+y^2}{\sigma})\right\|}\varphi(\frac{x^2+y^2}{\sigma}) \qquad \textbf{3-15}$$

where φ is a function used for systematic generation of images of slowly varying scale σ. A Gaussian is a commonly used function whose scale is determined by the variance σ. A multiscale edge detector can be derived from the spatial derivatives of φ.

Edges associated with abrupt transitions in the image were detected using a

multiscale Gaussian differential operator defined as below.

$$\vec{\psi}(x,y) = \frac{dG(x,y)}{dx}\hat{i} + \frac{dG(x,y)}{dy}\hat{j} \qquad \textbf{3-16}$$

We use a differential Gaussian function as the mother wavelet because this choice enhances edge information.

The scaled decomposition of the image can be performed by transforming the image data Z(x, y) with the differential Gaussian wavelet parameterized by scale σ. For a fixed value of scale, we can calculate the 2D CWT in frequency domain:

$$W(\sigma, w_1, w_2) = \sigma Z(w_1, w_2)\Psi^*(\sigma w_1, \sigma w_2). \qquad \textbf{3-17}$$

The resolution of the multiscale recognition technique corresponds to the resolution of the features within the image. This is nanometer-scale for AFM images and angstrom-scale for STM images.

Examples of AFM images and their corresponding CWTs are shown in Figure 3-6(a) and Figure 3-6 (b). For each image, the mass center is calculated, which is the point where the pixel intensities are balanced for any line through that point. By plotting the pixel intensities along horizontal and vertical lines through the mass centers of the CWT transformed images as shown in Figure 3-6 (c), it is clear that leukocytes and erythrocytes have a different number of peaks. The peaks correspond to edge pixels and hence the presence of a nucleus inside the cell is represented by the number of zero-crossings, which is the number of times that the pixel intensities cross the zero level. We define the zero level as the average value of the maximum and minimum pixel intensities along each line.

Two orthogonal lines are chosen for this analysis for robustness. We choose the number of zero-crossings as the feature which represents discriminating information for

erythrocytes and leukocytes, and will refer to the feature thus defined as the Edge Feature. Both leukocytes and erythrocytes have globular shapes. A distinguishing characteristic between them is that erythrocytes are anucleate. Continuous Wavelet Transform (CWT) method is used to successfully distinguish erythrocytes from leukocytes [45].

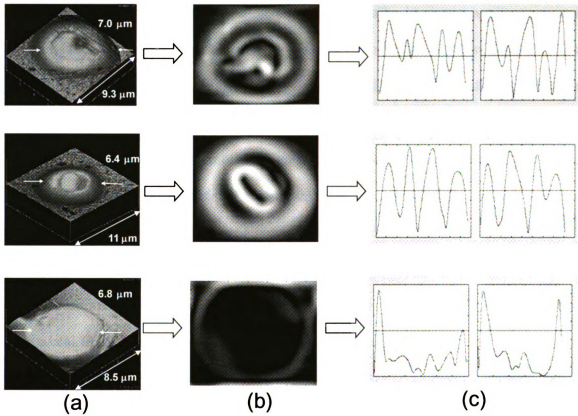

Figure 3-6 The definition of the Edge Feature is based on (a) AFM images; (b) Continuous wavelet transformed (CWT) images. (c) Pixel intensities on horizontal and vertical lines clearly show the Edge Feature for each cell type. Reproduced from Figure 4, Reference: Q. Chen, Y. Fan, L. Udpa, and V.M. Ayres, Vol. 2, Issue 2, pp. 181-189, Int. J. Nanomedicine (2007)

3.5 SPRM Operation Modes

The SPRM system has multi-function, off-line and on-line operation modes. Some applications, such as classification, need the whole information of objects, which can only be done after the scan of the whole region of interest is finished. Other applications need real-time capability. The SPRM system can be operated in either off-line mode or

on-line mode. In the off-line mode, powerful recognition and analysis ability of SPRM enable the user to get more information of samples under observation conveniently and efficiently. In the on-line mode, the SPRM system makes auto-focus/tracking on the region of interest in real-time possible. This ability is the most important feature of the SPRM system. It saves the operation time dramatically in many applications and segments the meaningful information from the background automatically. Users can also combine these two modes to be even more powerful. For example, after an object is scanned in on-line mode, its property can be analyzed under off-line mode. Since on-line auto-focus scan has already segments the meaningful data from the background, it makes any subsequent off-line analysis of the object more convenient, efficient and accurate. The next several chapters will present examples that illustrate these points.

How to choose the operation mode and how to combine them together depends on the applications. In the following four chapters, four important topics in biological and biomedical fields are discussed separately. However, the SPRM system is used in all of them to solve the application problems. Detail of techniques used in the SPRM system and realizations of the SPRM system are also covered in these four different applications.

3.6 Novelty & Importance of SPRM versus State of the Art AFM

3.6.1 Novelty and importance of SPRM versus standard SPM

Compared with standard SPM techniques, SPRM system improves the speed of SPM, which is one of the most commonly observed problems of SPM techniques. In SPRM system, only the region of interest is scanned, therefore, the overall time taken for imaging can be decreased. Therefore, SPRM system has the advantage of saving operation time.

Speed improvement for SPM is a state of the art research issue. Various groups have recently reported successes in the overall improvement of conventional SPM speed through improvements in the individual sub system components [46]. SPRM can take advantage of the new improvement in overall system speed while contributing new capabilities.

The SPRM system provides more powerful feature/property analysis abilities compared with SPM. Auto-tracking specific regions of interest can provide more meaningful information of samples automatically, efficiently and accurately. The power of SPRM allows us to investigate situations in which standard SPM is insufficient to deal with. Two examples are given in this thesis. One is the properties investigations of individual nanofibers within a tissue scaffold used for regenerative medicine. This example is presented in detail in this thesis. Another example is discussed in Chapter 10: Future Work. This is an ongoing SPRM investigation of nanowire-based nanoelectronics in which SPRM is used to access information in a previously unavailable part of the circuit.

Another big advantage of SPRM system over SPM is that multiple data on same sample area can be obtained in SPRM system by its recognition and auto-tracking capability. It gives SPRM the potential for data fusion, which combines different types of information into a composite picture more truly representative object under investigation.

The design and development of SPRM system includes many works from hardware to software, from algorithms to data management, from tip control to result display. Basic functionalities of SPRM are implemented at first, which is the kernel part of the system. When SPRM is applied to investigate real nanobiological phenomenon, additional

functionalities specific to applications are added and integrated into SPRM as optional functionalities.

3.6.2 Novelty and importance of SPRM versus optical techniques

SPRM is an improved technique based on Scanning Probe Microscopy. Therefore, it inherits all the advantages of SPM but improves some of the limitations of SPM.

Both SPM and advanced optical techniques, such as confocal microscopy and two-photon microscopy can image living specimens and provide 3D information of samples. But when SPM technique is compared with these advanced optical techniques, it has the advantages of direct interacting with specimens rather than looking at them. The direct interaction with sample surface enables SPM to serve as a microindenter that probes soft samples to reveal information about the mechanical properties of samples. In SPRM system, this advantage can be extended with flexibility to probe any region of interest on sample surface and get mechanical properties of desired region. The mechanical properties of living specimens are important for many biological investigations. Thus, SPRM technique enhances the power of SPM for its application in biological fields.

The disadvantage of SPM compared with optical techniques is that SPM is not looking inside. This problem can be solved by combining the two techniques together. Combination the two techniques can also bridge the gap of scales between optical techniques and scanning probe microscopy techniques. Information gotten from optical techniques can also be used to guide SPM investigation. Our group has the intention to be able to integrate optical technique into SPRM system in the future for a powerful

combined instrument.

3.6.3 Novelty and importance of SPRM versus HRTEM

SPM and HRTEM techniques provide comparable image resolution. But SPM has several advantages over HRTEM. Unlike the electron microscope which provides a two-dimensional projection or a two-dimensional image of a sample, the SPM provides a true three-dimensional surface profile.

Additionally, samples viewed by SPM do not require any special treatments that would irreversibly change or damage the sample. While an electron microscope needs an expensive vacuum environment for proper operation, which usually killed living samples. Most SPM modes can work perfectly well in ambient air or even a liquid environment. This makes SPM be able to study living biological samples. SPM studies can also be done under physiological conditions allowing for the imaging of dynamic biological processes taking place in real time.

In SPRM system, the same living biological object can be imaged repeatedly based on recognition and auto-focus ability of SPRM. It makes possible to image the progress of the same biological object under living condition as time elapse. This is very useful for many biological experiments.

Part II SPRM

Applications in Nanobiology

Part II SPRM APPLICATIONS IN NANOBIOLOGY

SPRM was developed with powerful recognition capability as explained in the first part of this dissertation. Its successful application in analyzing nanoscale 3D cues for spinal cord repair research is addressed in this part. The motivation and background of SPRM in spinal cord repair are introduced first in Chapter 4. Chapter 5 discusses the auto-tracking ability of SPRM which enables the system to scan only on individual nanofibers within the tissue scaffolds used for regenerative medicine, thereby, collecting the first accurate nanofiber properties analyses. In Chapter 6, the topographic, mechanical and chemical properties of nanofibers which influence neural cell attachment are addressed and analysis of these properties are done by using SPRM. Cell responses to different substrates are explored and compared in Chapter 7. Chapter 8 discussed the correlation of electronspinning parameters with nanofiber properties analysis.

The candidate developed the first adaptation of SPRM for investigation of a significant nanobiomedical problem: analyzing nanoscale 3D cues for spinal cord repair research. The candidate also made significant contributions to the development of the auto-tracking implementation, and to material properties analyses.

CHAPTER 4

4 MOTIVATION & BACKGROUND OF SPRM IN TISSUE ENGINEERING: SPINAL CORD REPAIR

4.1 Introduction of Tissue Engineering: Spinal Cord Repair

The use of scaffolds composed of biocompatible materials as vehicles to deliver or promote growth/differentiation of cells within damaged tissues of the body is an exciting new tool for the field of regenerative medicine. Tissue scaffolds composed of artificial nanofibers that mimic natural collagen nanofibers can enable the entrained re-growth of cells into damaged areas and this is of great medical importance. Tissue scaffolds fabricated from artificial nanofibers have recently been successfully used in kidney repair[47], knee joint repair[48], and reproductive tract repair with fully restored natural function [47-49].

Electrospun nanofibers in tissue scaffolds generated tremendous interest due to their potential as scaffolds for regenerating tissue. The tissue scaffolds explored in this thesis are: slowly degradable tissue scaffolds fabricated from electrospun [50, 51] polyamide nanofibers by the Donaldson Company. The nanofibers were electrospun using an adapted electrospinning probe procedure described in Reference [52].

The design of prosthetic implantable scaffolds to promote tissue repair in vivo will require the accurate incorporation of the topographic, mechanical and chemical signaling properties that best mimic endogenous support tissue. Sophisticated tissue scaffolds with properties designed for the re-growth of specific cells types, while maintaining maximum biocompatibility, would greatly increase the quality and number of applications. To optimize the performance of these scaffolds for each type of tissue or application, new

analytical methods must be developed that can examine the interaction of these cells with the surfaces of these scaffolds in vitro under a variety of biochemical and physical conditions at a resolution in the nanometer range.

The support surface for cell organization in natural tissues is termed the extracellular matrix/basement membrane (ECM/BM). This is especially necessary in the spinal cord repair. Repair of damage to the spinal cord and optimal recovery of motor and sensory functions can only occur when the specific physical and chemical cues are engineered into an implantable system to provide proper guidance for oriented axonal regeneration that bridges the spinal cord defective area.

During development of, and also following injury to, the nervous system, the growth and regeneration of axons is strongly influenced by the extracellular matrix (ECM) [53] and Schwann cell-derived basement membrane (BM) [54]. (The basement membrane is a structurally compact form of the extracellular matrix). Therefore, artificial scaffolds that are extracellular matrix/base membrane - mimetic might provide ideal substrates for neuronal growth, particularly for in vivo applications that require regenerative scaffolds to be compatible with the original tissues.

It is necessary to examine the natural in vivo environment in order to reproduce it. Almost all cells are attachment-dependent, which means that they much first successfully attach to substrate (cell adhesion) in order to begin cell growth (spreading) followed by cell division (mitosis leading to proliferation) processes. (For comparison, a red blood cell is one of the few non-attachment dependent cells, as its function requires that it float freely within its environment). The neural cells: astrocytes and neurons investigated by SPRM in this thesis are attachment-dependent cells. Astrocytes and neurons are a paired

system in which neurons attach to astrocytes which provide them with nutrients, waste-removal and mechanical support, while astrocytes attach to a specialized extracellular matrix (ECM)/basement membrane (BM), which provides them with filtration and mechanical support. Astrocytes obtain nutrients and pass waste molecules through exchange with capillaries which are encased by the ECM/BM filtration system called the basal lamina as shown in Figure 4-1. Regulatory proteins embedded within the ECM/BM assist these processes. Therefore, an artificial tissue scaffold must reproduce the topographical, mechanical and surface chemistry cues of the natural basal lamina environment.

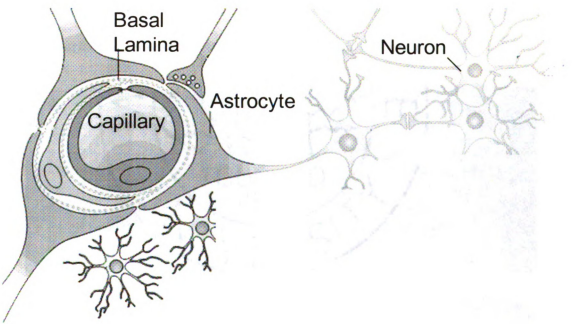

Figure 4-1 Cellular constituents of the blood-brain barrier. Images from reference [55]

4.2 Environmental Nanoscale Cues for Cell Growth

To tap the potential of artificial slowly degradable nanofibers as scaffolds for many different cell types, it is necessary to quantify the properties that provide all necessary environmental cues for a truly biomimetic situation. A literature search was performed to

indentify specific properties that have been shown to influence cell attachment and growth. Recent research has identified individual external triggers in the cell environment that stimulate dynamic cell responses include surface roughness [56], elasticity [57] and surface chemistry[58]. An additional trigger, 3D nanoscale topography has recently been shown to influence cell attachment and growth. A brief review of examples of each is provided.

(1) Surface roughness

Investigations of human bone marrow cells examined the effect of specifically graded surface roughness of hydroxyapatite (HA) substrate on cellular adhesion and proliferation as shown in Figure 4-2 [59]. For bone marrow cells, the results indicated that high surface roughness best promoted cell adhesion and proliferation.

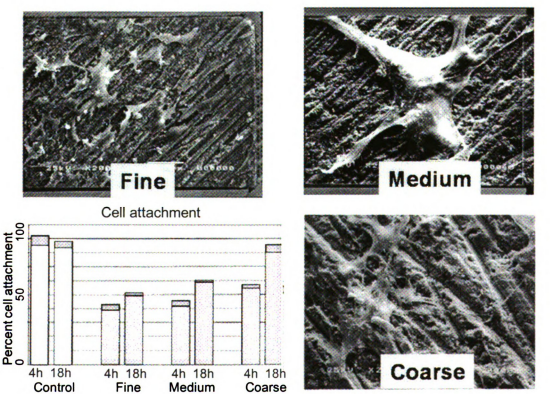

Figure 4-2 SEM micrograph showing the bone marrow cell morphology on substrates with different surface roughness, Images from reference [59]

(2) Elasticity

Research work was performed to investigate the response of NIH 3T3 Fibroblasts cultured on polyamine substrates with different rigidities, provided by different amounts of cross-linking. Experimental results indicated that fibroblasts cells move in favor of rigid substrate areas as shown in Figure 4-3 [60]. This means elasticity properties of substrate will influence cell in growth.

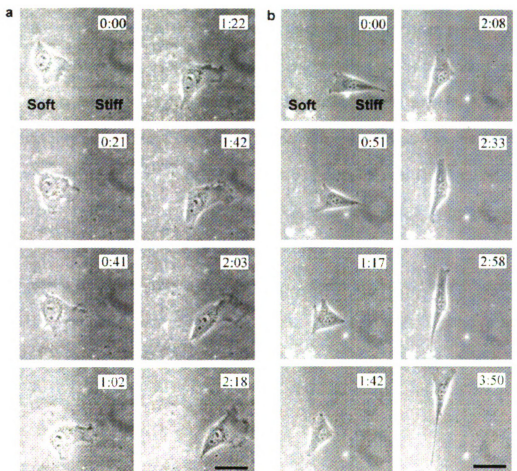

Figure 4-3 Movements of National Institutes of Health 3T3 cells on substrates with a rigidity gradient (*a*) A cell moved from the soft side of the substrate toward the gradient. The cell turned by ~90° and moved into the stiff side of the substrate. Note the increase in spreading area as the cell passed the boundary. (*b*) A cell moved from the stiff side of the substrate toward the gradient. The cell changed its direction as it entered the gradient and moved along the boundary. Bar, 40 μm. Images from reference [60]

(3) Surface chemistry

It is well known that regulatory proteins are complexed with the extracellular matrix and that these provide chemical cues for healthy cell function. Therefore, the surface chemistry property of implantable tissue scaffold nanofibers is important issue in tissue engineering. Research in our collaborator's laboratory (S. Meiners) has focused on the growth-promoting actions of bioactive neuro-regulatory molecule embedded in the extracellular matrix in vivo. One of these is the fibronectin type III region of tenascin-C. The active site of this peptide for neurite outgrowth for cerebellar granule, cerebral cortical, spinal cord motor, and dorsal root ganglion neurons has been localized to an amino acid sequence VFDNFVLKIRDTKK [58], called the D5 peptide. A D5 peptide was covalently complexed to the electrospun nanofibers investigated in this dissertation. The results provide an example of the importance of chemical cues for neural cells.

Astrocytes cultured on even bare nanofibers adopted a stellate morphology that is typical of their in vivo counterparts, whereas astrocytes cultured on poly-L-lysine (PLL) coated plastic coverslips had a flat, cobblestone appearance which is never seen in the body. The nanofibers were then covalently modified with the D5 peptide and this additional chemical cue resulted in aligned axonal regeneration by neurons in vivo as shown in Figure 4-4 [58].

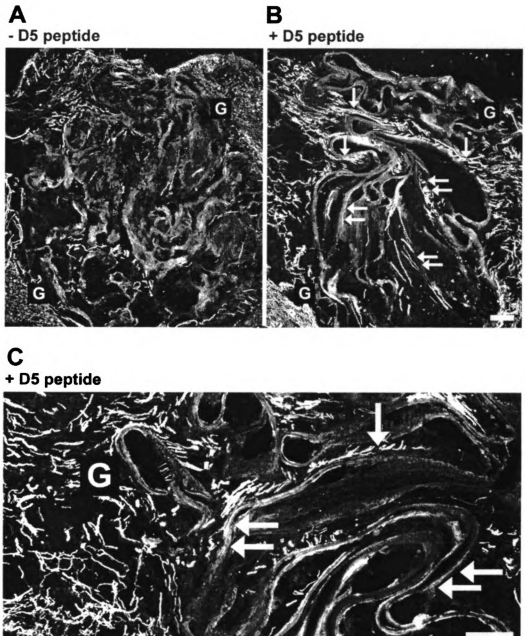

Figure 4-4 Peptide modification enhances the ability of nanofibers to promote axonal regrowth. Rostral is to the left. G, host-graft interface. Curves were adjusted in Adobe Photoshop for each panel to enhance the visibility of the axons against the autofluorescence of the nanofibers. (A) Neurofilament M-labeled axons were observed within the implant of unmodified nanofibers. (B) Axonal growth was more robust within the implant of nanofibers modified with the D5' peptide. Bar, 150 μm. (C) Axons were observed on the surface of the nanofibers following folds in the nanofibrillar fabric. The top of the image is ~ 300 μm ventral to the top of the spinal cord. Bar, 300 μm. Single arrows in (B) and (C) denote axons growing more or less parallel to the axis of the spinal cord. Double arrows denote axons that deviated from a parallel path. Reference: S. Meiners, I. Ahmed, A. S. Ponery, N. Amor, S. L. Harris, V. Ayres, Y. Fan, Q. Chen, R. Delgado-Rivera, and A. N. Babu, Polymer International, vol. 56, pp. 1340-1348, 2007

Therefore, we present a quantitative investigation of surface roughness, elasticity, surface chemistry, as these may be expected to influence the cell regeneration in its search for a biomimetically attractive environment.

SPRM-enhanced atomic force microscopy (SPRM-AFM) was used by the candidate to investigate the curvature, surface roughness and elasticity of individual nanofibers. The detail of neural cell response to a set of well quantified properties was then investigated. This provided the first data obtained along individual nanofibers using a technique that maintains uniformity of experimental conditions.

(4) Nanoscale topography.

Recent work strongly suggests that substrate topography influences cell attachment and that this influence is nanoscale in nature. The recent investigations are based on newly available nano patterning techniques such as electron beam, photo and ink jet soft lithography, and oriented growth of nanowires/ nano pillars [61]. Experiments performed using these as guides indicate a strong cell response to nanoscale topography for many cell types. Quantification and understanding of the observed cell responses is now an active research area.

As previously discussed and as shown in Figure 4-5, astrocytes cultured on even bare nanofibers adopted a stellate morphology (a) that is typical of their in vivo counterparts, whereas astrocytes cultured on poly-L-lysine (PLL) coated plastic coverslips had a flat, cobblestone appearance (b) which is never seen in the body. Until this work, PLL had been required for astrocyte growth in culture. This indicates the strong positive influence of 3D nanoscale curvature in itself as a topographic trigger for astrocyte growth.

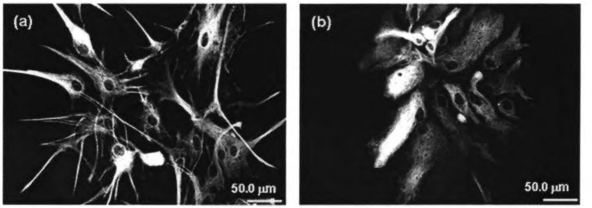

Figure 4-5 Astrocytes cultured on even bare nanofibers adopted a stellate morphology (a) that is typical of their in vivo counterparts, whereas astrocytes cultured on poly-L-lysine (PLL) coated plastic coverslips had a flat, cobblestone appearance (b) which is never seen in the body. To date, PLL has been required for astrocyte growth in culture. Reference: S. Meiners, I. Ahmed, A. S. Ponery, N. Amor, S. L. Harris, V. Ayres, Y. Fan, Q. Chen, R. Delgado-Rivera, and A. N. Babu, Polymer International, vol. 56, pp. 1340-1348, 2007

4.3 Ultimate Goal

In spinal cord repair, individual external triggers in the cell environment that stimulate dynamic cell responses include surface roughness, elasticity and surface chemistry. Other additional triggers, such as porosity and mesh density, are also shown to influence cell attachment and growth. The ultimate goal is to find the best tissue scaffold with most appropriate topographical, mechanical and chemical properties for specific cells or cell classes. These properties of nanofibers can be analyzed by using the new Scanning Probe Recognition Microscopy technique. And cell response can also be investigated by SPRM and other optical techniques. Information can be combined to provide a composite picture representative of a cell's perception of its environment. Then, the electrospinning materials or parameters can be adjusted adaptively until the properties of the produced nanofibers are found to be best for cell regeneration. The whole procedure will provide an automatic guide to design tissue scaffold for regenerative medicine.

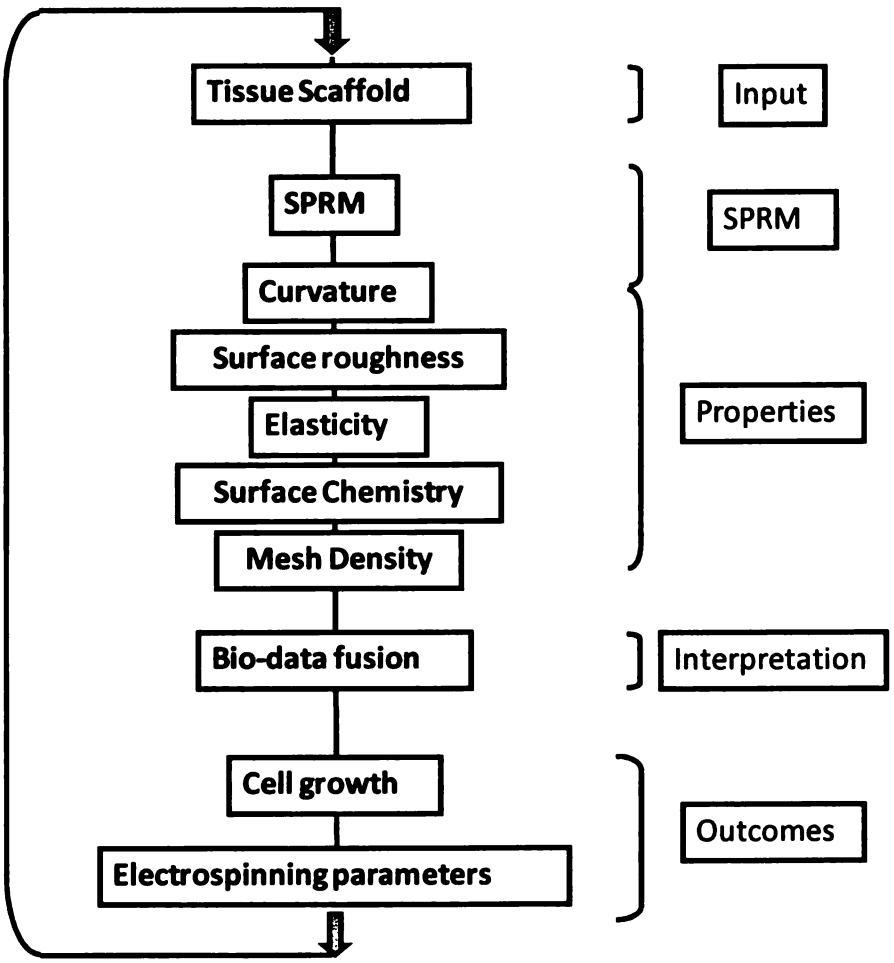

Figure 4-6 Application of SPRM in spinal cord repair

CHAPTER 5

5 SPRM AUTO-TRACKING IMPLEMENTATION ON TISSUE SCAFFOLD NANOFIBERS

As explained in previous chapter, electrospun tissue scaffold nanofibers structurally mimic the extracellular matrix on which cells attach and grow in vivo. This property gives electrospun nanofibers great potential for use in tissue engineering applications. However, much fundamental understanding is still needed to design tissue scaffolds with the most appropriate mechanical, topographical and chemical properties for particular cells or cell classes. SPM methods are essential to measure the nanoscale triggers that cells respond to. It is also essential for individual nanofibers within a tissue scaffold to be scanned for accurate mechanical or topographical properties investigations. SPRM provides the first ability to do this.

5.1 Importance of Auto-Tracking of Individual Nanofibers

In a standard SPM of a candidate tissue scaffold, an extra image segmentation technique would be necessary after getting the image of the whole scan region in order to get the information along each individual nanofiber. This would be extremely difficult to realize using off-line segmentation techniques as shown in Figure 5-1 and Figure 5-2. By contrast, when nanofibers only are automatically tracked during an SPRM scan, the segmentation is already done in the scan step. The useful information on nanofibers is extracted from the environment automatically.

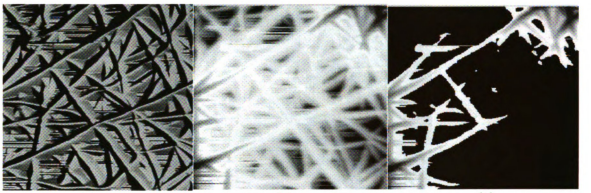

Figure 5-1 Off-line segmentation results at scan size equals 15 microns a) AFM height image; b) Recovered image by reading exported ASCII file; c) Off-line segmentation results using thresholding method.

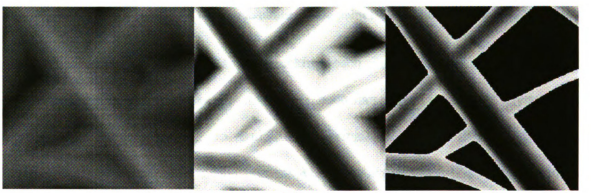

Figure 5-2 Off-line segmentation results at scan size equals 3 microns (a) AFM height image; (b) Recovered image by reading exported ASCII file; (c) Off-line segmentation results by using thresholding method.

A second important feature of auto-tracking is data collection over a reliable region of interest. An attempt to measure the elasticity of a tissue scaffold nanofiber using standard SPM illustrates this point. In tissue scaffold nanofibers, there are three types of regions as shown in Figure 5-3. Regions as data point (1) are not region of interest; regions as data point (2) are right on top of a nanofiber; regions as data point (3) are on the side of a nanofiber. Only regions as data point (2) contain reliable data in these three types. SPRM has the capability to collect information only along these reliable regions.

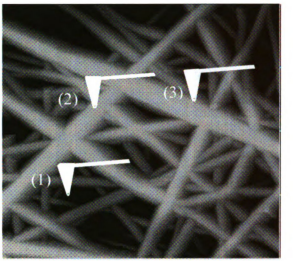

Figure 5-3 Different types of regions on tissue scaffold nanofibers: Data point (1) is out of region of interest; data point (2) is right on top of a nanofiber; data point (3) is on the side of a nanofiber. Scan size: 10 microns [62].

A third important feature of auto-tracking each individual nanofiber is that it maintains the uniformity of experiments. When each nanofiber is automatically scanned by tracking from beginning to end, the information on nanofiber is collected independently to other parts of environment which are not scanned. This will provide a uniformity of scanning probe experimental condition as long as other operation parameters are same. The experimental uniformity is extremely important when the research interest is to compare different samples.

The new Scanning Probe Recognition Microscopy is designed to provide auto-tracking ability. As shown in Figure 5-4 (and also as a movie at http://www.egr.msu.edu/ebnl, Research, Scanning Probe Recognition Microscopy), SPRM can scan along individual nanofibers in tissue scaffolds by tracking them one by one, which will automatically provides reliable information of individual nanofiber in real-time.

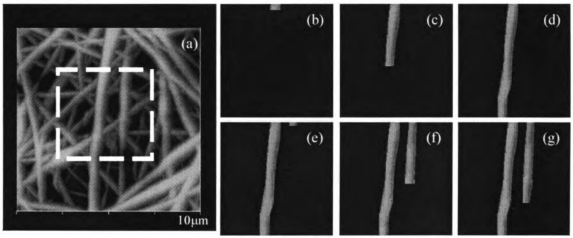

Figure 5-4 SPRM auto-tracking capability to scan along individual nanofibers (a) AFM height image; (b)-(g) A series of images shows the time sequence of scanned results by using SPRM. [62]

5.2 SPRM Auto-Tracking Capability

The flow chart to realize auto-tracking capability of SPRM for auto-tracking along nanofibers is shown in Figure 5-5.

A coarse scan and fine scan is used alternatively to scan all the nanofibers in scan range with high efficiency. The basic idea of tracking nanofiber is to use real-time information to detect the boundary of a single nanofiber while using coarse scan. The coarse scan is set to have relatively large step size and a relatively high scan velocity. On the contrary, fine scan has relatively small step size and relatively low scan velocity. Once a boundary of nanofiber is detected, it triggers the initiation of a fine scan set to have a small step size and a relatively low scan velocity. The new auto-tracking scan is combined with boundary prediction when enough information is accumulated in previous lines of scanning, usually 10-20 lines. With boundary prediction, SPRM is able to stay along the nanofiber even though there are other nanofibers crossing it. Adaptive learning ability is also integrated in our algorithms to improve performance.

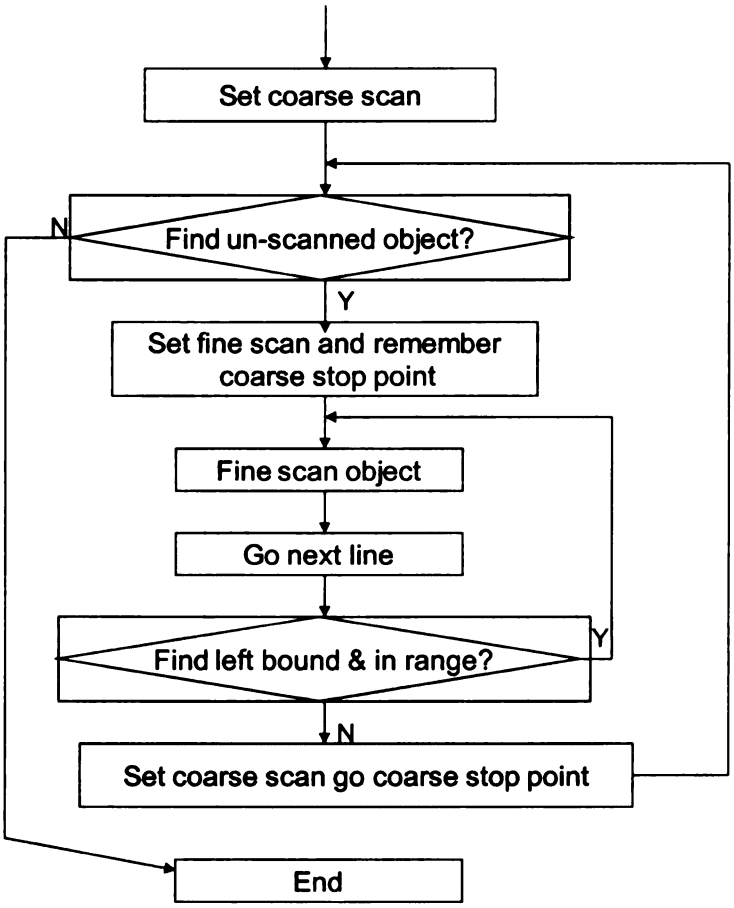

Figure 5-5 Flow chart of auto-tracking scan

(1) Coarse scan versus fine scan

A coarse scan is used to detect individual nanofiber while fine scan is used to actually scan along the detected nanofiber. This scheme enables SPRM to scan nanofiber one by one as shown in Figure 5-6, which will increase overall imaging efficiency without losing resolution of imaging.

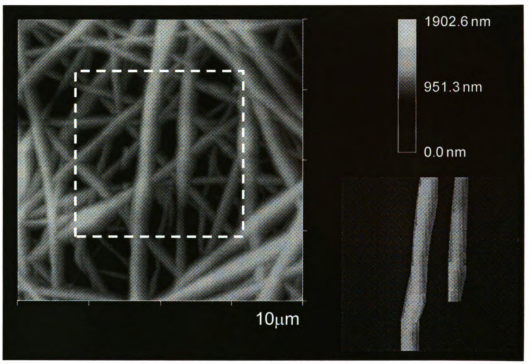

Figure 5-6 SPRM scan along individual nanofibers in a tissue scaffold. Left image is the standard AFM image, region in black box are target scan region by SPRM. Right image shows the scan result of using SPRM, two individual nanofibers are scanned one after the other, other regions not scanned are padded 0 for display.

(2) Statistics analysis

After boundary of the next line is predicted, the scan range in the next line will be controlled only from the left predicted boundary to the right predicted boundary, which will make the scan stays within the targeted region of interest. In order to increase the accuracy of the system, boundary detection technique is applied after each line of scan. With both predicted boundary and detected boundary at hand, a criterion is needed to decide whether the detected boundary matches the predicted boundary. When the detected boundary matches predicted boundary within a reasonable error range, the detected boundary is used to predict boundary of next line since it records the newest information. When the detected boundary is too far away predicted boundary, which means that there is special situation which makes the detected boundary not the boundary

of the target nanofibers, detected boundary will not be used to predict boundary information in the future because it doesn't record the correct boundary information of the target nanofiber. In the tissue scaffold application, this problem normally happens when there are several nanofibers crossing over one another as shown in Figure 5-7.

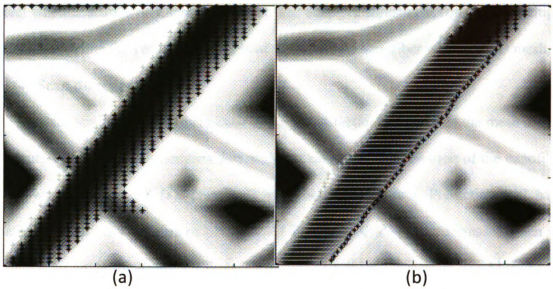

Figure 5-7 Scan plan to stay on individual nanofiber (a) without boundary prediction; (b) with boundary prediction

Hypothesis test in statistics[63] are applied to give a criterion of how far away the distance between detected boundary and predicted boundary is acceptable. Therefore, accuracy of boundary detection can be analyzed statistically. When the detected boundary is not the real boundary, the predicted boundary will be used instead.

(3) Adaptive learning

It is important for SPRM system to have adaptive learning ability in real-time because there are many types of noise when SPRM is imaging in tissue scaffolds, for example, sample tilting issue will cause the height information of the sample surface to have tilting too. With adaptive learning algorithm, important parameters in algorithms can be adjusted automatically in real-time in order to capture changes of sample surfaces.

The newest information is updated into the information database and used to replace the oldest information in algorithms. Therefore, the SPRM system can still stay within individual nanofibers in spite of complex situation of sample surface.

The key parameter needed to be adjusted adaptively is the thresholding value to detect whether scan is on nanofibers or not. The adaptive adjustment considered multiple factors that define the vertical placement of an individual nanofiber within its 3D mesh.

(4) Scan direction

In tissue scaffolds, nanofibers exist in random directions to produce the mesh shown in Figure 5-8. When the scan direction is almost same as the orientation of the nanofiber as shown in Figure 5-8 (a), there will be fewer lines of data. Prediction will have relatively larger error because of limitation of data. This error will be decreased when we change scan angle by 90 degree as shown in Figure 5-8 (b). Therefore, SPRM gives the flexibility of changing scan angle to get best performance.

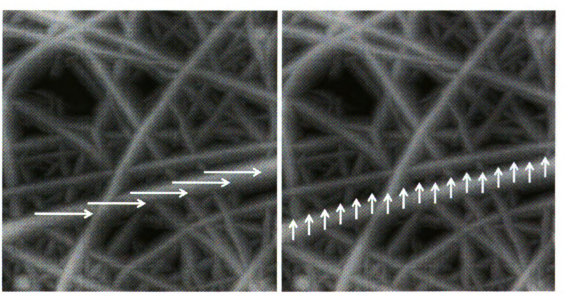

(a) (b)

Figure 5-8 Demonstration of Scan angle in imaging Tissue scaffold nanofibers using SPRM (a) horizontal scan direction; (b)vertical scan direction

5.3 Examples of SPRM

Samples of tissue scaffolds fabricated from electrospun carbon nanofibers were obtained from the Donaldson Company. The SPRM is used to selectively scan only along individual nanofibers.

The standard AFM contact mode was used first to get an image of the tissue scaffolds sample as shown in Figure 5-9 (a). The SPRM system can be and was run under simulation mode to confirm that the SPRM can automatically scan only on the nanofibers one by one as shown in Figure 5-9 (b). Then a real-time scan along individual nanofibers was performed. The real-time scan result of the SPRM is shown in Figure 5-9 (c). It is clear that the SPRM system can auto-track on the nanofibers as desired.

The scan direction can also be changed in the SPRM depending on requirements. The scan result of the same tissue scaffold sample at the same region but with a different scan direction is shown in Figure 5-10.

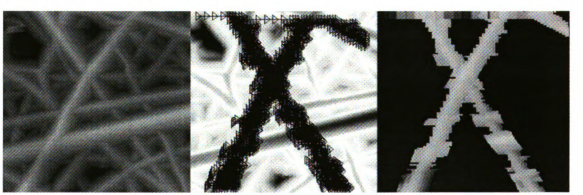

(a) (b) (c)

Figure 5-9 (a) Standard AFM image of tissue scaffolds with scan size equals 6 microns; (b) simulation scan result of SPRM by using horizontal scan direction; (c) real-time scan result of SPRM by using horizontal scan direction.

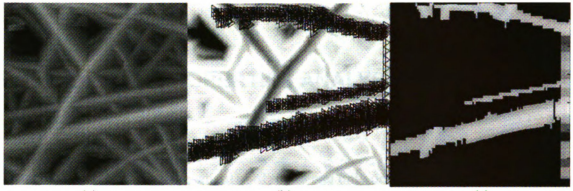

(a) (b) (c)

Figure 5-10 (a) Standard AFM image of tissue scaffolds with scan size equals 6 microns; (b) simulation scan result of SPRM by using vetical scan direction; (c) real-time scan result of SPRM by using vertical scan direction.

From the scan results shown in the Figure 5-9 and Figure 5-10, it is clear that SPRM scanned most of the nanofibers in the tissue scaffolds one by one. The experimental results show that operation time can be saved dramatically by applying SPRM to selective scan only on nanofibers. Only meaningful data is captured in SPRM; the background regions were not scanned at all. It makes the analysis of properties of nanofibers much easier after this step of useful information extraction. Another advantage of using SPRM is that users have flexibility in imaging the samples. SPRM can repeat the scan of same nanofiber because of its on-line recognition ability.

In conclusion, the auto-tracking ability of SPRM is realized based on algorithms and techniques in pattern recognition and image processing fields. Adaptive learning and prediction are implemented to make detection and recognition quicker and more reliable. Error analysis and hypothesis test techniques in statistics are also used to improve performance of SPRM. Experimental results show that SPRM can auto-track on individual nanofibers one by one efficiently and accurately, which makes the property analysis of nanofibers very convenient. The detailed analysis of topographic and mechanical properties of nanofibers will be explained in the next chapter.

CHAPTER 6

6 NANOFIBER PROPERTIES ANALYSIS BY USING SPRM

As discussed in Chapter 4, spinal cord repair can only occur when the specific physical and chemical cues are engineered into an implantable device to provide proper guidance for the axons across the spinal cord defect. Therefore, it is necessary to be able to analyze physical and chemical cues, including curvature, surface roughness, elasticity and surface chemistry, which are all known to affect cell attachment and growth. As explained in chapter 5, Scanning Probe Recognition Microscopy allows us to adaptively follow along individual nanofibers within a tissue scaffold. The ability of SPRM to auto-track on individual nanofibers was also demonstrated. In this chapter, the result of a physical and mechanical property analysis of electrospun polyamide nanofibers by using SPRM is presented in detail. Statistically significant data for multiple properties can be collected and calculated by scanning only over individual nanofibers, and information can be combined by repetitively scan over the same nanofibers if necessary.

6.1 Tissue Scaffold Samples and Experimental Parameters

Three samples of tissue scaffolds fabricated from electrospun [50, 51] carbon nanofibers were obtained from the Donaldson Company. These will be referred to as samples A, B, and C. The nanofibers were electrospun using an adapted electrospinning probe procedure described in Reference [52]. No further information about the tissue scaffolds samples was provided.

The new Scanning Probe Recognition Microscopy was performed in atomic force microscopy contact mode in ambient air. Other instrumental parameters include the use of a J scanner with a maximum 125x125 square micron x-y scan range and silicon nitride tips with a nominal 20 nm tip radius of curvature. Transmission electron microscopy (TEM) of the nanofibers was performed to provide an independent check of nanofiber diameter/curvature. TEM with selected area electron diffraction (SAED) was performed using a JEOL 100CXII TEM. Scanning electron microscopy (SEM) was performed to ensure that the nanofiber mesh scanned by SPRM was representative of the tissue scaffold as a whole. SEM was performed using a Hitachi S-4700II field emission SEM.

Atomic force microscope (AFM) images of tissue scaffold samples A, B, and C are shown in Figure 6-1 (a)-(c). Scanning electron microscope (SEM) images, shown in Figure 6-1 (d)-(f), were also used to ensure that the AFM results were representative over larger scaffold areas. The general appearance of the nanofibers was similar for samples A, B, and C. Tissue scaffold samples A, B, and C were then analyzed using Scanning Probe Recognition Microscopy for the more specific environmental triggers surface roughness and elasticity.

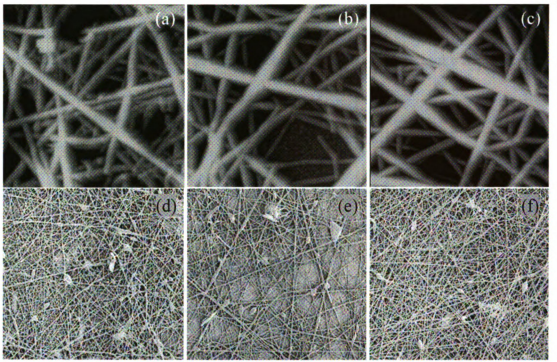

Figure 6-1 AFM and SEM images of electrospun carbon nanofiber tissue scaffolds. (a)-(c) AFM images of Sample A, B and C. The scan area of each image is 5 square microns and the z-height projection is 1500 nanometers. (d)-(f) SEM images of Sample A, B and C. The scan area of each image is 20 square microns. Reproduced from Figure 1, Reference: Y. Fan, Q. Chen, et al. in press, Vol. 2, Issue 4, *Int. J. Nanomedicine* (2007)

6.2 Nanofiber Property Analysis by Using SPRM

6.2.1 Surface roughness

The surface roughness of the substrate has been shown to influence cell attachment. It is therefore important to obtain this information accurately and conveniently along individual tissue scaffold nanofibers.

In the majority of studies, the surface roughness is the Root Mean Square (RMS) of height values in a region of interest as defined in equation below.

$$RMS = \sqrt{\frac{\sum_{i=1}^{N}(Z_i - Z_{ave})^2}{N}} \qquad \textbf{6-1}$$

For AFM-based measurements, N is the number of total pixilated data points in this region; Z_i is the height value at each pixel and $Z_{ave} = \frac{1}{N}\sum_{i=1}^{N} Z_i$ is the average value of all height values in this region.

The AFM nanoscope software provides the ability to calculate surface roughness as shown in Figure 6-2. The user can draw any rectangular box in the image, and the surface roughness in the box is calculated based on the above equation.

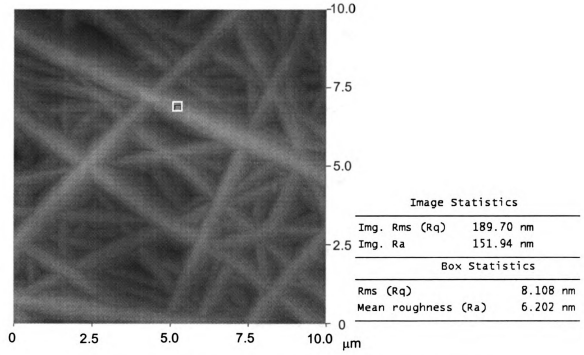

Figure 6-2 surface roughness calculation of Scanning Probe Microscopy

First, this method will introduce some error when it is used to measure the surface roughness of nanofibers. Height data, Z, is used to calculate the surface roughness in this way. This is acceptable for samples whose surfaces are relatively flat because then the variation in height data will reflect the variation in their surface roughness. This assumption is no longer appropriate for tissue scaffolds because the nanofibers have a cylinder shape. Therefore, the variation of height data, Z, includes not only its surface

roughness variation, but also the variation caused by the non-planar shape.

Second, the surface roughness information is acquired through manual application of a rectangular region of interest box[64]. The surface roughness within the box is then calculated. There are several problems with the conventional approach to surface roughness investigation when the sample is a tissue scaffold nanofiber. The shape of the region of interest (ROI) may not be rectangular, necessitating the application of several small ROI boxes which follow the curvature of the nanofiber. Only a single value is provided for each time of operation. Therefore, in order to get surface roughness along a nanofiber, this operation would need to be repeated for many times, which is time-consuming and inefficient.

In Scanning Probe Recognition Microscopy, the surface roughness property measurement ability was designed to be able to do accurate and efficient measurement along individual nanofibers, i.e. along non-planar substrates. These two discussed problem will be solved.

In SPRM, distance data, D, instead of height data, Z, was used to get the real roughness of the sample surface. The Kåsa circle fit method [65] was implemented to get the center (X_{center}, Z_{center}) of the most fitted circle as shown in Figure 6-3. Then the distance D_i between each point on the surface and the center was evaluated as equation below and used to calculate the surface.

$$D_i = \sqrt{(Z_i - Z_{center})^2 + (X_i - X_{center})^2} \qquad \textbf{6-2}$$

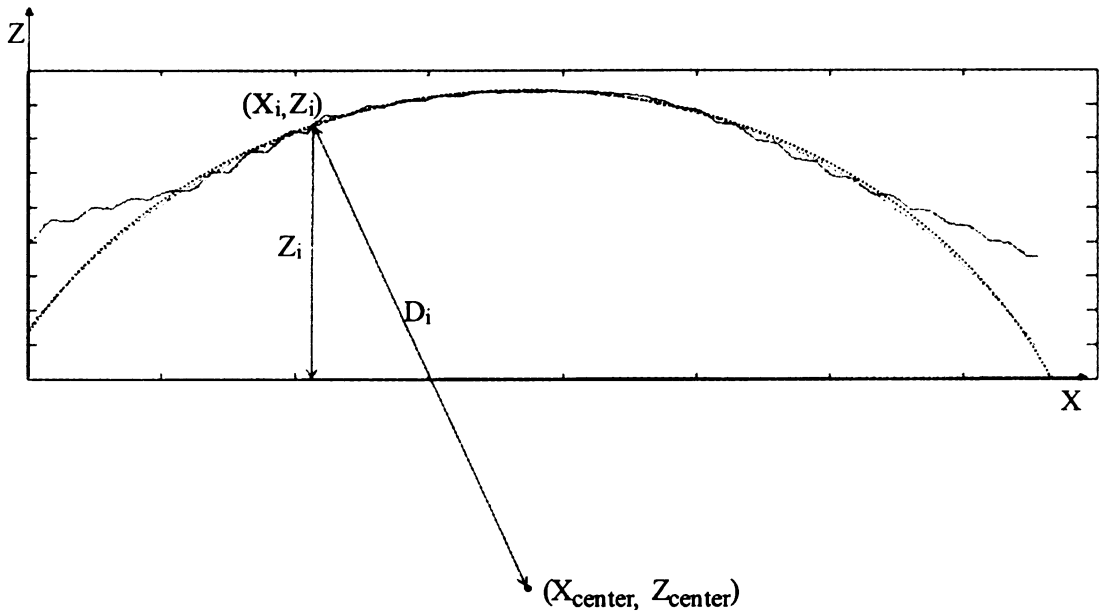

Figure 6-3 Circle fit based on Kåsa method. Reproduced from Figure 5, Reference: Y. Fan, Q. Chen, et al. in press, Vol. 2, Issue 4, *Int. J. Nanomedicine* (2007)

Only the center part of the height data was used to find the best fit circle. The boundary regions are unreliable due to tip-shape dilation effects. Dilation, or broadening of the image, is a result of the side of the tip coming into contact with the curved side of the nanofiber [66, 67]. When an SPRM scan is tracking an individual nanofiber, both the edge and center data is acquired. However, only the center part of the nanofiber provides reliable data because of the tip convolution effect [68, 69]. The ideal AFM would have an infinitely sharp tip to reach as much of the surface as possible and an infinitely sharp impulse response in its feedback system to instantly adjust the height of the tip as it is scanned over the surface. In reality, the tip has a pyramidal or conical shape with some finite end radius so it is durable enough to withstand the surface interaction forces. The effects of the tip shape cannot be avoided and these result in characteristic tip-dilation artifacts, as shown in Figure 6-4. We restricted the properties evaluations to regions of reliable data through the use of an erosion operation. This is an important consideration

when analyzing tissue scaffold nanofiber geometries using AFM-based methods (instead of planar substrates).

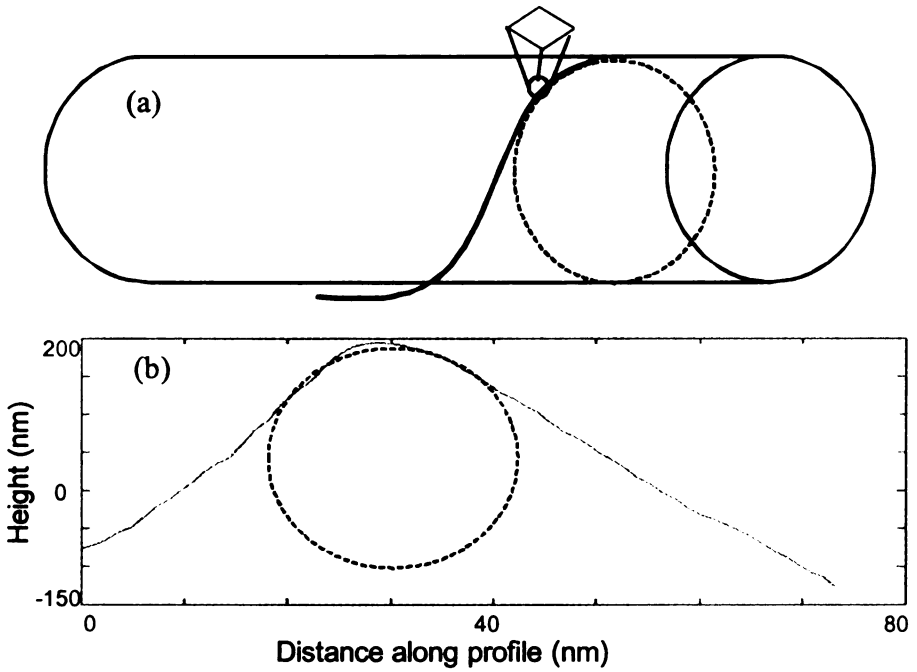

Figure 6-4 (a) Characteristic tip-dilation artifacts (b) The cross section of a real AFM nano fiber image and the best fit circle. Reproduced from Figure 6, Reference: Y. Fan, Q. Chen, et al. in press, Vol. 2, Issue 4, *Int. J. Nanomedicine* (2007)

In the SPRM system, a recognition-based scan plan can be generated to automatically control tip motion along an individual nanofiber [70]. Adaptive scanning enables SPRM to follow along an individual nanofiber even when it crosses another. Therefore, the whole nanofiber, or whole nanofiber mesh becomes the region of interest.

For the second problem, the surface roughness was calculated on each pixel based on a local neighborhood region by using data obtained by SPRM along individual nanofibers. The shape and size of the local neighborhood region can be adjusted by the user, which makes the system adaptable to different samples. We chose a rectangular box around each pixel as the local neighborhood region, with a box size close to the nanofiber diameter. Multiple sets of overlapping surface roughness information were generated,

with the provision that any box that extended outside the nanofiber boundaries was automatically truncated. A roughness map along individual nanofibers was then generated efficiently.

Figure 6-5 (b) shows a typical surface roughness map along an individual nanofiber in tissue scaffold. This is the first time that statistically meaningful information has been extracted along individual nanofibers using an automatic procedure that maintains uniformity of experimental conditions.

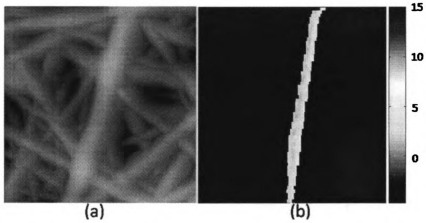

Figure 6-5 SPRM analysis of surface roughness (a) AFM image; (b) surface roughness map of an individual nanofiber

The histograms of the surface roughness for samples A, B and C are shown in Figure 6-6. From the histograms, the mode, the mean value, the range, and the variance of the surface roughness were investigated for several nanofibers for each tissue scaffold sample. The distribution was also approximately analyzed. Table 6-1 shows the results from the statistical analysis.

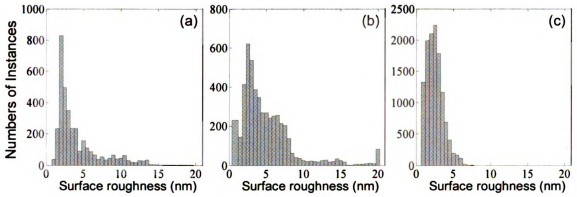

Figure 6-6 Histograms of surface roughness (a) Sample A; (b) Sample B; (c) Sample C. Reproduced from Figure 3, Reference: Y. Fan, Q. Chen, et al. in press, Vol. 2, Issue 4, *Int. J. Nanomedicine* (2007)

Table 6-1 Surface Roughness Statistical Analysis

Sample	Data Points	Mode (nm)	Mean (nm)	Range(nm)	Variance(nm^2)
A	3482	2.0	4.17	0.8~19.7	9.1
B	5063	2.5	5.10	0.4~20.0	15.5
C	12205	2.5	2.53	0.7~7.4	1.2

The mode values were close for all three samples. The mean values might indicate a progression between the samples: Sample C (least) < Sample A < Sample B (greatest). However, the surface roughness distributions of samples A and B were wide spread with prominent tails and irregular values while the surface roughness distribution for samples C was narrow, peaked and smoothly connected. Analysis of the surface roughness distribution therefore indicated that sample C was different from samples A and B. The corresponding range and variance values further indicated that samples A and B were similar to each other but different from Sample C.

The histogram analysis shows the possibilities for misinterpretation of data using conventional AFM methods. The surface roughness mode values for the three samples were all very close. An individually applied ROI box would be most likely to return the

mode value. However, the variances and distributions differed substantially between the samples. This was the true difference between the surface roughness of the samples, and it specifically indicated that sample C was different from samples A and B.

6.2.2 Elasticity

Getting one (or a series of) force curves at the desired position (or region) is very important for measuring mechanical properties of samples. Atomic force microscopy can be used to measure elastic properties by collecting force curves over points on the surface of the sample. A single force curve records the force felt by the tip as it approaches and is then drawn away from the sample [71, 72]. It is more useful to collect arrays of force curves across the sample surface at regular intervals and this is known as force volume imaging [73]. A force volume data set can be used to generate a 3-D map of interaction forces between the sample and tip as shown in Figure 6-7.

The problem of using force volume imaging mode to get force curves to analyze elasticity property lies in the following two aspects:

First, force volume imaging takes about hours to get force curves at each pixel as shown in Figure 6-7. But most of the force curves captured on the regions outside nanofibers are not necessary when the only interest is the elasticity of nanofibers. Time is wasted in getting unnecessary information. Therefore, applying SPRM to accurately recognize region of interest and then get force curves only along nanofibers is vital.

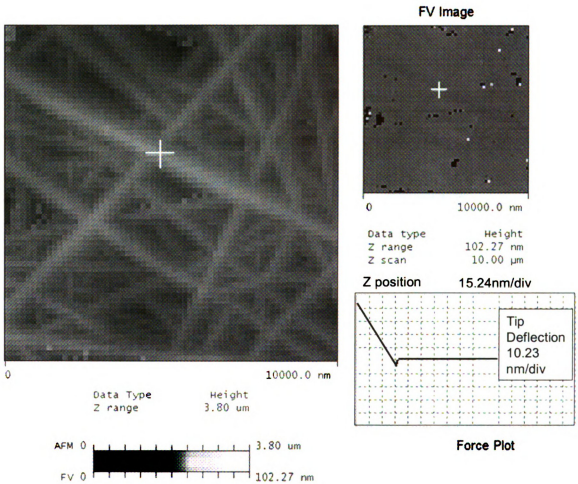

Figure 6-7 Force volume imaging of Atomic Force Microscopy

The second problem is that force volume imaging technique probes sample surface at given interval. The probe position might be anywhere, on top of nanofibers or at the side of nanofibers. But in order to using Hertz model [74] to calculate elasticity property, the force curves are required to be on top of the nanofibers as shown in Figure 6-8 (a). When tip is probing side of nanofibers as shown in Figure 6-8 (b), the force will not be normal to sample surface. This won't satisfy one of the assumptions of using Hertz model, which makes Hertz model not appropriate to be applied to calculate elasticity under this situation. Therefore, it is important to use SPRM to automatically track the top position of individual nanofibers and guarantee that force is normal to the sample surface.

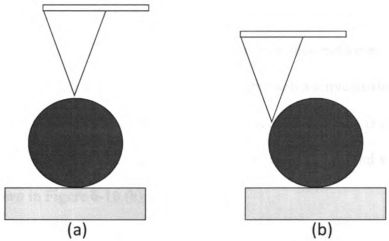

Figure 6-8 Tip probing position (a) tip probes top of nanofiber, force is normal to sample surface; (b) tip probes side of nanofiber, force is not normal to sample surface

The new SPRM system solved these problems by integrating recognition ability into the AFM system. Same as force volume imaging, tip will probe sample surface to generate force curve, but only meaningful and useful probes are done by recognition the top of individual nanofibers. Therefore, operation time will be decreased dramatically because only force curves on the top of nanofibers are collected. And forces are normal to the sample surface in these force curves is guaranteed at the same time.

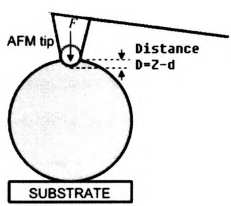

Figure 6-9 Force distance records the indentation of tip into soft sample

The force curves record the cantilever deflection (d) versus the height of the sample

surface (Z) as shown in Figure 6-10 (a). The elasticity analysis is based on the approaching part of the force curves. Rather than using the sample surface position (Z), it is more useful to obtain an absolute distance (D) that is relative to the separation between the tip and the sample surface which records the indentation of the tip into soft sample as shown in Figure 6-9. A force-distance curve can be obtained from the force curve which is defined by the cantilever deflection versus the absolution distance (D) between the tip and sample surface ($D = Z - d$) as shown in Figure 6-10 (b).

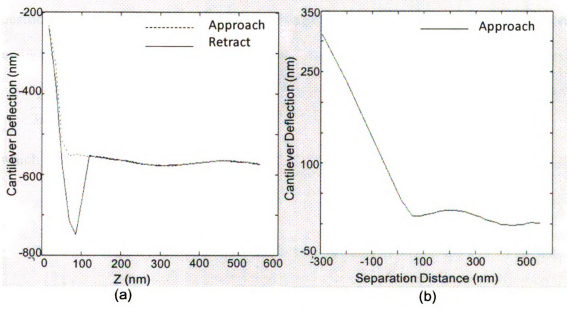

Figure 6-10 (a) force curve, both approach part and retract part are displayed; (b) force distance curve, only approach part curve is displayed, which is used to calculate elasticity property

The Force Integration to Equal Limits (FIEL) [75] mapping method is used to produce a robust measurement of relative elasticity. This method has the advantage of being independent of the tip-sample contact point, and of not requiring calibration of the AFM cantilever's spring force constant. Using the Hertz model[74], which has been widely applied to AFM data, if the tip of an AFM is approximated by a sphere, then the force on the cantilever (F) is decided by indentation (δ), elastic modulus (E), Poisson ration (v) and

radius of the probe sphere(R).

$$F = \frac{4E\sqrt{R}}{3(1-\nu)}\delta^{3/2} \qquad \textbf{6-3}$$

Let $k = \frac{1-\nu}{\pi E}$, $F = \frac{4\sqrt{R}}{3\pi \cdot k}\delta^{3/2}$ **6-4**

To compare the elastic properties at two different positions, a pair of force-distance curves is collected at positions P1 and P2 using the relative trigger mode in which the sample is probed until a preset same cantilever deflection (relative to the zero deflection) position is reached [32]. Therefore, force F1 equals force F_2 at these two points. It results in the following equation.

$$\frac{4\sqrt{R}}{3\pi \cdot k_1}\delta_1^{3/2} = \frac{4\sqrt{R}}{3\pi \cdot k_2}\delta_2^{3/2} \qquad \textbf{6-5}$$

which reduces to

$$\frac{k_1}{k_2} = \left(\frac{\delta_1}{\delta_2}\right)^{3/2} \qquad \textbf{6-6}$$

The work done by the cantilever at each position is the area under a force-distance curve, and is given by

$$w_1 = \int_0^{\delta_1} F_1 d\delta = \frac{8}{15}\frac{\sqrt{R}}{\pi \cdot k_1}\delta_1^{5/2} \qquad \textbf{6-7}$$

and

$$w_2 = \int_0^{\delta_2} F_2 d\delta = \frac{8}{15}\frac{\sqrt{R}}{\pi \cdot k_2}\delta_2^{5/2} \qquad \textbf{6-8}$$

Therefore, the relationship between the elasticity and the force-distance curve at two different data positions is

$$\frac{w_1}{w_2} = \frac{k_2}{k_1}\left(\frac{\delta_1}{\delta_2}\right)^{5/2} \qquad \textbf{6-9}$$

From equation 6-6, the following equation is derived.

$$\frac{w_1}{w_2} = \left(\frac{k_1}{k_2}\right)^{2/3} \qquad \textbf{6-10}$$

where k is inversely proportional to E, the elastic constant which represents the local elasticity of the sample. The area under the force distance curve can be calculated and used to represent the inverse relative elasticity of the tissue scaffolding. Similar to reference [75], this area value was used to compare different samples.

In order to compare one tissue scaffold with another, it is required to maintain the maximum relative deflection to be a constant, which means the force (F) will be a constant. Constant maximum relative deflection should be provided.

Each force curve in all three samples was triggered to exhibit the same maximum relative deflection of 45nm. The histograms of elasticity for samples A, B and C are shown in Figure 6-11. As before, the mode, the mean value, the range, and the variance were investigated for each tissue scaffold sample, and the distribution was approximately analyzed. The results are shown in Table 6-2.

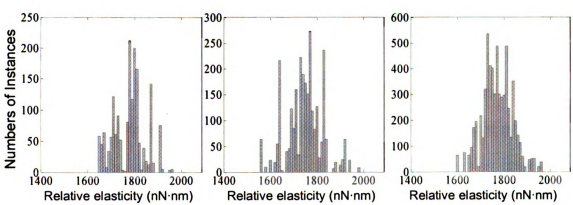

Figure 6-11 Elasticity histograms for (a) Sample A; (b) Sample B; (c) Sample C. Reproduced from Figure 4, Reference: Y. Fan, Q. Chen, et al. in press, Vol. 2, Issue 4, *Int. J. Nanomedicine* (2007)

The distribution of sample C was almost a normal distribution, while samples A and sample B had a symmetric but irregular distribution at both sides.

Two points were identified from the histogram analysis. The first was that samples A and B had similar distributions, but sample C had a different distribution even though the mode and mean of all three were close. The second was that sample B had the widest range, the largest variance and the most irregular distribution.

Table 6-2 Elasticity/Area Map Statistical Analysis

Sample	Data Points	Mode (nN· nm)	Mean (nN· nm)	Range (nN· nm)	Variance ((nN· nm)^2)
A	1739	1780.0	1777.8	1953.6~ 1961.4	4463.3
B	2757	1770.0	1747.5	1563.7~ 1979.2	5760.5
C	6325	1730.0	1770.7	1602.5~ 1961.4	4144.3

6.3 Comparison of Nanofiber Diameter by Transmission Electron Microscopy

TEM images of several nanofibers were taken to provide independent verification of nanofiber diameter, and from this, an estimate of the severity of tip-dilation artifacts present in the AFM images. Representative TEM images are shown in Figure 6-12. The nanofiber diameter measurements within the TEM images were taken using Scion Image software (http://www.scioncorp.com/). Scion Image was used to obtain a conversion factor relating pixels to nanometers using the scale bar in the lower right corner of the TEM images. Scion Image uses this conversion factor to measure lines drawn in the program's image editor in units of physical length. For each TEM image, three measurements of the nanofiber diameter were taken at distinct points along the length of

the wire. Care was taken to identify fluctuations in diameter that would be reflected in the mean and variance of the measurements.

Nanofiber diameter measurements within the AFM images were taken using the Nanoscope software. The software can be used to take a series of cross sections of the image orthogonal to the longitudinal axis of the nanofiber being measured. These cross sections are returned to the user as 1-dimensional signals representing height versus distance parallel to the cross section. The software can then be used to position markers at various points along the signal, allowing the user to measure the distance between them. As in the TEM images, three measurements were taken at a variety of points along the length of the chief nanofiber in each image. Variations in diameter were not as apparent in the AFM images, so care was taken to space the measurements evenly along the length of the nanofiber.

The discrepancy between the diameters measured using the TEM images and the diameters measured using the AFM images are given in table below. Based on these measurements, a dilation factor of over 100% was estimated for AFM measurements of all three samples. These results are demonstrative of the severity of tip dilation effects in AFM techniques. As previously discussed, an erosion operation was applied to both the surface roughness and elasticity data to restrict the properties analysis to the most reliable data.

Table 6-3 Nanofiber Diameter Measurements Using TEM and AFM Images

Image	Section 1 (nm)	Section 2 (nm)	Section 3 (nm)	Mean (nm)	Standard Deviation (nm)
TEM a1	120	100	130	116.6667	12.47219
TEM a2	110	120	150	126.6667	16.99673
TEM a3	109.86	99.78	105.74	105.1267	4.137933
TEM b1	117.67	117.02	106.88	113.8567	4.94038
TEM b4	111.3	77.52	97.52	95.44667	13.86834
TEM b9	65.91	111.96	98.03	91.96667	19.28252
TEM b12	110.01	94.34	91.89	98.74667	8.026939
TEM c3	69.14	82.53	84.76	78.81	6.898063
TEM c4	390	380	350	373.3333	16.99673
TEM c5	390	380	350	373.3333	16.99673
TEM c7	312.96	313.21	309.12	311.7633	1.871903
TEM c8	351.19	348.64	329.44	343.09	9.707986
TEM c9	345.83	325.06	327.96	332.95	9.184164
TEM c11	345.71	346.33	345.36	345.8	0.401082
TEM c14	415.95	388.83	345.04	383.2733	29.21432
TEM c16	377.23	369.2	337.71	361.38	17.05524
AFM A	647	589.91	494.77	577.2267	62.79142
AFM B	781.25	722.66	742.19	748.7	24.35819
AFM C	761.72	800.78	644.53	735.6767	66.39381
Average Dilation of A		**509.5275%**			
Average Dilation of B		**739.6577%**			
Average Dilation of C		**220.8495%**			

6.4 Comparison of Nanofiber Properties by Transmission Electron Microscopy

Typical TEM images of samples A, B, and C with corresponding selective area electron diffraction (SAED) images are shown in Figure 6-12. Samples A and B both showed a dark contrast outer layer surrounding a light contrast inner core, possibly hollow, while sample C was solid throughout. Diffraction images for samples A and B showed prominent rings typical of disordered structures while diffraction images for sample C showed spots typical of an ordered (crystalline) structure. These results indicated that the atomic arrangement of sample C nanofibers was substantially different from sample A and B nanofibers.

Close-up TEM images of samples B and C are shown in Figure 6-13. These images are consistent with the normal and narrow surface roughness distribution of sample C as well as the wide variance and irregular surface roughness distribution of sample B. Therefore the TEM results were consistent with the results obtained by SPRM which consistently indicated 1) that sample C was different from both samples A and B, and 2) that samples A and B, while similar, had differences with sample B having the more extreme values.

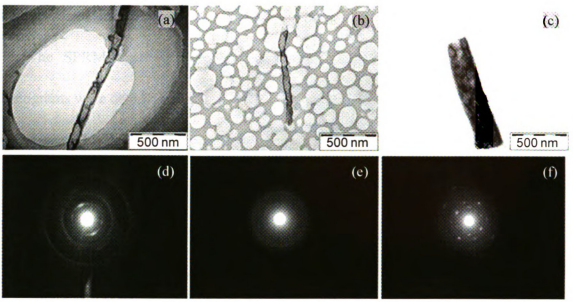

Figure 6-12 TEM images of (a) Sample A; (b) Sample B; (c) Sample C, with corresponding selective area electron diffraction (SAED) images shown beneath. Reproduced from Figure 7, Reference: Y. Fan, Q. Chen, et al. in press, Vol. 2, Issue 4, *Int. J. Nanomedicine* (2007)

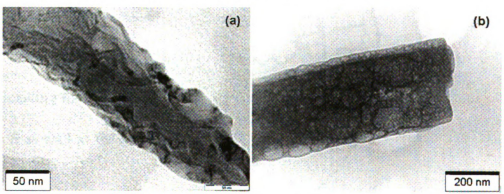

Figure 6-13 Close up images (a) Sample B; (b) Sample C. Reproduced from Figure 8, Reference: Y. Fan, Q. Chen, et al. in press, Vol. 2, Issue 4, *Int. J. Nanomedicine* (2007)

6.5 Conclusion & Discussion

Using SPRM, we have performed investigations of tissue scaffold properties directly along individual nanofibers. We have investigated surface roughness and elasticity properties that influence cell attachment. This is the first time that statistically meaningful information has been extracted along individual nanofibers using an automatic procedure

that maintains uniformity of experimental conditions.

The SPRM approach provided a wealth of data. Statistical methods based on histograms were developed to analyze the surface roughness and elasticity properties of the tissue scaffold nanofibers. The mode, mean range variance and distribution of surface roughness and elasticity were analyzed for tissue scaffold samples A, B and C. Sample C consistently showed properties that differed from samples A and B. The most prominent differences were observed in the surface roughness and elasticity distributions rather than in the individual mode values.

TEM with electron diffraction analysis confirmed that both the structure and surface properties of sample C differed from those of samples A and B. The electron microscopy results were consistent with the results of the histogram analyses using SPRM generated data, including the large property variances and wide irregular distributions observed for sample B as well as for the small variances and narrow smooth distributions observed for sample C.

Preliminary investigations indicated that normal rat kidney cells (NRK2) showed good adhesion to sample C and poor adhesion to sample B tissue scaffolds [76]. Systematic cell studies with SPRM-characterized tissue scaffolds are reported in next two chapters.

SPRM has the obvious advantage of saving operation time by scanning only regions of interest. This is especially useful for investigations of tissue scaffold properties, as a scaffold is composed of many individual nanofibers. SPRM also enabled us to discriminate and use only the most reliable data from each nanofiber for the properties evaluations.

CHAPTER 7

7 CELL RESPONSE ANALYSIS

As discussed in Chapter 5, SPRM has been used for first-time investigations of surface roughness and elasticity directly along individual nanofiber within a tissue scaffold. The true nanofiber curvature was also identified by using deconvolution techniques to identify the "missed" artifact regions, and the true nanofiber diameter was estimated by using the Kasa circle fit techniques. Surface roughness, elasticity and 3D nanoscale curvature are all parameters which have been demonstrated to evoke strong cell attachment responses.

As discussed in Chapter 4, specific combination of these three properties plus regulatory protein surface chemistry should mimic the natural environment for successful regrowth of neural cells. The candidate's dissertation research explored the response of astrocytes to a series of 2D planar substrates, 3D unmodified nanofiber substrates and 3D peptide-modified nanofiber substrates designed to mimic the basal lamina. The unmodified and peptide-modified nanofiber substrates were characterized by SPRM.

Fibroblasts were investigated as a first model system for astrocytes. Then the astrocyte response was analyzed as a second model system. Fibroblasts and astrocytes are both actin-based cells, which means that they actively probe their environment through their extension of protrusions called lamellipodia (broad) and filopodia (narrow). The extensions form through the polymerization of actin filaments within the cells as a

reconfiguration endo-skeleton.

For actin-based cells, such as fibroblasts and astrocytes, cell motility towards and adhesion to tissue scaffolds results from the extension of cell protrusions due to actin polymerization. Motility and adhesion are triggered through a complex interaction of receptors at the leading edge of the protrusion with the external environment ahead, as well as with the cell internal environment behind. Cell sensing of surface roughness (haptotaxis), elasticity (durotaxis) and surface chemistry (chemotaxis)[61, 77, 78] are all known to trigger cell motility towards conditions which promote adhesion. Leading edge formation corresponds to a 10's of nanometers sensing area at the cell's extending tip. The environmental triggers should therefore be assessed on a comparable scale. Atomic force microscopy is an investigative tool with the correct nanometer-scale resolution and which may be used to investigate minimally conductive biological surfaces[79].

In a situation that reproduces its natural biological environment, cells will extend protrusions towards the scaffold. The initial attachment of the cell with scaffold surface is triggered through a complex interaction of chemical and mechanical receptors at the leading edge of the protrusion. Actin-based cells develop the protrusions through a dynamic cycle of assembly and disassembly of intracellular actin filaments. Recent research has provided new insight into the internal signaling cascades that promote the reorganization of actin filaments into aligned and branched internal structures that result in the extension of the two different types of protrusions, narrow filopodia and broad lamellipodia as shown in Figure 7-1 [80].

The use of scaffolds composed of biocompatible materials as vehicles to deliver or promote growth of cells within damaged tissues of the body is an exciting new tool for the field of regenerative medicine. To optimize the performance of these scaffolds for each type of tissue or application, new analytical methods must be developed that can examine the interaction of these cells with the surfaces of these scaffolds in vitro under a variety of biochemical and physical conditions at a resolution in the nanometer range.

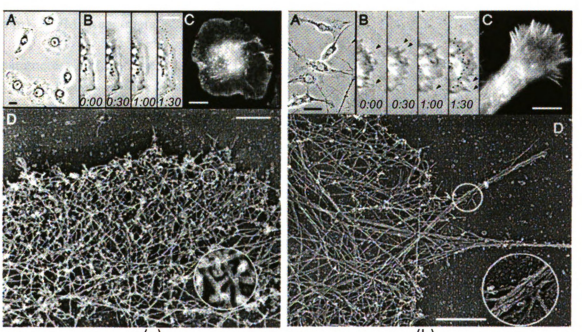

Figure 7-1 (a) Characterization ofS2R+ cells: A, Morphology of cell. Many cells display broad circumferential lamellipodia; B. Protrusive activity (time-lapse sequence). Lamellipodium protrudes with regular and smooth outline. Dotted line shows the initial position of the cell edge. Time in min:sec. C. Actin cytoskeleton (phalloidin staining). Circumferential lamellipodium is rich in actin. D. Structural organization of lamellipodia; (b) Characterization of BG2 cells. A. Morphology of cell population. Cells display polarized lamella. B. Protrusive activity (time-lapse sequence). Leading edge moves forward by combination of filopodial (arrowheads) and lamellipodial protrusion. Dotted line shows the initial position of the cell edge. Time in min:sec. C. Actin cytoskeleton (phalloidin staining). D. Structural organization of lamellipodia. Images from reference [80]

The topographic, mechanical and chemical properties of a series of tissue scaffolds fabricated from electrospun carbon nanofibers tissue scaffolds were investigated by

SPRM. Atomic force microscopy, phase contrast microscopy, selective staining & fluorescence microscopy were used to observe cell responses to these tissue scaffolds nanofibers. Phase Contrast Microscopy was performed on live cells using an Olmpus 1X70 inverted microscope. The images were captured by using IP lab scientific imaging software. The desiccated samples were optically examined during AFM imaging using a Sony XC-999P CCD color video camera microscope with a VCL-12S12XM lens (f = 12 mm). AFM was operated based on contact mode in ambient air. Other instrument parameters included the use of a J scanner with a maximum 125x125 square micron x-y scan range and silicon nitride tips with a nominal 20 nm tip radius of curvature.

The differences in cell responses corresponding to the differences in substrate properties are discussed.

7.1 Tissue Scaffold Samples & Experimental Techniques

7.1.1 Tissue scaffold samples

Samples of tissue scaffolds fabricated from electrospun [50, 51] carbon nanofibers were obtained from Donaldson Co., Inc. (Minneapolis, MN). The nanofibers were electrospun using an adapted electrospinning probe procedure described in Reference[52]. They were electrospun onto plastic coverslip for in-vitro study.

Four different surfaces: 2D, NANS, SANS and SANS + XL + D5/FGF-2, as shown in Figure 7-2, are target substrates to be investigated. Where 2D is planar plastic

coverslip; NANS are non-activated unmodified nanofibers; SANS are surface-activated nanofibers, functionalized with an amine group; and SANS + XL + D5/FGF-2 are SANS crosslinked and modified with D5 peptide or Fibroblast Growth Factor 2 (FGF-2). These nanofibers were randomly oriented polyamide nanofibers (a continuous fiber that collects as a nonwoven fabric). They were electrospun from a blend of two polymers [(C28O4N4H47)n and (C27O4.4N4H50)n] onto plastic coverslips.

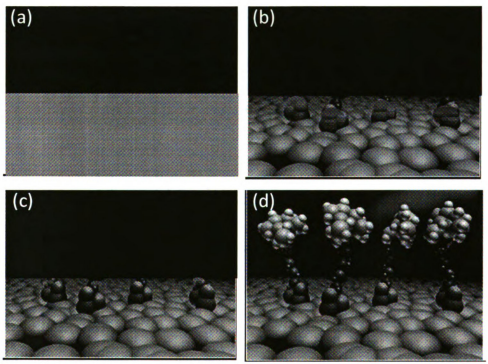

Figure 7-2 Four target substrates (a) 2D: planar plastic coverslip; (b) NANS: Non-activated nanofibers; (c) SANS: surface-activated nanofibers, functionalized with amine group; (d) SANS + XL + D5/FGF-2: crosslinked and modified with D5 peptide or FGF-2 growth factor.

7.1.2 SPRM Properties investigation of nanofibers

The new Scanning Probe Recognition Microscopy was used to analyze topographic, mechanical and chemical properties of NANS and SANSS+XL+FGF-2 nanofibers as discussed in chapter 6.

7.1.2.1 Surface roughness

The Surface Roughness property of unmodified and FGF-2 modified nanofiber substrates was analyzed as discussed in Chapter 6, with the creation of surface roughness maps and histograms, created from the collection of reliable data points from SPRM scan along individual nanofibers. The comparison between distributions of surface roughness property is shown in Figure 7-3. The result shows that NANS nanofibers have a slightly smaller surface roughness mode value. ~3 nm versus ~5 nm. The FGF-2 modified nanofibers have a larger surface roughness variance: more ~5-10 nm points.

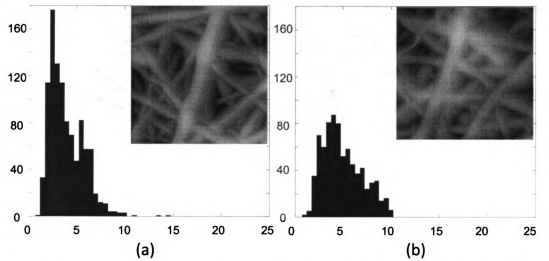

Figure 7-3 Histogram of surface roughness map for (a) NANS: unmodified nanofibers; (b) SANS + XL + FGF-2: crosslinked and FGF-2 modified nanofibers. AFM images of these two substrates are shown as the inside images, scan size: 5 μm.

7.1.2.2 Elasticity

The force curves are collected at the top of the nanofiber where the force vector is exactly normal to the sample surface as shown in Figure 7-4 by using the new Scanning Probe Recognition Microscopy as explained in chapter 6. Comparison of the results

shows that the FGF-2 modified nanofibers have a lower median Young's modulus and their variance is less too.

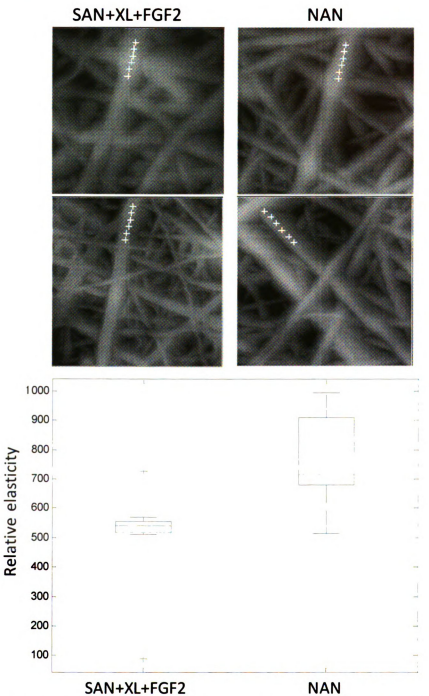

Figure 7-4 Box plots of elasticity for two different nanofiber substrates SAN+XL+FGF-2 and NAN. The top images are AFM images of these nanofibers, scan size: 5 μm. Points shown as crosses on AFM images are the positions where force curves are collected to calculate elasticity.

7.1.2.3 Surface chemistry

Chemistry as well as geometry of the extracellular matrix is critical for proper neuronal function. It is necessary to optimize chemical cues of a biomimetic surface for spinal cord repair. Fibroblast Growth Factor 2 (FGF-2) has demonstrated activity in the regulation of pathways that control regeneration and repair. FGF-2 is also observed to exist in astrocyte-capillary system in-vivo as shown in Figure 7-5. Therefore, it can be attached to nanofibers to recreate chemical cues in tissue engineering and regenerative medicine. FGF-2 provides an example of a peptide-modification that might enhance the function of a nanofibrillar scaffold.

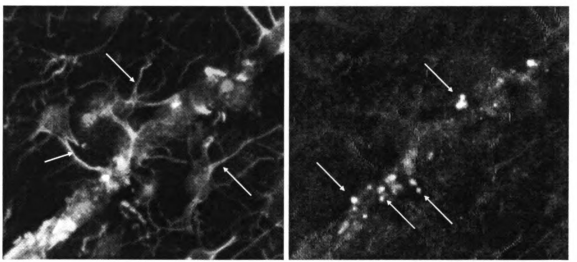

Figure 7-5 In vivo astrocyte-capillary system: astrocytes are pointed by arrows in (a); FGF-2s are dots pointed by arrows in (b). S. Meiners, et al. UMDNJ

(1) Phase Imaging technique to obtain chemical information

In tapping mode AFM, a stiff cantilever, which has a sharp tip at its free end, is excited at or near its free resonance frequency. The oscillation amplitude is used as the

setpoint parameter. The feedback loop adjusts the tip-sample distance to maintain constant oscillation amplitude in order to measure the topography of the sample surface [33]. Additionally, material properties variations could be mapped by recording the phase shift between the driving force and the tip oscillation. Tapping mode AFM allows us to obtain both topographic and compositional information in samples by recording the phase angle difference between the external excitation and the tip motion, which is called phase imaging. It has been shown in work by Garcia et al [81] that two tip-sample interaction regimes exist in tapping mode. These are designated the phase-repulsive and the phase attractive regime. The difference between them is shown in Figure 7-6 .

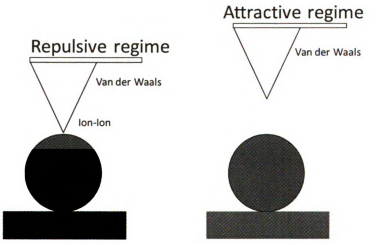

Figure 7-6 Repulsive regime versus attractive regime in Phase Imaging.

In the repulsive regime, the tip-sample interaction includes the strong ion-ion repulsion Coulomb force. In the phase attractive regime, scanning takes place with the tip at a distance from the sample surface which corresponds to a tip-sample interaction by Van der Waals Forces only. The height above the sample surface that corresponds to the division between the two regimes can be identified through analysis of force distance

curves as shown in Figure 7-7. The removal of the strong ion-ion repulsion has proved to be very important for imaging biological samples. An example taken from Garcia's work is shown in Figure 7-8.

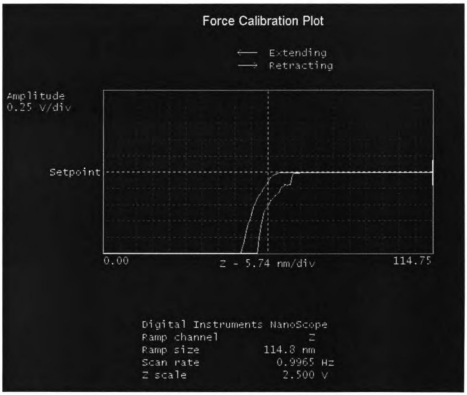

Figure 7-7 Force distance curve showing the division between the two regimes, this curve was taken on a SANS+XL+FGF-2 nanofiber sample.

The morphology and dimensions of the fragments that form antibodies are clearly visible in the image obtained at phase attractive mode as shown in Figure 7-8 (a), while the image obtained at phase repulsive mode has no clear evidence of the domain structure as shown in Figure 7-8 (b) [81].

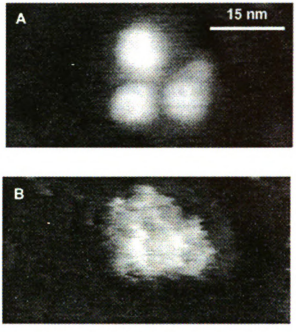

Figure 7-8 Characteristic morphologies of a-HSA antibody (a) phase attractive mode; (b) phase repulsive mode [81]

(2) Experimental results of using Phase Imaging technique

In our tapping mode experiments, imaging in the phase attractive mode is used to investigate surface chemical properties of unmodified nanofibers (NANS) and modified nanofibers (SANS+XL+FGF-2). Atomic force microscopy is performed in tapping mode in ambient air. Other instrumental parameters include the use of an E scanner with a maximum 10x10 square micron x-y scan range and silicon tips with a nominal 10 nm tip radius of curvature.

The phase images at attractive regime shows in Figure 7-9 (e)-(f) are recording the phase angle difference between the external excitation and the tip motion. Comparison between the phase images of unmodified nanofibers and modified nanofibers shows that this technique provided macromolecular resolution. The unmodified nanofibers have a

smooth phase image, while structures at nanometer level (about 15 nm) appear on the modified nanofibers as shown in Figure 7-9. 15 nm is consistent with the expected size of FGF-2 protein. Therefore, imaging in the phase attractive regime provided first-time direct quantification of the FGF-2 peptide modification. Based on these images, the peptide-modified nanofiber appears to be densely covered with FGF-2 macromolecules. Coverage density is a very important property to quantify and should reproduce in vivo or wound healing overages. For comparison, phase images taken in phase repulsive mode are shown in Figure (c)-(d). The results are consistent with those obtained by Garcia: no clear evidence of peptide domain structures could be obtained in phase repulsive mode.

Phase imaging of modified nanofibers in attractive mode provided detailed information of the structures on the nanofiber as shown in Figure 7-9 (e), but it is hard to maintain the weak tip-sample interaction when there are large variations at the sample surface. Therefore, Phase Imaging in the attractive regime displayed loss of contact when imaging boundary regions of nanofibers.

SPRM is currently being adapted for use in Tapping Mode/Phase Imaging along nanofibers. SPRM auto-tracking will enable phase attractive imaging through decrease of surface variations.

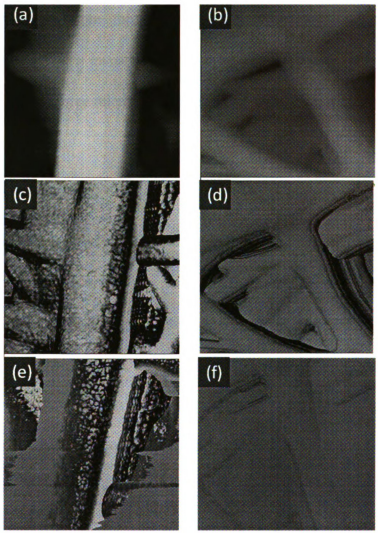

Figure 7-9 surface chemistry characteristics (a) height image of SANS+XL+ FGF-2, Z range for height image is 500 nm; (b) height image of NANS, Z range is 1000 nm; (c) phase image of SANS+XL+FGF-2 at repulsive mode, Z range is 75 °; (d) phase image of NANS at repulsive mode, Z range is 20 °; (e) phase image of SANS+XL+FGF-2 at attractive mode, Z range is 75 °; (f) phase image of NANS at attractive mode, Z range is 20 °. Image scan size is 1 μm.

7.2 First Model System: Fibroblasts on 2D versus Nanoscale 3D Nanofibers

The responses of 3T3 NIH fibroblasts to 2D planar surfaces versus their response to nanofiber mat surfaces, which have 3D nanoscale curvature effects, were investigated by our group as first model system for astrocytes. The interactions of filopodia and

lamellipodia emanating from the NIH 3T3 fibroblasts with 2D planar and 3D nanofibrillar surfaces were investigated by using phase contrast microscopy, optical microscopy and atomic force microscopy. The 3D nanofibrillar surfaces were previously investigated using SPRM.

7.2.1 Cell culture

NIH 3T3 fibroblast cells were cultured for 24 hours on two different surfaces, planar (2D) tissue culture plastic and amine coated nanofibers (SANS). The amine coated nanofibers (SANS) were randomly oriented polyamide nanofibers electrospun by Donaldson Co., Inc. (Minneapolis, MN). They were electrospun from a blend of two polymers [(C28O4N4H47)n and (C27O4.4N4H50)n] onto plastic coverslips. The polymeric nanofiber mat was cross-linked in the presence of an acid catalyst and formed a dense network of filaments 50-80 nm in diameter with minimal porosity. The nanofibers were covalently coated with a proprietary polyamine polymer by Surmodics, Inc. (Eden Prairie, MN) to provide functional groups for further covalent modification of the nanofibers with bioactive peptides.

Samples for optical and AFM microscopy were fixed with 2.5% glutaraldehyde in 0.1% phosphate buffer for 15 minutes, briefly rinsed with 0.1M phosphate buffer and washed 3 times with triple distilled water. The samples were then permitted to desiccate in air for 48 hours prior to optical and AFM imaging.

7.2.2 Experimental investigation of fibroblasts response

3T3 NIH fibroblasts are cultured on two different surfaces, tissue culture plastic (2D) and amine coated nanofibers. In order to investigate cell response, fibroblasts cultured on these two surfaces were observed and compared by using different techniques.

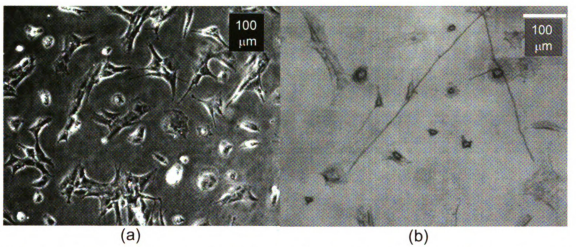

Figure 7-10 Fibroblasts cultured on 2D surface. (a) Phase contrast microscopy of live cells, and (b) Optical microscopy of fixed cells indicate similar morphologies. Reproduced from Figure 1, Reference: Q. Chen, Y. Fan, et al, Mater. Res. Soc. Symp FF. Proc. (2007)

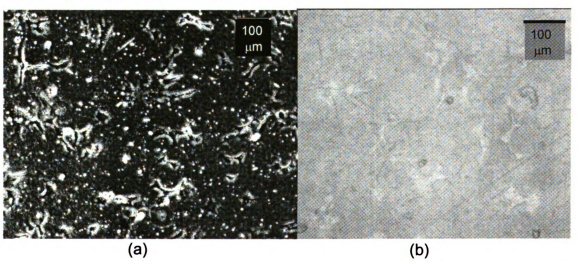

Figure 7-11 Fibroblasts cultured on amine coated nanofibers. (a) Phase contrast microscopy of live cells, and (b) Optical microscopy of fixed cells indicate similar morphologies. Reproduced from Figure 2, Reference: Q. Chen, Y. Fan, et al. Mater. Res. Soc. Symp FF. Proc. (2007)

Phase contrast images of living fibroblasts at the end of the first 24 hours are shown

in Figure 7-10 (a) and Figure 7-11 (a). Bright field images of the desiccated cells shown in Figure 7-10(b) and Figure 7-11 (b) show similar morphologies. A difference in cell morphology was observed using phase contrast and bright field microscopy.

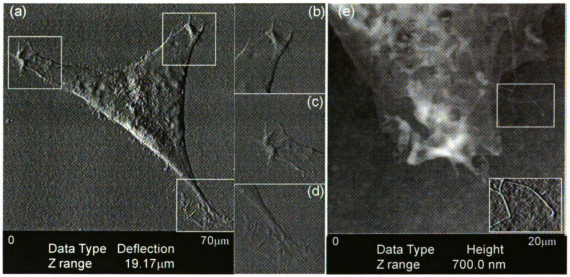

Figure 7-12 AFM images of 3T3 NIH fibroblast cultured on 2D surface. (a) Deflection image of a typical fibroblast; (b) Close-up deflection image of top right region; (c) Close-up deflection image of top left region; (d) Close-up deflection image of bottom right region; (e) Height image of vertex region for another cell showing structures (close-up deflection image in inset). Reproduced from Figure 3, Reference: Q. Chen, Y. Fan, et al. Mater. Res. Soc. Symp FF. Proc. (2007)

AFM images shown in Figure 7-12 and Figure 7-13 provided more detailed information about size, and shape of fibroblasts growing on the two different surfaces. The cell body size of fibroblasts was about 50µm in both cases. However, fibroblasts grown on the tissue culture plastic 2D surface showed fine filopodia-like structures at the ends of pointed projections, as shown in Figure 7-12. Fibroblasts grown on the amine coated nanofibers showed blunted lamellipodia-like projections extending over several nanofibers. These projections lacked the fine filopodia-like end structures. Fibroblasts grown on the amine coated nanofibers were also observed to show a great number of

cell-cell interactions between the blunted vertices as shown in Figure 7-13. Both factors contributed to the changed appearance of the 2D and nanofiber cultured fibroblasts observed in the images obtained using phase contrast and bright field microscopy.

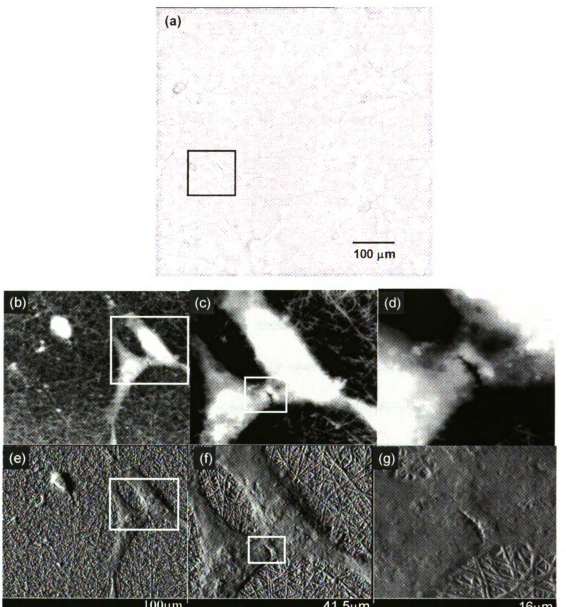

Figure 7-13 3T3 NIH fibroblast cultured on amine coated nanofibers (SANS). (a) Multiple cell-cell interactions on the SANS are observed in the optical microscopy image. The cells in the black box are shown in close-up AFM images in (b) through (g). (b) through (d): increasing close-up AFM height images; (e) through (g): corresponding increasing close-up AFM deflection images. Reproduced from Figure 4, Reference: Q. Chen, Y. Fan, et al. Mater. Res. Soc. Symp FF. Proc. (2007)

7.2.3 Comparison of fibroblasts response and conclusion

3T3 NIH fibroblasts cultured on two different types of surfaces: tissue culture plastic and amine coated nanofibers (SANS) are observed by using phase contrast microscopy, optical microscopy and atomic force microscopy. The cell body size of fibroblasts was about 50μm in both cases. However, fibroblasts grown on the tissue culture plastic 2D surface showed fine filopodia-like structures at the ends of pointed vertices while fibroblasts grown on the amine coated nanofibers showed blunted lamellipodia-like vertices extending over multiple nanofibers. Fibroblasts grown on the amine coated nanofibers (SANS) were also observed to show a greater number of cell-cell interactions between the blunted vertices. Both factors contributed to the changed appearance of the 2D and nanofiber cultured fibroblasts observed. The appearance of the vertices and the greater number of observed cell-cell interactions suggests the possible formation of a greater number of adherens junctions. If this is so, it further suggests that amine-coated nanofibers (SANS) may stimulate Rac activation since Rac activation stimulates the formation of adherens junctions.

The remarkably different response of the actin based cells to a nanoscale 3D versus the planar 2D situation may prove to be medically important. 3T3 and embryonic fibroblasts are being used by our group as first model system for astrocytes which are another actin based cell system.

7.3 Second Model System: Astrocytes on 2D versus Nanoscale 3D Nanofibers

The astrocyte system was next investigated, which is another actin based cell system. Astrocytes perform multiple functions for brain and spine neuronal systems, including biochemical support of endothelial cells which form the blood-brain barrier, providing food and waste removal for the nervous tissue, and a principal role in the repair and scarring process in the brain [82]. Astrocytes can provide direct cell body-cell body mechanical support for neuron cell bodies. Astrocytes can also provide indirect mechanical support for neuronal systems through the generation of astrocyte-derived extracellular matrix molecules [53].

Astrocytes have environmental requirements which enable healthy function. Healthy versus pathological astrocyte development on nanoscale 3D nanofibers versus planar substrates are observed. Promising result of in vivo implantation of slowly degradable nanofiber scaffolds composed of electrospun polyamide nanofiber random meshes in the rat confirms these observations [83]. We will focus on the response of astrocyte, such as attachment and division, to 2D planar substrate and 3D nanofibrillar substrate, as this step is important for nerve system regeneration. Surface chemistry of nanofibers would affect astrocyte regeneration in its search for an attractive environment. Therefore, both unmodified nanofibers and FGF-2 modified nanofibers are included in the analysis.

7.3.1 Cell culture

Astrocyte cells were cultured on three different surfaces, 2D, NANS and SANS+XL+FGF-2 for 24 hours in one group and on the same three substrates for 48 hours in another group. Samples for optical and AFM microscopy were fixed with 2.5% glutaraldehyde in 0.1% phosphate buffer for 15 minutes, briefly rinsed with 0.1M phosphate buffer and washed 3 times with triple distilled water. The samples were then permitted to desiccate in air for 48 hours prior to optical, AFM imaging.

7.3.2 Experimental investigation of astrocytes response

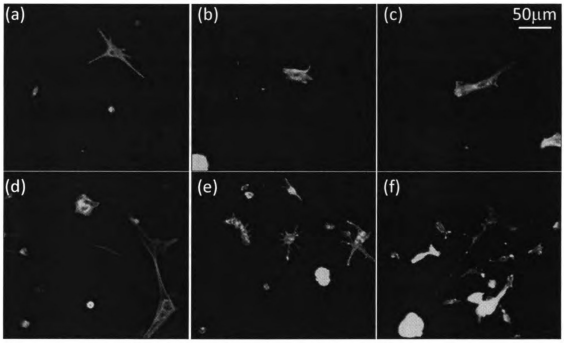

Figure 7-14 Actin stain + Fluorescent Microscopy images of astrocytes on different substrate (a) astrocytes on 2D substrate imaged at 24 hours; (b) astrocytes on NANS at imaged 24 hours; (c) astrocytes on modified NANS imaged at 24 hours; (d) astrocytes on 2D substrate imaged at 48 hours; (e) astrocytes on NANS imaged at 48 hours; (f) astrocytes on modified NANS imaged at 48 hours

Astrocytes are cultured on 2D, NANS and peptide-modified SANS+XL+FGF-2 for 24 hours in one group and for 48 hours in another group. Both groups were observed by

fluorescent microscopy after actin stained as shown in Figure 7-14. At 24 hours, all cells are probing their environments. By 48 hours, astrocytes on nanofibers have a more in vivo-like morphology indicating a good environment as shown in Figure 7-14.

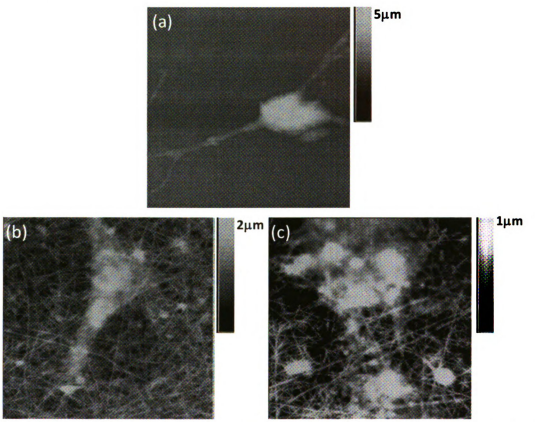

Figure 7-15 AFM images of astrocytes grown on different substrates for 24 hours (a) 2D substrate; (b) NANS; (c) modified NANS. Image scan size : 50 μm

Atomic force microscopy is performed in contact mode in ambient air. Other instrumental parameters include the use of a J scanner with a maximum 125x125 square micron x-y scan range and silicon nitride tips with a nominal 20 nm tip radius of curvature.

Even at 24 hours, AFM images of astrocytes on different substrates show differences as shown in Figure 7-15. Astrocytes on nanofibers develop very thin (~1 actin layer thick) broad processes to probe their environments. This was similar to the cell response

observed for NIH 3T3 fibroblasts previously discussed. Also astrocytes on nanofibers show more cell-cell interactions. The number of cell-cell interactions appeared to increase for FGF-2-modified nanofibers.

7.3.3 Conclusion

The new Scanning Probe Recognition Microscopy has been successfully used to quantify 3D nanoscale cues: elasticity, surface roughness and peptide modification in tissues scaffold nanofibers. Cell responses to these different nanofibers are also reported. Therefore, successful assessment cell response to variations in nanofiber properties accurately quantified using SPRM may provide vital insights that lead to successful spinal cord repair techniques.

CHAPTER 8

8 ELECTROSPINNING PARAMETERS

As discussed in Chapter 4, In spinal cord repair, individual external triggers in the cell environment that stimulate dynamic cell responses include surface roughness, elasticity and surface chemistry. The ultimate goal is to find the best tissue scaffold with most appropriate topographical, mechanical and chemical properties for specific cells or cell classes. These properties of nanofibers can be analyzed by using the new Scanning Probe Recognition Microscopy technique. Cell responses can also be investigated by SPRM and other optical techniques. Information can be combined to provide a composite picture representative of a cell's perception of its environment. Then, the electrospinning materials or parameters can be adjusted adaptively until the properties of the produced nanofibers are found to be best for cell regeneration. The whole procedure will provide an automatic guide to design tissue scaffold for its application in regenerative medicine.

The new Scanning Probe Recognition Microscopy was used to investigate of the influence of droplet size on electrospun carbon nanofiber properties. The key property under investigation is the effect of electrospinning conditions on the resulting carbon nanofiber elasticity. [84]

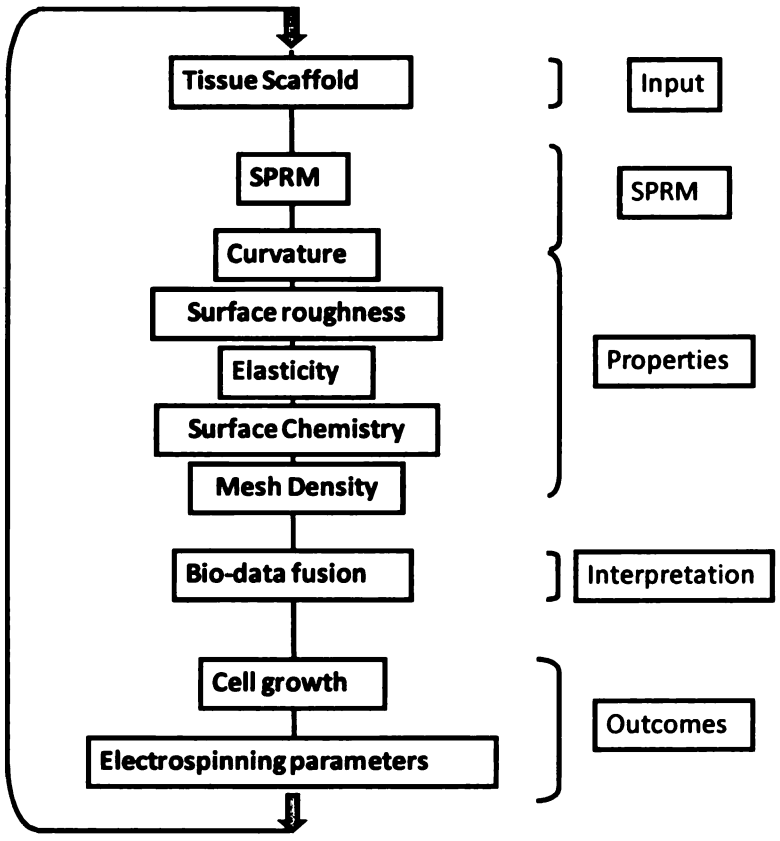

Figure 4-6 (repeated) Application of SPRM in spinal cord repair

8.1 Introduction

Electrospun carbon nanofibers are hollow core carbon structures produced by self-assembly within an evaporating liquid jet. They are of great interest as biocompatible carbon-based structures for tissue scaffold applications.

Electrospinning-based self-assembly is achieved by the application of an electrostatic force between a charged droplet containing polymer monomers in liquid suspension and a collecting metal electrode [85, 86]. A charged droplet of monomer in liquid suspension is formed at a capillary tip, conveniently a metal syringe tip of known bore radius. A 20-30 kV potential difference is applied between the syringe tip and a metal collecting

plate, held 10-20 cm apart. At a critical field, the force due to the electric field overcomes the surface tension forces holding the droplet, and the solution starts flowing towards the collecting electrode in the form of a charged jet. Initially, the charged droplet deforms into a cone, which then separates into splayed charged jets due to mutual repulsion. As the liquid in each splayed jet evaporates, the jet diameter shrinks rapidly, creating the conditions for self assembly of the polymers into nanofibers. The diameters of the collected electrospun carbon nanofibers may range from a few microns to as low as 10 nanometers depending on the complicated interplay of Coulomb forces. Electrospun carbon nanofibers used in tissue scaffold applications typically have diameters on the order of ~100 nm.

Results of an investigation of monomer choice, to control the initial droplet charge state, and syringe bore size, to control the initial droplet radius/surface tension, are presented in this chapter. In Series 1, 15% weight of poly methyl methacrylate suspended in tetrahydrofuran (THF)/Dimethylformamide (DMF) was electrospun using a 200 micron fixed bore radius, without and with the addition of 6% single walled carbon nanotubes produced by NASA-GSFC Cooled Welding Method added to the suspension. In Series 2, 15% weight of poly (ε-caprolactone) suspended in Methylene Chloride (MC)/ Dimethylformamide (DMF) was electrospun using bore radii of 152.4, 254.0 and 406.4 microns. The tip to collector plate distance was held constant at 10 cm. The voltage was held constant at 25kV. A key property under investigation in our group is the effect of electrospinning conditions on resulting carbon nanofiber elasticity.

8.2 Experimental Setting

Poly (methyl methacrylate) (PMMA) with a molecular weight of 120,000 and poly (ε-caprolactone) with a number average molecular weight (Mn) of 80,000 from Aldrich Chemical were used in these experiments Figure 8-1 (a-b). Single walled carbon nanotubes, 6 % by weight, produced by NASA-GSFC Cooled Welding Method were added to one batch of PMMA experiments. The electrospinning set-up consisted of a Sorensen 230-3/12P R&D high voltage DC power supply, with a syringe and an 8x12" aluminum collecting foil held 10 cm apart. The experiments were horizontally configured, with the syringe tilted about 300 to facilitate droplet formation Figure 8-1 (c).

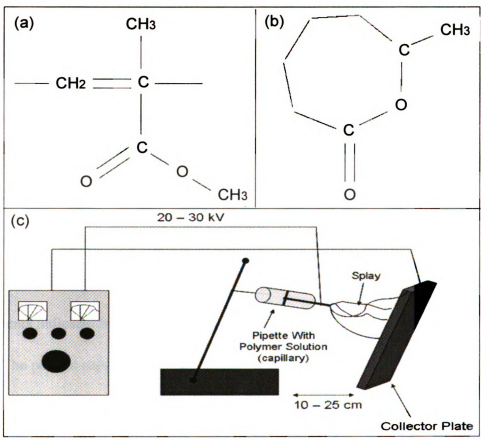

Figure 8-1Polymer monomers (a) poly (methyl methacrylate), and (b) poly (ε-caprolactone). (c) Experimental configuration of electrospinning experiment.

Field emission scanning electron microscopy (FESEM) of gold coated samples was used to assess the initial non-woven mat topography and nanofiber diameter, and to confirm that subsequent atomic force microscopy results were truly representative. Field emission scanning electron microscopy was performed using a Hitachi S-4700II Field Emission SEM operated at 1.0 kV.

Atomic force microscopy (AFM) was performed using a Veeco Nanoscope IIIA Scanning Probe Station, in contact mode with a nominal tip radius of 25 nm, operated in ambient air. A silicon nitride tip was used. The silicon nitride tip (hardness $\approx$ 35 GPa), was assumed to be much harder than any of the tissues scaffold samples.

8.3 Experimental Results

The PMMA monomers with and without single walled carbon nanotubes were electrospun under conditions of 200 microns bore radius,10 cm between the tip and the collector foil, and 25kV electrostatic potential difference. The results are shown in Figure 8-2. Electrospinning of both resulted in micron-scale diameter fibers. This is too large for tissue scaffold applications and PMMA was not investigated further. Anomalous beam and tip deflections observed during the electron and atomic force microscopy experiments indicated highly charged surface states.

The poly (ε-caprolactone) monomers were electrospun under conditions of 10 cm between the tip and the collector foil and 25kV electrostatic potential difference. The bore radius was varied through (a) 152.4, (b) 254.0, and (c) 406.4 microns. The results

are shown in Figure 8-3. The nanofiber average diameter was ~ 90-110 nm, increasing slightly as the bore size was increased. Nuisance bubbles were observed in addition to the nanofibers. The average diameter of the nuisance bubbles deceased by ~50% as the bore size was increased.

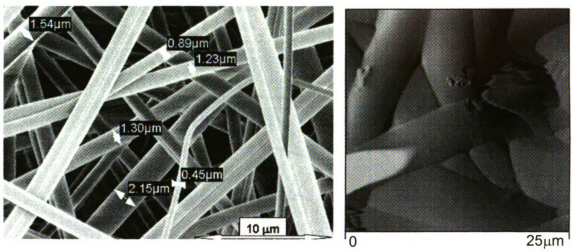

Figure 8-2 (a) Field emission SEM of PMMA-based carbon nanofibers and (b) atomic force microscopy of PMMA-based carbon nanofibers with 6% weight of single walled carbon nanotubes added. A 200 micron bore radius resulted in micron-scale diameter nanofibers. Reproduced from Figure 2, Reference: Rutledge, S.L., Shaw, H. C., Benavides, J. B., Yowell, L. L., Chen, Q., Jacobs, B. W., Song, S. P., Ayres, V. M., Diamond and Related Materials, 2006. 15(4-8): p. 1070-1074 [84]

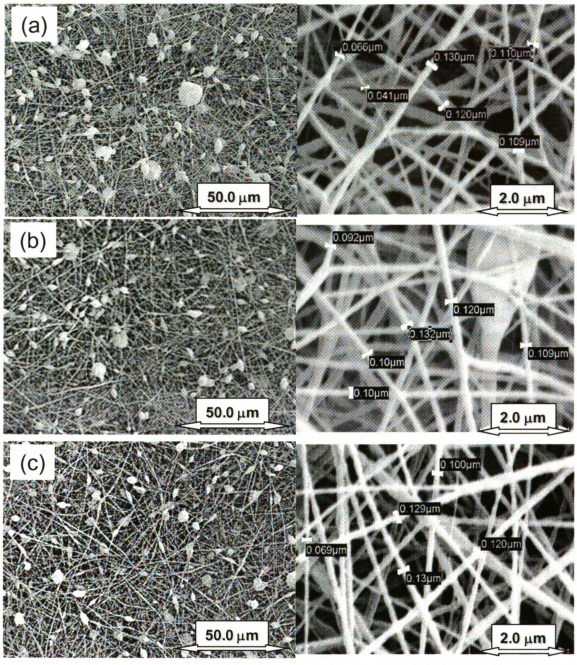

Figure 8-3 Field emission SEM of poly (ε-caprolactone) carbon nanofibers spun at bore radii (a) 152.4, (b) 254.0, and (c) 406.4 microns. As the bore size was increased, a slight increase in fiber diameter with a large decrease in bubble size was observed. Reproduced from Figure 3, Reference: Rutledge, S.L., Shaw, H. C., Benavides, J. B., Yowell, L. L., Chen, Q., Jacobs, B. W., Song, S. P., Ayres, V. M., Diamond and Related Materials, 2006. 15(4-8): p. 1070-1074 [84]

SPRM was used to measure the relative elasticity between the three poly (ε-caprolactone) nanofiber samples and the metal foil. As the AFM tip is vertically

indenting a cylindrical object, only data collected along the top and center of each nanofiber matches the model. Then new SPRM technique can collect reliable force curves along this region by its recognition capability. Elasticity property of these three nanofibers electrospun with different bore sizes can be investigated by using SPRM technique as explained in chapter 6. Results show that the mean force distance curve areas increased with increasing bore radius, which indicate a decrease in sample elasticity with increasing bore radius as shown in the following Figure.

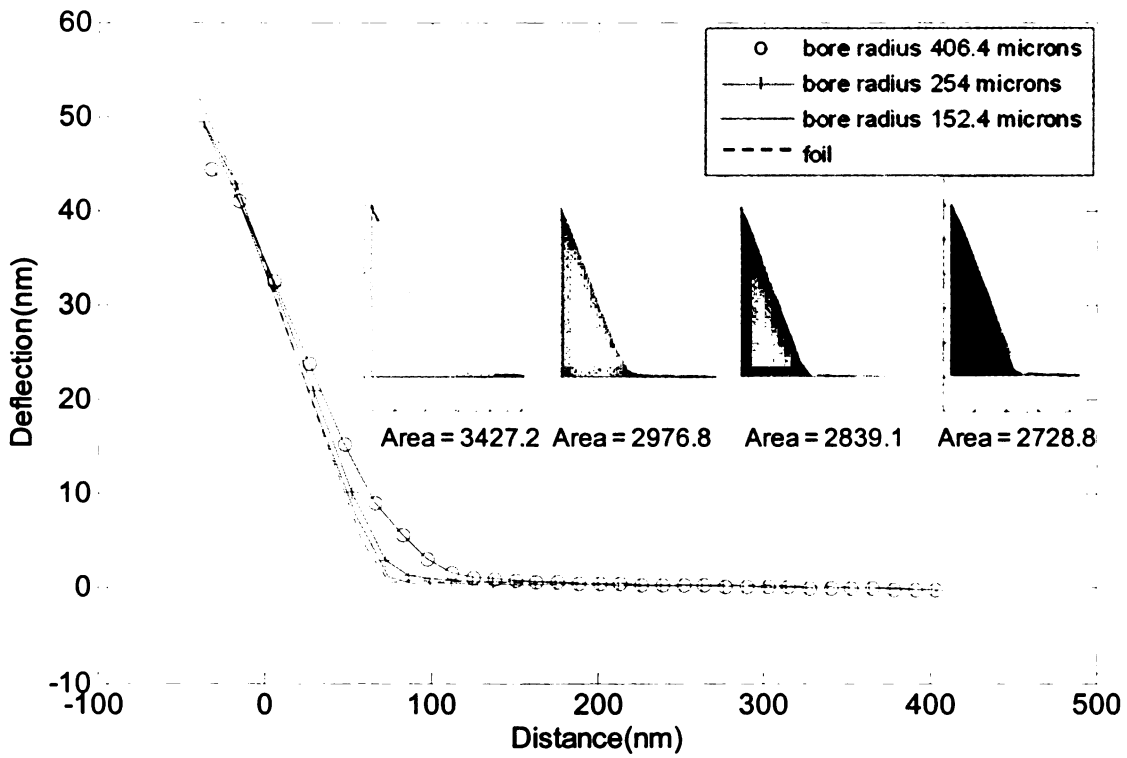

Figure 8-4 Mean force distance curves for three nanofibers samples electrospun with different bore radii and the aluminum foil. The mean force distance curve areas increased with increasing bore radius (insets), indicating a decrease in nanofiber elasticity with increasing bore radius. Reproduced from Figure 5, Reference: Rutledge, S.L., Shaw, H. C., Benavides, J. B., Yowell, L. L., Chen, Q., Jacobs, B. W., Song, S. P., Ayres, V. M., Diamond and Related Materials, 2006. 15(4-8): p. 1070-1074 [84]

8.4 Discussion and Conclusion

A 15% weight of poly (ε-caprolactone) suspended in Methylene Chloride (MC)/Dimethylformamide (DMF) was shown to produce electrospun carbon nanofibers with average diameters ~ 90-110 nm. The average nanofiber diameter was observed to increase slightly as the bore size was increased. There is a large body of research on control of electrospun nanofiber diameter, which indicates that the monomer charge density and polymer solution concentration have the greatest influence, by varying the charge concentrations, and hence the Coulomb forces. For electrospun carbon nanofibers used in tissue scaffold applications, diameters that mimic the structural portion of the extracellular matrix (ECM) are desirable. The ECM is composed of fibrillar collagen 50-300 nm in diameter. Therefore, the Series 2 nanofibers had acceptable diameters for potential tissues scaffold applications.

The mean value force distance curves for data analyzed along several nanofibers indicated a decrease in relative elasticity with increasing bore radius. This is a new result. The correlations between electrospinning parameters (bore radius) and properties of produced nanofibers (diameter, elasticity) may lead to dynamically adjusting electrospinning parameters in order to get desired nanofibers properties. It will be very important for many applications of nanofibers, for example, applying electronspun nanofibers as implantable artificial tissues in regenerative medicine.

Part III Conclusion & Future Work

Part III CONCLUSION & FUTURE WORK

CHAPTER 9

9 CONCLUSION & DISCUSSION

9.1 Conclusion

A new scanning probe microscopy modality: Scanning Probe Recognition Microscopy system has been developed. The new SPRM system gives the scanning probe microscopy itself the ability to auto-track regions of interest through incorporation of recognition-based tip control. A low resolution scan to identify regions of interest is followed by auto-track high resolution scans of just these areas. SPRM has the advantages of providing more meaningful information about samples automatically, efficiently and accurately. SPRM enables investigations in many situations in which standard SPM is insufficient. Investigations of biomimetic properties along individual nanofibers in actual tissue scaffolds used for regenerative medicine in spinal core repair showcases the power of SPRM within a significant biomedical investigation.

Tissue scaffolds for spinal cord repair are a specific example of regenerative medicine, with national importance and current emphasis. Electrospun polyamide nanofibers are nanoscale 3D platforms for regenerative medicine. Nanoscale curvature is indicated as a key biomimetic aspect. Tissue scaffolds made from nanoscale 3D nanofibers must reproduce the physical properties and the functions of the basal lamina/basement membrane. The SPRM system developed by our group enables SPM to have recognition ability and be able to auto-track regions of interest, which are individual

nanofibers. Therefore, investigations of tissue scaffold properties directly along individual nanofibers are possible. We have performed investigations of curvature, surface roughness, elasticity and surface chemistry properties that have been shown to influence cell attachment in statistically meaningful detail.

Investigations of cell attachment to the 2D and nanoscale 3D nanofiber surfaces, which have different topographical, mechanical and chemical properties, are observed. The remarkably different response of the actin based cells to planar 2D versus nanoscale 3D situation provide vital insights that head to use tissue scaffolds made of electrospun nanofibers for successful spinal cord repair techniques. The correlation of cell responses with nanofiber properties analysis are discussed.

9.2 Discussion

The new Scanning Probe Recognition Microscopy has great potential to be used in many research fields where macro/nano-scale resolution is required. SPRM also has the flexibility to be able to extend into different applications. As one reviewer of one of our successful grant applications expressed it, "This is enabling technology for nanoscience". Initial research work is done in applying SPRM into the following research topics. More future work at these aspects will be discussed in detail in the next chapter.

CHAPTER 10

10 FUTURE WORK

The new Scanning Probe Recognition Microscopy has been successfully used to solve problems in tissue engineering that require macro/nano-scale resolution. It also has great potential to be applied to many other research fields because of its flexibility to extend into different applications. Several directions of future work that are under investigation are listed.

10.1 Improvement of SPRM Recognition Capability

More image processing and pattern recognition techniques can be integrated in SPRM to make it more powerful in feature recognition and information processing. Additional algorithms are under investigation to make SPRM to run more efficiently, accurately and reliably.

Different types of information are available from Scanning Probe Microscopy, such as height information, deflect information and friction information in contact AFM. How to combine and fuse all these information to get the best feature recognition ability and optimal algorithms is also an ongoing work.

10.2 Extended Work in Spinal Cord Repair

In spinal cord repair, several other aspects can also be investigated by the new Scanning Probe Recognition Microscopy technique. Future work will develop SPRM-based porosity and mesh density investigations, as this is known to be an

important property for cell motility and adhesion[58].

The ultimate goal is to find the tissue scaffold with most appropriate topographical, mechanical and chemical properties from cell regeneration. These properties of nanofibers can be analyzed by using the new Scanning Probe Recognition Microscopy technique. The next step is to adjust the electrospinning materials or parameters adaptively until the properties of the produced nanofibers are best for cell regeneration as shown in Figure 10-1. It will provide an automatic guide in tissue scaffold design.

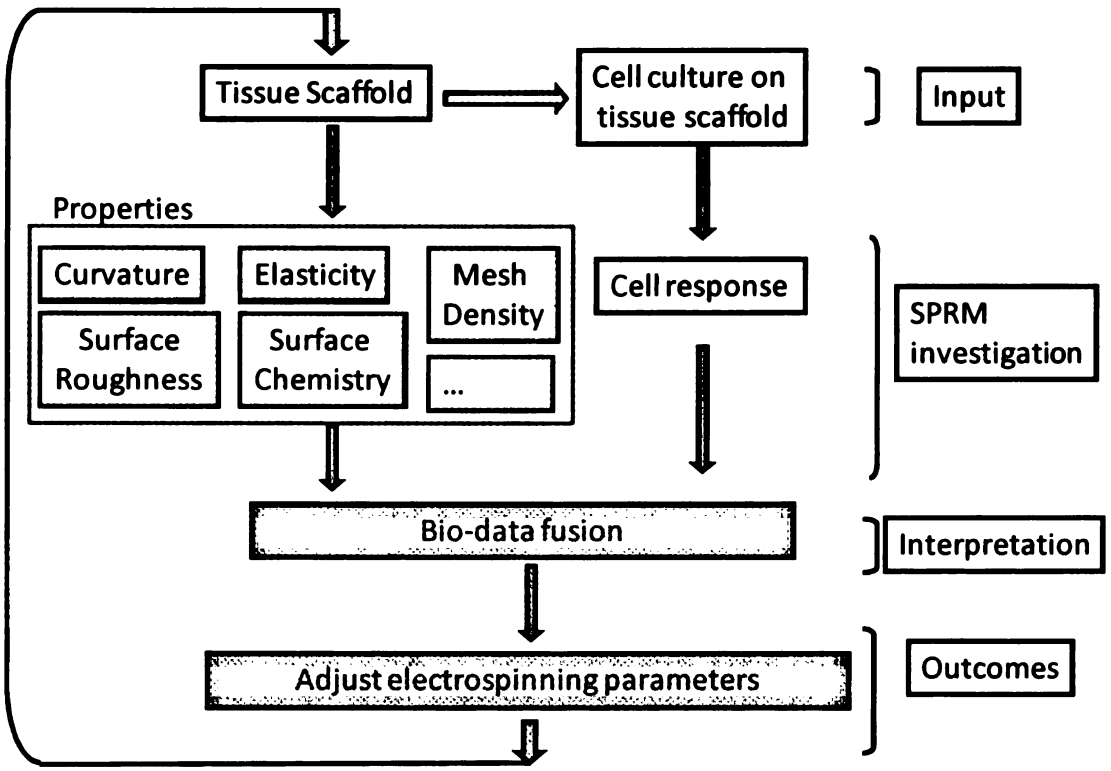

Figure 10-1 Diagram of providing an automatic guide for tissue scaffold design

10.3 Extension of SPRM to Additional Research Problems:

Nanocircuits

Nanowire made from a wide variety of materials has demonstrated extraordinary electronic, mechanical and chemical characteristics. The new Scanning Probe

Recognition Microscopy can be used to detect the contact pad and nanowire radial boundary.

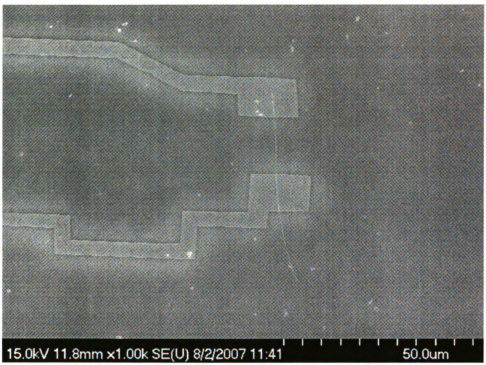

Figure 10-2 SEM images of nano circuits

For the nanocircuits investigation, several aspects of investigation require the ability to auto-track the scan path to proceed from the conducting contact pad onto the semiconducting nanowire, while avoiding the insulating oxide layer.

Initial experiments are done to auto-track a nanowire by using SPRM working under contact mode AFM setting. Experimental results indicate the nanowire can be tracked by using recognition based tip control of SPRM as shown in Figure 10-3. The image captured by standard AFM is shown in Figure 10-3 (a). Figure 10-3 (b) shows the simulation result, which indicate that the scanning scheme can detect the edges very well

and predict the boundaries accurately. Therefore, the nanowire can be auto-tracked reliably. Experimental result in real-time are displayed in Figure 10-3 (c) where the regions that are not really scanned are padded with 0 (dark region) for display.

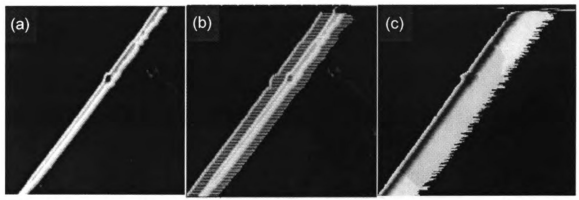

Figure 10-3 Scanning scheme implementation for GaN anocircuit: (a) Image captured by standard SPM, the image side is 5 x 5 microns; (b) Scanning scheme simulation showing lines of the scan plan; (c) Real-time image captured by SPRM system using self-defined scanning scheme along the nanowire. Reproduced from Figure 4, Reference: B.W. Jacobs, V.M. Ayres, M.A. Tupta, R.E. Stallcup, A. Hartman, J.B. Halpern, M-Q. He, M.A. Crimp, A.D. Baczewski, N.V. Tram, Q. Chen, Y. Fan, S. Kumar, L. Udpa , 2006 6th IEEE Conference on Nanotechnology Proceedings

Another potential application of the new Scanning Probe Recognition Microscopy is to use its recognition ability to locate the nanowire in the nanocircuits automatically with a fast scan with low resolution. Once the nanowire is detected, SPRM can start a relatively low scan scheme with high resolution to get more detail information of the nanowire. The initial experimental results shown in Figure 10-4 demonstrate the ability of SPRM to automatically locate the position of nanowire and scan along the nanowire.

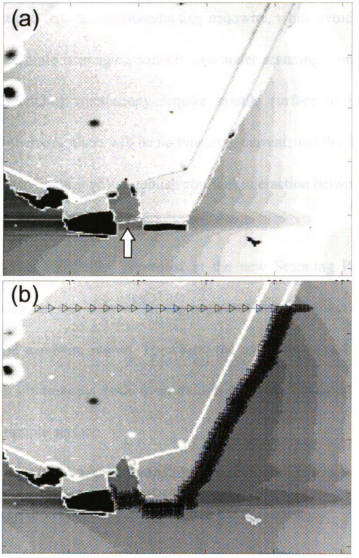

Figure 10-4 SPRM scan strategy to locate nanowire in nanocircuits (a) AFM images of nanocircuits, the arrow points to the nanowire; (b) simulation scan result shows locating the nanowire by following edges of nanocircuits. Image Size: 50μm.

Since both ends of the nanowire are attached to nanocircuits, the scan strategy of the new SPRM is to follow the edge of nanocircuits once an edge is detected. The scan angle can turn 90 degree automatically when the edge of the nanocircuits changes. After the nanowire is found, SPRM scan scheme is to start high resolution scan on nanowire region with relatively low scan rate, which will provide detail information about the nanowire.

Many nanocircuits investigation require the scan path to proceed from the

conducting contact pad onto the semiconducting nanowire, while avoiding the insulating oxide layer. One example is imaging nanocircuits under scanning tunneling microscopy mode. Scanning tunneling microscopy require sample surface to be conductive or semi-conductive, otherwise, there will be no tunneling current, and the feedback loop will fail to work, then there is no way to establish constant interaction between tip and sample surface.

With the recognition ability presented in the new Scanning Probe Recognition Microscopy, the scan can stay only within the region of interest which can be defined as the contact pad and nanowire region. Therefore, the nanocircuits can be imaged under scanning tunneling microscopy mode even though there are insulating region which is oxide layer in the sample surface.

A new set of SPRM feature definitions involving highly planar surfaces with nanoscale height variation is under development at the present time.

REFERENCE

1. Dufrene, Y.F., *Atomic Force Microscopy, a Powerful Tool in Microbiology.* Journal of Bacteriology, 2002. **184**(19): p. 5205-5213.

2. Fotiadis, D., et al., *Atomic-force microscopy: Rhodopsin dimers in native disc membranes.* Nature, 2003. **42**: p. 127-128.

3. Gadegaard, N., *Atomic force microscopy in biology: technology and techniques.* Biotechnic & Histochemistry, 2006. **81**(2 - 3): p. 87-97.

4. *Phase contrast microscopy.* Wikipedia 2007 [cited.

5. Wang, X.F. and B. Herman, *Fluorescence Imaging Spectroscopy and Microscopy.* 1996, New York: Wiley.

6. Amos, W.B. and J.G. White, *How the confocal laser scanning microscope entered biological research.* Biology of the Cell 2003. **95**: p. 335–342.

7. Sandison, D.R. and W.W. Webb, *Background rejection and signal-to-noise optimization in the confocal and alternative fluorescence microscopes.* Appl. Opt. , 1994. **33**: p. 603-610.

8. Kleinfeld, D., et al., *Fluctuations and Stimulus-Induced Changes in Blood Flow Observed in Individual Capillaries in Layers 2 through 4 of Rat Neocortex.* Proc Natl Acad Sci U. S. A., 1998. **95**: p. 15741-15746.

9. Bozzola, J.J. and L.D. Russell, *Electron Microscopy: Principles and Techniques for Biologists.* 1998, Sudbury (MA): Jones and Bartlett.

10. Bonetta, L., *Zooming in on electron tomography.* Nature methods, 2005. **2**(2): p. 139-144.

11. Hansma, H.G., *Surface biology of DNA by atomic force microscopy.* Annual Rev. of Phys. Chem., 2001. **52**: p. 71-92.

12. Liang, Y., et al., *Organization of the G-Protein-coupled receptor rhodospin and opsin in native memebranes.* J. Biol. Chem, 2003. **278**: p. 21655-21662.

13. Moller, C., et al., *Determining the molecular forces that stabilize human aquaporin-1.* J. Struct. Biol., 2003. **142**: p. 369-378.

14. Engel, A., *Microscopic assessment of membrane protein structure and function.* Histochem Cell. Biol., , 2003. **120**: p. 93-102

15. Shao, D.C.a.Z., *Submolecular Resolution of Single Macromolecules with Atomic Force Microscopy.* FEBS Letters, 1998. **430**: p. 51-54.

16. Florin, E.L., V.T. Moy, and H.E. Gaub, *Adhesion Forces between individual ligand-receptor pairs.* Science, 1994. **265**: p. 415-417.

17. Hoh, J.H. and P.K. Hansma, *Atomic force microscopy for high-resolution imaging in cell biology.* Trends in Cell Biology, 1992. **2**(7): p. 208-213.

18. F.Braet, et al., *Imagining surface and submembranous structures with the atomic force microscope: a study on living cancer cells, fibroblasts and macrophages.* J. Microscopy, 1997. **190**: p. 328-338.

19. Fillmore, H.L., et al., *Atomic force microscopy observations of tumour cell invadopodia: novel cellular nanomorphologies on collagen substrates.* Nanotechnology, 2003. **14**: p. 557-561.

20. Chasiotis, I., H.L. Fillmore, and G.T. Gillies, *Atomic force microscopy measurement of cytostructural elements involved in the nanodynamics of tumour cell invasion.* Nanotechnology, 2003. **14**: p. 73-76.

21. Leighton, X., et al., *Significant allelic loss of ANX7 region (10q21) in hormone receptor negative breast carcinomas.* Cancer Letters., 2004. **210**(2): p. 239-244.

22. Subramaniam, V., A.K. Kirsch, and T.M. Jovin, *Cell biological applications of scanning near-field optical microscopy (SNOM).* Cellular and Molecular Biology, 1998. **44**: p. 689-700.

23. Binnig, G., C.F. Quate, and C. Gerber, *Atomic Force Microscope.* Physical Review Letters, 1986. **56**(9): p. 930.

24. Pesen, D. and J.H. Hoh, *Modes of Remodeling in the Cortical Cytoskeleton of Vascular Endothelial Cells.* FEBS Lett., 2005. **579**: p. 473-476.

25. Hansma, H.G. and J.H. Hoh, *Biomolecular Imaging with the Atomic Force Microscope.* Annual Review of Biophysics and Biomolecular Structure, 1994. **23**(1): p. 115-140.

26. Rivetti C, C.S., Dieci G, Bustamante C., *Visualizing RNA extrusion and DNA*

wrapping in transcription elongation complexes of bacterial and eukaryotic RNA polymerases. J Mol Biol 2003. **326**(5): p. 1413-1426.

27. Lee, G.U., D.A. Kidwell, and R.J. Colton, *Sensing discrete streptavidin-biotin interactions with atomic force microscopy.* Langmuir, 1994. **10**(2): p. 354-361.

28. Wojcikiewicz, E.P., X. Zhang, and V.T. Moy, *Force and Compliance Measurements on Living Cells Using Atomic Force Microscopy(AFM).* Biol Proced Online, 2004. **6**: p. 1-9.

29. Ayres, V.M., *Microscopy, Scanning Tunneling* in *Encyclopedia of Medical Devices and Instrumentation (Second Edition)*, J. Webster, Editor. 2006, John Wiley and Sons Inc.: Hoboken, NJ. p. pp.516-523.

30. Tanaka, H. and T. Kawai, *Visualization of detailed structures within DNA.* Surface Sci Lett, 2003. **539**: p. 531-536.

31. *The Nobel Prize in Physics 1986.* nobelprize 1986 [cited.

32. *MultiMode SPM Instruction Manual*, Veeco Instruments Inc.

33. Howland, R. and L. Benatar, *A Practical Guide to Scanning Probe Microscopy.* 1996, Sunnyvale CA: Park Scientific Instruments.

34. Giessibl, F.J., *Advances in atomic force microscopy.* Reviews of Modern Physics, 2003. **75**(3): p. 949-35.

35. Hansma, P.K., et al., *APPLIED PHYSICS: High-Speed Atomic Force Microscopy.* Rev. Sci. Instrum., 1996. **314**(5799): p. 601-602.

36. Walters, D.A., et al., *Short cantilevers for atomic force microscopy.* Review of Scientific Instruments, 1996. **67**(10): p. 3583-3590

37. Humphris, A., M. Miles, and J. Hobbs, *A mechanical microscope – high speed atomic force microscopy.* Applied Physics Letters, 2005. **86**: p. 034106.

38. Schitter, G., F. Allgower, and F. Stemmer, *A new control strategy for. high-speed atomic force microscopy.* Nanotechnology, 2004. **15**: p. 108–114.

39. Kodera, N., H. Yamashita, and T. Ando, *Active Damping of the Scanner for High-speed Atomic Force Microscopy.* Rev. Sci. Instrum., 2005. **76**: p. 053708.

40. Hobbs, J.K., C. Vasilev, and A.D.L. Humphris, *Real time observation of*

crystallization in polyethylene oxide with video rate atomic force microscopy. Polymer, 2005. **46**(23): p. 10226-10236.

41. Wire, B. 2006 [cited.

42. *NanoScope Signal Accesss Module (SAM)-Description & Use.* 1997, Santa Barbara, CA: Digital Instruments.

43. Xu, Y., et al., *Wavelet transform domain filters: a spatially selective noise filtration technique.* Image Processing, IEEE Transactions on, 1994. **3**(6): p. 747-758.

44. Chen, Q., V.M. Ayres, and L. Udpa, *Biological Investigation Using Scanning Probe Recognition Microscopy.* Proceedings of the 3rd IEEE Conference on Nanotechnology (IEEE-NANO 2003), 2003. **2**: p. 863-865.

45. Goolsby, B., et al., *Scanning probe microscopy with landmark referenced control for direct biological investigations.* J Nanosci Nanotechnol, 2003. **3**(4): p. 347-50.

46. Fantner, G.E., et al., *Components for high speed atomic force microscopy.* Ultramicroscopy, 2006. **106**(8-9): p. 881-887.

47. Atala, A., *Technology insight: Applications of tissue engineering and biological substitutes in urology.* Nat Clin Pract Urol, 2005. **2**(3): p. 143-9.

48. Hu, J.C. and K.A. Athanasiou, *A self-assembling process in articular cartilage tissue engineering.* Tissue Eng, 2006. **12**(4): p. 969-79.

49. Xu, M., et al., *Tissue-Engineered Follicles Produce Live, Fertile Offspring.* Tissue Eng, 2006. **12**(10): p. 2739-2746.

50. Dzenis, Y., *Spinning Continuous Fibers for Nanotechnology.* Science, 2004. **304**(5679): p. 1917-1919.

51. Taylor, G., *Electrically Driven Jets.* Proceedings of the Royal Society of London. Series A, Mathematical and Physical Sciences, 1969. **313**(1515): p. 453-475.

52. Chung, H.Y., et al., *Polymer, polymer microfiber, polymer nanofiber and applications including filter structures.* 2004, Donaldson Company, Inc United States Patent No. 6743273.

53. Silver, J. and J.H. Miller, *Regeneration beyond the glial scar.* Nat Rev Neurosci,

2004. **5**(2): p. 146-156.

54. Chernousov, M.A. and D.J. Carey, *Schwann cell extracellular matrix molecules and their receptors.* Histol Histopathol, 2000. **15**(2): p. 593.

55. Abbott, N.J., L. Ronnback, and E. Hansson, *Astrocyte-endothelial interactions at the blood-brain barrier.* Nat Rev Neurosci, 2006. **7**(1): p. 41-53.

56. Deligianni, D.D., et al., *Effect of surface roughness of hydroxyapatite on human bone marrow cell adhesion, proliferation, differentiation and detachment strength.* Biomaterials, 2001. **22**(1): p. 87-96.

57. Discher, D.E., P. Janmey, and Y.-l. Wang, *Tissue Cells Feel and Respond to the Stiffness of Their Substrate.* Science, 2005. **310**(5751): p. 1139-1143.

58. Ahmed, I., et al., *Three-dimensional nanofibrillar surfaces covalently modified with tenascin-C-derived peptides enhance neuronal growth in vitro.* Journal of Biomedical Materials Research Part A, 2006. **76A**(4): p. 851-860.

59. Deligianni, D., et al., *Effect of Surface Roughness of Hydroxyapatite on Human Bone Marrow Cell Adhesion, Proliferation, Differentiation and Detachment Strength.* Biomaterials, 2001. **22**: p. 2001.

60. Lo, C.-M., et al., *Cell Movement Is Guided by the Rigidity of the Substrate.* Biophys. J., 2000. **79**(1): p. 144-152.

61. Arnold, M., et al., *Activation of Integrin Function by Nanopatterned Adhesive Interfaces.* ChemPhysChem, 2004. **5**(3): p. 383-388.

62. Fan, Y., *Image Processing Enhancements for Scanning Probe Recognition Microscopy*, in *Electrical & Computer Engineering*. 2007, Michigan State University.

63. Chatterjee, S. and A.S. Hadi, *Influential Observations, High Leverage Points, and Outliers in Linear Regression.* Statistical Science, 1986. **1**(3): p. 379-393.

64. *Chapter 14.6*, in *Command Reference Manual.* 2003, Digital Instruments p. 381-400.

65. Kasa, I., *A curve fitting procedure and its error analysis.* IEEE Trans. Inst. Meas., 1976. **25**(1): p. 8-14.

66. Keller, D., *Reconstruction of STM and AFM images distorted by finite-size tips.* Surface Science, 1991. **253**(1-3): p. 353-364.

67. Villarrubia, J.S., *Morphological estimation of tip geometry for scanned probe microscopy.* Surface Science, 1994. **321**(3): p. 287-300.

68. Villarrubia, J.S., *Algorithms for scanned probe microscope image simulation, surface reconstruction, and tip estimation.* Journal of Research of the National Institute of Standards and Technology, 1997. **102**(4): p. 425-454.

69. Udpa, L., et al., *Deconvolution of atomic force microscopy data for cellular and molecular imaging.* Signal Processing Magazine, IEEE, 2006. **23**(3): p. 73-83.

70. Fan, Y., et al., *Scanning Probe Recognition Microscopy Investigation of Cell Elastic Properties*, in *2005 APS March Meeting*. 2005: Los Angeles, CA.

71. Butt, H.-J., B. Cappella, and M. Kappl, *Force measurements with the atomic force microscope: Technique, interpretation and applications.* Surface Science Reports, 2005. **59**(1-6): p. 1-152.

72. Cappella, B. and G. Dietler, *Force-distance curves by atomic force microscopy.* Surface Science Reports, 1999. **34**(1-3): p. 1-104.

73. Hoh, J.H., W.F. Heinz, and E. A-Hassan, *Force Volume*, in *Support Note No. 240.* 1997, Digital Instruments.

74. Hertz, H., *Uber den Kontakt elastischer Köper.* J. Reine Angew. Mathematik, 1881. **92**: p. 156.

75. A-Hassan, E., et al., *Relative Microelastic Mapping of Living Cells by Atomic Force Microscopy.* Biophys. J., 1998. **74**(3): p. 1564-1578.

76. Schindler, M.S., *Private Communication:M.S. Schindler*. 2006.

77. Stevens, M.M. and J.H. George, *Exploring and Engineering the Cell Surface Interface.* Science, 2005. **310**(5751): p. 1135-1138.

78. Murray, J.D., *Chapter 4*, in *Mathematical biology II: Spatial Models and Biomedical Applications*. 2003, Springer: New York. p. 192-248.

79. Braga, P.C. and D. Ricci, *Atomic Force Microscopy: Biomedical Methods and Applications*. Methods in Molecular Biology. Vol. 242. 2003, New Jersey:

Humana Press. 408.

80. Biyasheva, A., et al., *Cascade pathway of filopodia formation downstream of SCAR.* J Cell Sci, 2004. **117**(6): p. 837-848.

81. Garcia, R. and R. Perez, *Dynamic atomic force microscopy methods.* Surface Science Reports, 2002. **47**(6-8): p. 197-301.

82. *Astrocyte.* Wikipedia 2007 [cited; Available from: http://en.wikipedia.org/wiki/Tissue_engineering.

83. Meiners, S., et al., *Engineering electrospun nanofibrillar surfaces for spinal cord repair: a discussion.* Polymer International, 2007. **56**(11): p. 1340-1348.

84. Rutledge, S.L., et al., *Self assembly and correlated properties of electrospun carbon nanofibers.* Diamond and Related Materials, 2006. **15**(4-8): p. 1070-1074.

85. Bibekananda, S., et al., *Electrospinning of continuous aligned polymer fibers.* Applied Physics Letters, 2004. **84**(7): p. 1222-1224.

86. Lee, K.H., et al., *Characterization of nano-structured poly([var epsilon]-caprolactone) nonwoven mats via electrospinning.* Polymer, 2003. **44**(4): p. 1287-1294.


MICHIGAN STATE UNIVERSITY LIB
3 1293 02956 64